Distinct roles for the mTOR pathway in postnatal morphogenesis, maturation and function of pancreatic islets

Katie L. Sinagoga[1], William J. Stone[1], Jacqueline V. Schiesser[1], Jamie I. Schweitzer[1], Leesa Sampson[3], Yi Zheng[3], James M. Wells*[1,2]

[1]Division of Developmental Biology, [2]Division of Endocrinology, [3]Division of Experimental Hematology and Cancer Biology, Cincinnati Children's Hospital Medical Center, 3333 Burnet Ave, Cincinnati OH 45229-3039

*Author for correspondence:
james.wells@cchmc.org

Keywords: islet, pancreas, mTOR, postnatal, diabetes

Summary Statement

The nutrient-sensing pathway, mTOR, and its downstream effectors are required in the first 2 weeks of life for morphogenesis, maturation, and function of pancreatic islets.

Abstract

While much is known about the molecular pathways that regulate embryonic development and adult homeostasis of the endocrine pancreas, little is known about what regulates early postnatal development and maturation of islets. Given that birth marks the first exposure to enteral nutrition, we investigated how nutrient-regulated signaling pathways influence postnatal islet development. To do this we performed loss-of-function studies of mechanistic target of rapamycin (mTOR), a highly conserved kinase within a nutrient-sensing pathway known to regulate cellular growth, morphogenesis and metabolism. Deletion of mTOR in pancreatic endocrine cells had no significant effect on their embryonic development. However, within the first 2 weeks after birth, mTOR-deficient islets became dysmorphic, β–cell maturation and function was impaired, and animals lost islet mass. Moreover, we discovered these distinct functions of mTOR are mediated by separate downstream branches of the pathway, in that mTORC1 (Raptor) is the main complex mediating maturation and function of islets, whereas mTORC2 (Rictor) impacts islet mass and architecture. Taken together, these findings suggest that nutrient-sensing may be a trigger for postnatal β cell maturation and islet development.

Introduction

While only making up about 1-2% of total pancreatic mass, the endocrine pancreas is part of a vital system controlling nutrient and metabolic homeostasis. To do this, β cells, α cells, δ cells, and pancreatic polypeptide (PP) cells secrete insulin, glucagon, somatostatin and PP in a coordinated fashion in response to nutrient and metabolic demands. During embryonic and postnatal development, these endocrine cells are specified and undergo maturation, migration, and morphogenesis to form clusters known as the islets of Langerhans.

Extensive studies in model organisms have identified numerous signaling pathways and responding transcriptional networks that regulate key stages of embryonic endocrine pancreas development (reviewed in Mastracci and Sussel, 2012; Pan and Wright, 2011). In contrast, little is known about early postnatal endocrine cell development, where endocrine cells expand in number and mature into fully functional islets that are capable of controlling nutrient homeostasis. Certain regulators of postnatal maturation have been identified that influence the function of the adult endocrine pancreas. Rodent β cells begin as an embryonic Mafb+ population but transition and ultimately mature into Mafa single-positive cells after birth (Artner et al., 2010; Hang et al., 2014; Nishimura et al., 2006). While having significant roles during embryonic development, Mafb and Arx remain factors required for the α-cell population in mature murine islets (Wilcox et al., 2013). Exclusive to the β-cell population in mice, Urocortin3 (Ucn3) is up-regulated in the postnatal pancreas starting at P6 (Blum et al., 2012) and potentiates a mature paracrine feedback loop necessary for proper glycemic control (van der Meulen et al., 2015). During this time, expression of Pdx1 within β cells also increases and is necessary for β-cell survival and identity (Ahlgren et al., 1998; Gao et al., 2014). Additional transcription factors have been found to be required for adult endocrine maintenance and subsequent function of the islet. Among other roles, Nkx2.2, Isl1, and Pax6 regulate glucose transporter 2 (Glut2) expression (Doyle and Sussel, 2007; Ediger et al., 2014; Gosmain et al., 2013). Glut2 is a necessary carrier protein that is part of the glucose sensing machinery of a β cell and as such, is an integral part of glucose stimulated insulin secretion (GSIS). In mouse models, down-regulation or loss of key postnatal maturation factors leads to a loss of β-cell functionality, decreased responsiveness to glucose, and diabetes.

There are vast changes in the gastrointestinal tract after birth, primarily in response to oral feeding (Zhang et al., 1998). Published findings suggest that islets are glucose-responsive during this time, but are not able to perform oxidative metabolism, nor maintain efficient whole-body glucose homeostasis like adult islets (Bliss and Sharp, 1992). At later postnatal stages, changes in diet, such as milk to chow transition, can drastically affect the maturation and function of the islet (Stolovich-Rain et al., 2015). These studies have shown that timing, weaning, and diet composition all play major roles in the final stages of postnatal islet development and glycemic control. In addition,

several studies demonstrate the importance of nutrient sensing in adult islet function. In contrast, nothing is known about the impact of nutrients on islet development just after birth.

Mechanistic target of Rapamycin (mTOR) is comprised of two nutrient-sensitive serine-threonine kinase complexes that have known roles in proliferation, transcription, translation, cytoskeletal rearrangement, and cell survival. One key role of mTOR is to modulate cellular metabolism and homeostasis in response to availability of growth factors and nutrients. The two complexes, mTORC1 and mTORC2, differ in both the adaptor proteins associated with the complex as well as their sensitivity to the drug rapamycin. mTORC1 utilizes adaptor protein Raptor which directly phosphorylates S6K and 4ebp1, both of which promote synthesis of proteins. mTORC2 includes the adaptor protein Rictor and plays roles in cytoskeletal reorganization and cell size. While mTORC1 is highly sensitive to rapamycin, short-term exposure to the drug has no effect on mTORC2.

While few studies have detailed mTOR's role during embryonic or postnatal endocrine pancreas development, the mTOR pathway is known to be involved in several aspects of adult β-cell biology. Aberrant regulation of mTOR has been implicated in obesity and type2 diabetes, and inhibition of mTOR signaling via rapamycin improves blood glucose levels in some patients with hyperinsulinemic hypoglycemia (Alexandrescu et al., 2010; Senniappan et al., 2014). However, in normal glycemic mice, rapamycin exposure leads to decreased glucose sensitivity and diabetes (Schindler et al., 2014). In addition, mTORC1 activation promotes adult β-cell proliferation via regulation of cyclin D2 synthesis and stability (Balcazar et al., 2009), while mTORC2 has been implicated in the balance between cell size and proliferation in the adult β cell (Gu et al., 2011). Deletion of the negative regulator of mTOR signaling, TSC1, can actually improve glucose-sensing mechanisms and increase insulin production (Mori and Guan, 2012) while up-regulation of the pathway via Lkb1 deletion has been shown to enhance β-cell mass, glucose tolerance, and insulin content (Fu et al., 2009; Granot et al., 2009). A more detailed description of mTOR signaling in the adult islet is reviewed elsewhere (Wang et al., 2016), however, these data imply that mTOR signaling plays critical roles

in the function of adult β cells and influences glucose metabolism in both normal and pathological contexts.

Birth marks the start of enteral nutrition in mammals, which then must develop the ability to sense and regulate systemic glucose. Correspondingly, the endocrine pancreas undergoes profound changes including expansion of endocrine cell mass, the formation of islets, and the maturation of β cells. To investigate how nutrient-sensing pathways are involved in these postnatal changes in endocrine pancreas development, we studied the impact of inactivating mTOR on postnatal islet development. We deleted mTOR in the developing endocrine pancreas using a *Neurog3^{Cre};mTOR$^{f/f}$* mouse model and found that mTOR was not required for embryonic specification or differentiation of endocrine cells. In contrast, mTOR was essential in the first weeks of life for expansion of endocrine mass, β-cell maturation and functionality, as well as islet morphogenesis. Further examination revealed distinct roles for mTORC1 and 2 during postnatal development, in which C1 signaling was the primary complex affecting islet maturation and function. Ultimately, these late developmental defects caused β-cell failure and hyperglycemia in young adult mice.

Results

mTOR is required for normal postnatal islet development

To investigate the role of mTOR in islet development, we used Neurog3Cre to delete mTOR from the developing endocrine pancreas (Figure 1A). For the first 4 weeks after birth, *Neurog3^{Cre};mTOR$^{f/f}$* (mutant) mice grew in parallel with their control littermates and using immunohistochemistry, we confirmed efficient deletion of mTOR within the endocrine compartment (Figure 1B, Figure S1A). However, by 7 weeks of age, both male and female mutant mice showed signs of impaired health and most animals perished by 8 weeks. To identify when *Neurog3^{Cre};mTOR$^{f/f}$* (mutant) mice first exhibited an endocrine pancreas phenotype we analyzed animals from postnatal day 7 to 8 weeks of life for fasted blood-glucose levels and circulating insulin levels. Mutant mice first showed signs of impaired glucose regulation at P14 and were fully diabetic at P28 (Figure 1C). Whole-mount immunofluorescence staining of insulin in the pancreas revealed drastically fewer islets in adult mutant mice (Figure 1D top panels, Video S1, S2). Moreover, remaining islets were dysmorphic, smaller, and lacked functional

markers of mature β cells such as Glut2 (Figure 1D, bottom panels). For the first 3 weeks of postnatal life, the growth of mutant mice was the same as control littermates (Figure S1A), suggesting that feeding behavior and nutrient absorption was normal. We also stained for PECAM and synaptophysin and found normal vascularization and innervation of islets (Figure S1B). These data suggested that hyperglycemia and β-cell failure was primarily the result of a cell-autonomous role for mTOR within the postnatal islet, and not the culmination of intestinal or CNS effects on the β cell. Lastly, we detected a subtle phenotype in heterozygous mTOR mice through slightly reduced β-cell numbers (Figure S2A,B), however this phenotype did not culminate in elevated blood glucose levels or lowered glucose-sensing mechanisms, even at 1 year of age (Figure S2C). Therefore, we focused all remaining analyses on homozygous mutant mice.

Since *Neurogenin3* is expressed embryonically, we needed to first determine if postnatal effects were due to an earlier role of mTOR during embryonic endocrine development. Analysis of pancreas samples from embryonic day e18.5 of wildtype and mutant animals indicated no statistical difference in the relative proportions of α, β, and δ cells (Figure 2A). In addition, analysis of key regulators of endocrine-cell migration from the duct, such as Sox9, E-cadherin, and Snail2, indicated that islet morphogenesis before birth in *Neurog3^{Cre};mTOR$^{f/f}$* mice was similar to control mice (Figure S3A). Given that mTOR mutant animals became diabetic between 3-4 weeks of life, we hypothesized that mTOR primarily affected postnatal islet development. We therefore investigated when mTOR signaling was most active during postnatal pancreas development by analyzing phospho-mTOR levels, a readout of active mTOR signaling. mTOR signaling was highest in the first few weeks after birth in both the endocrine and exocrine compartments, after which the pathway became progressively less active as the mice aged (Figure S3B). Together these data indicated that mTOR was dispensable for embryonic development, instead having a prominent role during postnatal stages of islet development.

Loss of postnatal endocrine cell mass in mTOR mutant islets

Given the high levels of mTOR signaling in the first few weeks of life, we interrogated *Neurog3^{Cre};mTOR$^{f/f}$* animals at early postnatal stages for alterations in islet mass, β cell maturation and function, as well as islet architecture. Analysis of islet mass

using flow cytometry at P7 indicated no significant differences in endocrine populations within mutant islets (Figure 2A). However, there were noticeably fewer endocrine cells present at P14, with a decrease in α, β, and δ cell populations as compared to controls (Figure 2B). These reductions culminated in fewer large islets at P14 in mutant mice (Figure S3C). We investigated if this was due to apoptosis, however analysis of TUNEL staining from e18.5 through adult stages did not show any significant changes in cell death of endocrine cells (Figure S4B). We observed a similar finding with active Casp3 staining (data not shown), concluding that endocrine cells were not undergoing apoptosis in the absence of mTOR. Finally, lineage tracing of endocrine cells did not uncover trans-differentiation or dedifferentiation events in mTOR mutant mice (data not shown).

We next investigated if proliferation of endocrine cells was altered in mTOR mutant islets using BrdU incorporation as well as Ki67 and phosphohistone (PHH3) staining. By Ki67 immunofluorescence, we found significantly fewer proliferating cells just prior to birth, and a trend of decreased proliferation was also seen with PHH3 immunostaining (Figure S4C,D). Additionally, we assessed long-term proliferation through daily BrdU injections between 1 and 2 weeks of postnatal life and observed that while there was no statistical difference in BrdU incorporation between wildtype and mutant mice, there was a decreasing trend. This data suggested that mTOR mutant animals retained lower levels of postnatal proliferation (Figure S4C). From these data, we concluded that lower proliferation and numbers of endocrine cells during late embryonic/early postnatal development culminated in the reduced cell counts at P14 in mTOR mutant animals. Together these findings suggested that mTOR signaling was regulating islet mass and expansion during early postnatal islet development, which is consistent with its known role in adult animals to regulate β-cell mass (Balcazar Morales and Aguilar de Plata, 2012; Balcazar et al., 2009; Gu et al., 2011).

Maturation and function is compromised in mTOR mutant islets

Another key process that occurs during early postnatal islet development is functional maturation of β cells. Glucose sensing and transport is required for β-cell function and we investigated if glucose-sensing mechanisms were impaired in mutant mice by analyzing expression of the glucose transporter, Glut2. While Glut2 expression

was normal at P7, we noticed a significant decrease in Glut2 beginning at P14, ultimately leading to a complete loss at P21 in mTOR mutant mice (Figure 2C, Top). Despite the loss of Glut2, these islet cells retained β-cell identity as marked by expression of Pdx1 (Figure 2C, Bottom)(Gao et al., 2014). We concluded from these data that mTOR was affecting both islet-cell expansion and function in the first two weeks of postnatal life.

Previous work has identified several transcription factors that are necessary for β-cell maintenance, identity, and function postnatally. Alterations in these transcription factors could, in part, contribute to the phenotype in mTOR mutants at P14. We analyzed mRNA levels of a number of transcription factors at different stages ranging from birth to P14. At birth, islet transcription factors and hormones were expressed at normal levels in mTOR mutants, indicating that mTOR was functionally dispensable to embryonic islet development (Figure 3A, Figure S5B). However, at P7 and P14 several factors were significantly reduced including *Neurod1*, *Nkx6.1*, *Pax6*, *Foxa2,* and *Foxo1* (Figure 3A, Figure S5B). At the protein level, we also observed a decrease in Pax6 and Nkx2.2 at P14 (Figure 3B). Pax6 has been shown to be essential for the maintenance of adult islets, while Nkx2.2 is known to regulate β-cell function (Doyle and Sussel, 2007; Hart et al., 2013; Sander et al., 1997). In addition, Nkx6.1 and Foxo1 transcription factors are known to regulate β-cell growth (Okada et al., 2007; Taylor et al., 2015). Therefore, the significant reduction of all of these factors could contribute to the phenotypes observed in mTOR mutant islets.

To investigate the molecular basis for maturation defects in mTOR mutant islets, we analyzed β-cell maturation markers MafA and Urocortin 3 (Ucn3). Ucn3 protein and mRNA were reduced in P14 islets, as was *MafA* mRNA (Figure 3C). The reduced levels of MafA and Ucn3 observed in mTOR mutant animals at P14 was not due to a delay in islet maturation since P21 mutant mice also had further reduced Ucn3 levels, indicating persistent immaturity and loss of function (Figure 3C). Robust production of hormones is also a measure of islet function and we found that nearly all hormone transcripts were reduced in mTOR mutant animals by P14 (Figure 3D, S5B). One exception was a trend towards a transcriptional increase in the hormone *Ghrelin*, which is normally expressed in a subset of embryonic endocrine cells but decreases postnatally (Prado et

al., 2004). Despite an increase in *Ghrelin* mRNA, we did not observe increased levels of Ghrelin protein (data not shown). Lastly, we investigated the expression of selectively disallowed genes, which are down-regulated specifically during the neonatal period in β cells. The low-level expression of these genes ensures that the β cells respond exclusively to glucose within the body and not to other metabolites such as pyruvate (Thorrez et al., 2011). At P14 we did not observe any changes in lactase dehydrogenase (*Ldha*) or other selectively disallowed genes in mTOR mutant islets relative to controls (Figure S5C).

Postnatal maturation results in the formation of functional endocrine cells with the ability to accurately modulate glucose levels when animals transition from milk to a more complex diet. Production, processing, packaging and secretion of insulin are all hallmarks of a functional β cell and we investigated if these processes were affected in mTOR mutants. Preproinsulin processing by the prohormone convertase 1/3 is essential for β-cell function, and immunodetection for PC1/3 was similar between controls in mTOR mutant β cells (Figure 4A). However, at P7 and P14 we observed a significant reduction in *Slc30a8* (Znt8), a transporter that is responsible for the influx of zinc into β cells and the subsequent packaging of insulin into mature granules (Figure 4B, Figure S5D). Consistent with this, we observed a reduction in granule formation in both α and β cells by two separate measures; flow cytometry at P14 and transmission electron microscopy (TEM) at P21 (Figure 4C,D). Assessment of β-cell granularity by side scatter during flow cytometry has been previously reported (Katsuta et al., 2012) and while average side-scatter measurements were similar at P7, both α and β cells were less granular at P14 (Figure 4C, Figure S5E). In conjunction, TEM analysis at P21 revealed fewer insulin and glucagon granules within endocrine cells, most of which lacked a mature morphology (Figure 4D). Lastly, Sur1 and Kir6.2, which make up an essential K^+ transporter in the β cell, were reduced in mTOR mutants at P14 (Figure 4B). This would indicate a defect in the depolarization of the membrane and release of insulin granules from the β cell. To assess the functionality of β cell GSIS at P14, we performed a glucose challenge on mTOR mutant mice. While mutant mice were able to secrete comparable, wildtype levels of insulin in response to a bolus of glucose (Figure S5F), these same cells were unable to maintain normal glycemia after a 16-hour fast (Figure 4E). These data suggested that while mTOR-mutant beta cells were able to

respond appropriately to high levels of circulating glucose, they were less sensitive to basal glucose levels, likely due to loss of functional channels, transporters, and vesicles. Taken together, our data suggested that mTOR signaling was playing fundamental roles in regulation of postnatal endocrine maturation, formation of mature insulin secretory granules, and expression of transporters necessary for insulin secretion.

Islet morphogenesis is abnormal in mTOR mutant animals

One poorly understood process of postnatal pancreas development is the formation of islets of Langerhans. Just before birth, pancreatic endocrine cells are found along the major pancreatic ducts in large, disorganized clusters (See Figure S3A). Over the next few weeks, endocrine cells begin to aggregate and organize into islets that are distinct from the ducts. In mTOR mutant mice, these processes appear to be perturbed, resulting in dysmorphic islet architecture and continued close proximity to the duct. This was clearly evident at P14 in mTOR mutants, where we observed long aggregations of endocrine cells that failed to round off into individual islets and remained closely associated with ductal structures (Figure 5A). In order to thoroughly assess these morphogenic defects, we took four approaches to characterize these phenotypes. First, we examined immunofluorescence of serial-sectioned wildtype and mTOR mutant islets at P14 and P21 (Figure 5A). We then calculated a size and shape score for each of the islets within our P14 samples (see materials and methods for details regarding shape-score calculation). This revealed a significant decrease in the shape score of mutant islets, which was most apparent in the larger islets at P14 (Figure 5B, Figure S6A). Second, we performed whole-mount immunofluorescence staining and confocal analysis of the P21 pancreas to confirm in a 3D setting that large islets retained abnormal architecture and remained in close proximity to large ducts in mTOR mutants (Figure 5C, Video S3, S4). This also confirmed that the phenotype did not resolve with age. We also noted a decrease in the size of individual cells within islets, and this phenotype correlated with the size of the islet (Figure 5D). Next, we used dolichos biflorus agglutinin (DBA) as a ductal marker and calculated the distance of each islet to the nearest main duct. Islets in mTOR mutants remained closely associated with large ducts, indicating that endocrine cells failed to undergo normal islet morphogenesis (Figure 5B, Figure S6A). Lastly, we investigated the impact of mTOR deficiency on adhesion molecules known to regulate islet morphogenesis during development. Down-

regulation of E-cadherin expression is necessary for endocrine-cell delamination (Gouzi et al., 2011) and increased expression is correlated with a loss of endocrine-cell migration away from ductal structures (Greiner et al., 2009). We noted a trend of increased E-cadherin protein levels in mTOR mutant duct-associated islets, suggesting improper E to N-cadherin transition during segregation from ductal structures (Figure S6B,C). We also noted reduced *N-cadherin* expression and a slight decrease in connective tissue growth factor (*Ctgf*), which has been implicated in islet architecture defects as well (Figure 5E)(Crawford et al., 2009). From these data, we concluded that mTOR activity was required for normal morphogenesis of the postnatal islet.

mTOR Complex 1 and 2 each contribute to different aspects of postnatal islet development

mTOR is composed of two complexes, mTORC1 containing Raptor, and mTORC2 containing Rictor, each of which mediate different signaling effects of the mTOR pathway. mTORC1 signaling is primarily associated with transcriptional and translational changes within a cell, whereas mTORC2 signaling has been shown to mediate cellular morphogenic processes. Despite their differences, both complexes have been implicated in proliferation and islet mass in the adult pancreas (Balcazar Morales and Aguilar de Plata, 2012; Gu et al., 2011). We therefore investigated if the different phenotypes observed during early postnatal islet development in the mTOR mutants were complex-specific. Analysis of *Neurog3^{Cre};Rapt$^{f/f}$* mice revealed smaller, yet morphologically normal islets within the pancreas (Figure 6A). Raptor-deficient islets, however, had reduced Ucn3 and Glut2 immunostaining at P21, indicative of functional and maturation defects within the β cells (Figure 6B). In addition, Raptor mutant mice had reduced Pax6 protein, implying an altered transcriptional network, much like the mTOR mutant model (Figure 6B). These phenotypes culminated in elevated fasting blood glucose levels and reduced circulating insulin at three weeks of age (Figure 6C, Figure S7A). Although the mTOR and Raptor phenotypes shared many similarities such as reduced maturation and impaired function, these effects arose at P21 in Raptor mutants, whereas the mTOR phenotype was present at P14 (Figure S7B). Consistently, mTOR mutants died within 8 weeks, while Raptor mutants perished around 12 weeks of age (data not shown), which indicated latency in the phenotype.

While a functional and maturation defect was identified in Raptor mutants, we did not observe any morphological islet deformities within the pancreas. However, analysis of *Neurog3^{Cre};Rict$^{f/f}$* animals at P21 showed that Rictor-deficient islets had architecture defects similar to mTOR mutants (Figure 6D). Shape-score quantification of mutant islets did not reach statistical significance (Figure S7C), but suggested that both Raptor and Rictor complexes may contribute to morphogenic defects observed in mTOR mutant islets. Additionally, Rictor mutant islets displayed no changes in the maturation/functional markers Ucn3 or Glut2, respectively (Figure S7D) and had normal fasted blood glucose levels and circulating insulin at P21 (Figure 6C, Figure S7A). However, Rictor mutants did have reduced numbers of small/medium-sized islets at P21 (Figure 6D). Although there are no published reports of the impact of Rictor on early postnatal islet development, our data are consistent with known roles of Rictor in β-cell mass in the adult (Gu et al., 2011).

Since a functional defect was not present in Rictor mutants, this implicated a primary role for Raptor in postnatal islet development. From these data, we concluded that mTORC1 signaling is primarily responsible for the maturation and function of postnatal islets, whereas mTORC2 may play a lesser role in postnatal islet morphogenic events, but a consistent role in islet mass. It seems reasonable to conclude that the increased severity of the phenotypes observed in mTOR mutants are due to the additive effects of losing signaling through both mTOR complexes.

Discussion

In this study, we have identified several novel and separable functions for the mTOR signaling pathway during postnatal islet development. While previous studies have focused primarily on mTOR signaling in adult β cell maintenance and function, we show that mTOR is additionally required in the first few weeks after birth. Examination of postnatal animals revealed that mTOR is involved in three distinct aspects of postnatal islet development: 1) β cell maturation and function 2) islet mass and 3) islet morphogenesis (Figure 7). Moreover, we show that specific complexes, mTORC1 and mTORC2, are required during different stages of islet maturation/function and together may play an underappreciated role in islet morphogenesis.

One key function of the mTOR pathway is to sense the availability of nutrients and coordinate the appropriate cellular response. Interesting, we found that mTOR-deficient islets are normal at birth and do not require mTOR signaling until the beginning of postnatal life. During the two-week window after birth, it is critical for β cells to acquire the functional capacity to sense fluctuations in physiological glucose levels. This process, termed maturation (Blum et al., 2012; Pan and Wright, 2011), is not well-understood but can be monitored through the expression of critical transcription factors and proteins necessary for proper β-cell function (Ucn3, Glut2, Pax6, ect.), and physiologically through GSIS. During the same developmental time period, the entire gastrointestinal tract is undergoing major changes in response to oral nutrient exposure (Zhang et al., 1998). Changes to postnatal diet have been shown to impact islet development and maturation at weaning (P21) (Stolovich-Rain et al., 2015). However, the current study has identified a critical role for mTOR at just after birth, possibly by controlling β cell maturation in response to the introduction of oral nutrients. Beyond the scope of the current study, future experiments will need to identify the key regulators upstream of mTOR that stimulate this pathway to in response to enteral nutrition. We hypothesize that there could be many direct and indirect sources of mTOR activation, including components within the mother's milk and amino acids such as leucine (González and Hall, 2017; Haschke, 2016; Millward, 2012). In addition, the connection between enteroendocrine cells, the neuroendocrine system, and the endocrine pancreas in regulating global nutrient homeostasis has been well documented (Heijboer et al., 2006). We could therefore use the *Neurog3*^{Cre}*;mTOR*$^{f/f}$ system to study mTOR in neuro- and enteroendocrine cells. However, in the first 2 weeks of life, it appears that the predominant function of mTOR is in the endocrine pancreas, since we do not observe any changes in weight or feeding behavior that would be expected if satiety or digestion were grossly abnormal. Overall, our study is one of the first to highlight the importance of early nutrient-sensing mechanisms on postnatal pancreatic endocrine development for the overall function of the adult islet.

From previous studies, we know mTOR positively regulates Pax6 expression in the CNS and is required for maintenance of neuroepithelial and glial cells (Endo et al., 2009). Pax6 is a transcription factor that is essential in the adult islet for maintenance of cell identity and function, suggesting that the reduced function in mTOR islets is due, in

part, to loss of *Pax6* expression. Loss of Pax6 in the adult islet results in an increase in ghrelin and severe reductions in α, β, and δ cells (Hart et al., 2013), a phenotype that mirrors a loss of mTOR in islets. Pax6 and mTOR mutants additionally share similar maturation and functional defects as measured by reductions in Mafa and Glut2 in β cells (Gosmain et al., 2013). Glut2 has essential roles in GSIS (reviewed in Thorens, 2015) and down-regulation marks attenuated function of β cells. We additionally observed this in P14 mTOR mutant mice, where β cells were able to secrete insulin in response to a high bolus of glucose, but were unable to maintain normal basal glucose levels. This correlated with a significant loss of Glut2, most likely accounting for decreased glucose transport and inability to maintain glucose homeostasis during fasting conditions. In addition, reports have identified Mafa as a factor that promotes β-cell maturation through regulation of genes such as zinc transporter *Slc30a8*, which is essential for formation of mature insulin granules (Artner et al., 2010; Hang et al., 2014). In mTOR mutants, *Mafa* and *Slc30a8* were both significantly reduced, as was the granularity of both mutant β and α cells by EM. β cell EM from Slc30a8 and mTOR mutants appears strikingly similar, having fewer highly dense granules and more immature, less compact granules (Wijesekara et al., 2010). Overall, these data support a model whereby the mTOR pathway promotes postnatal endocrine maintenance, maturation, and the subsequent function of β cells in part through the regulation of Pax6 and its downstream transcriptional network.

Besides cellular maturation, pancreatic islets additionally change morphology after birth by transitioning from long strings of cells clustered next to ductal structures, to spherical, distinct islets. Surprisingly, we also observed striking morphological defects in mTOR mutants. Mutant islets retained elongated architecture and remained closely associated with ducts, which was reminiscent of earlier stages of development. Using a novel shape-score algorithm, we revealed significant differences at P14 in the overall architecture of large islets and confirmed these findings through a secondary, whole mount immunofluorescence approach at P21. Using this 3D imaging of the islet, we clearly observed dysmorphic islets and concluded that the phenotype did not resolve with age. We analyzed mTOR mutant islets for expression of Snail2, E-cadherin, and N-cadherin, all of which are involved in epithelial remodeling processes in many contexts. For example Snail2 has known roles in epithelial-mesenchymal transition

(EMT) and is expressed most highly at late embryonic/early postnatal stages of pancreatic endocrine development (Gouzi et al., 2011; Rukstalis and Habener, 2007). At e18.5 we found comparable levels of E-cadherin and Snail2 prior to birth between mTOR mutants and control animals. This indicated that mTOR-deficient endocrine cells are still able to delaminate from the ducts and cluster into nascent islets. However, at later postnatal stages we observed a decrease in N-cadherin and a slight increase in E-cadherin levels in our mutant islets, suggesting that a switch from E- to N-cadherin may be impaired (Gouzi et al., 2011). While these data show that mTOR signaling is required for normal islet morphogenesis, a more detailed description of normal islet morphogenesis postnatally will be essential to uncovering the exact mechanism of mTOR action in this process.

mTOR controls a wide range of cellular effects, some of which can be separated based on mTORC1 or mTORC2 downstream targets. The deletion of mTOR, or individual adaptor proteins Raptor (C1 signaling) and Rictor (C2 signaling) using *Neurog3*^{Cre} allowed us to examine the function of mTOR and each complex within all pancreatic endocrine cells during postnatal maturation. This is in contrast to previous work that focused on the roles for C1 and C2 in specifically in adult β-cells (Balcazar et al., 2009; Fu et al., 2009; Granot et al., 2009; Gu et al., 2011; Mori and Guan, 2012). Deletion of mTOR all islet cells prior to birth allowed us to identify that the kinase is required for the maturation, function, and granularity of postnatal endocrine populations. The Rictor and Raptor deletion studies identified that mTOR effects are mediated primarily through complex1 signaling, as Raptor mutant islets displayed nearly identical loss of transcription factor Pax6, maturation marker Ucn3, and functional marker Glut2. The morphogenesis defect observed in mTOR mutant islets was partially reproduced with the deletion of Rictor. While consistent with previous roles of Rictor in cytoskeletal reorganization, our data suggest that C1 and C2 have overlapping roles in regulating islet architecture and islet mass. We therefore propose a model through which complex 1 signaling is the primary inducer of postnatal islet maturation whereas both complexes 1 and 2 are involved in morphogenesis and islet mass. It would be of interest to analyze how the function of complex 1 and 2 change from postnatal stages into adulthood, and in turn, as diet composition switches during this time. Moreover, to understand how nutrient-sensing pathways contribute to the overall maturation of individual pancreatic

endocrine cell types, a more rigorous analysis of mTOR deletion specifically within the α, β, and δ subpopulations will need to be performed.

In conclusion, we have identified essential and separable roles for the mTOR pathway in early postnatal islet development. mTORC1-Raptor is essential for β cell maturation and acquisition of function while mTORC2-Rictor contributes to islet morphogenesis. Recently, studies of human juvenile islets determined that they are transcriptionally distinct from adult islets, implying that humans may also undergo significant postnatal maturation (Arda et al., 2016). Therefore, understanding the molecular basis of islet maturation and morphogenesis in response to enteral nutrients is of clinical importance. Moreover, given the therapeutic possibility of pharmacological manipulation of the mTOR pathway in premature infants, we could conceivably control the timing of maturation to correspond with normal gestational age. Lastly, our findings suggest that manipulation of nutrient-sensing pathways may be critical for controlling the maturation and functionality of human PSC-derived β cells.

Experimental Procedures

Mice

Mouse experiments were pre-approved by the Committee of Ethics of Animal Experiments at Cincinnati Children's Hospital Research Foundation (CCHRF) and were in accordance with Guide for the Care and Use of Laboratory Animals of the National Institutes of Health (IACUC2016-004). All mice in the study were housed in the CCHRF mouse facility and maintained in a normal 12-hour light/dark cycle and on regular chow. To obtain mutants, *Neurog3^{Cre}; f/+* mice were mated to *f/f* mice. Both male and female mice are represented in all experiments performed. Mouse strains, see Supplemental Methods.

Tissue Processing, Immunostaining and Imaging

In order to assess islet markers via immunofluorescence, pancreatic tissue was isolated, fixed, embedded, and sectioned using modified protocols found in Spence et al., 2009 and Jonatan et al., 2014, details of which can be found in the Supplemental Methods. Slides were imaged using a Nikon Confocal A1 inverted microscope and analyzed using Nikon Elements and Imaris software. Antibody lists can be found in Table S1.

qPCR analysis

Whole pancreatic tissue was collected at P0, P7, and P14. RNA was isolated using an RNAqueous-Micro Total RNA Isolation Kit (Life Technologies). cDNA was made using SuperScript Vilo cDNA synthesis kit (Invitrogen). qPCR was performed using a predesigned TaqMan Array 96-well fast plate (Life Technologies). Data was normalized to pan-endocrine transcription factor *Neurogenin3*.

Morphogenesis and Migration analysis

For shape-score analysis, P14 serial-section pancreas tissue was stained for insulin, glucagon, and somatostatin. 8 sections per slide (per animal) were tiled-scanned using a Nikon A1 inverted confocal microscope. Islet circularity, elongation, and convexity were calculated on NIS-Elements software to determine shape score (See Supplemental Methods).

Whole-Mount Pancreas Staining

Whole pancreas was isolated and processed using a modified version of passive clarity from Yang et al., 2014. See Supplemental Methods for protocol. Tissue was cleared using refractive index matching solution (RIMS) and imaged using a Nikon Confocal A1 inverted microscope.

Circulating Insulin and Glucose

Mice were fasted for 4 hours (or extended 16 hour-fast) and blood glucose levels were tested using a TrueTrack glucometer. The Mouse Ultrasensitive Insulin ELISA kit (ALPCO) was used to determine fasted circulating insulin levels. Data was analyzed using Prism software. Detailed methods and glucose tolerance test, see Supplemental Methods.

Flow cytometry analysis and Granularity

Whole pancreatic tissue was collected, dissociated, and immunostained with insulin, glucagon, and somatostatin (See Supplemental Methods for protocol). Cells were analyzed using a LSRII bench-top flow cytometer (BD Biosciences), and FACS plots were

processed using FACSDiva (BD Biosciences) and FlowJo (Tree Star Inc). A full list of antibodies can be found in Table S1.

Granularity via flow cytometry was determined from the mean side scatter measurement (SSC) of all endocrine cells analyzed per sample. SSC analysis was done at P7 and P14 with 6 litters analyzed in total.

Proliferation and apoptosis

BrdU (100 mg/kg) was IP injected daily into pups from P7 to P13 and tissue was collected at P14 for analysis. Tissue was processed and analyzed via flow cytometry.

TUNEL staining was performed using an *In Situ* Cell Death Detection Kit, Fluorescein (Roche). Slides were imaged using a Nikon Confocal A1 inverted microscope.

Statistical Methods

All quantitated data was assessed for significance using a one-tailed student's T-test, assuming normal distribution, and represented as ± S.E.M. Number of animals in each experiment as well as significance values can be found in Table S3.

Acknowledgements

We would like to thank members of the Wells, Zorn, and Huppert labs as well as the CCHMC PSCF Core for feedback and reagents. In addition, we thank Matt Kofron and Mike Muntifering for their expertise on imaging and analysis quantification. We acknowledge CCHMC Vet Services, CCHMC Pathology Core, the CCHMC Confocal Imaging Core and the Flow Cytometry Core. This work was supported by National Institutes of Health grants R01DK092456 and U19 AI116491 (J.M.W.) and core support from the Cincinnati Digestive Disease Center Award (P30 DK0789392). We declare no conflict of interest.

Author Contributions

KLS and JMW were responsible for the study as well as designed experiments, analyzed data, and co-wrote the manuscript. Feedback and additional experiments were performed by WJS, JIS, YZ and LS. Cell sorting and FACS analysis was performed by JVS.

References

Ahlgren, U., Jonsson, J., Jonsson, L., Simu, K. and Edlund, H. (1998). beta-cell-specific inactivation of the mouse Ipf1/Pdx1 gene results in loss of the beta-cell phenotype and maturity onset diabetes. *Genes Dev.* **12**, 1763–8.

Alexandrescu, S., Tatevian, N., Olutoye, O. and Brown, R. E. (2010). Persistent hyperinsulinemic hypoglycemia of infancy: constitutive activation of the mTOR pathway with associated exocrine-islet transdifferentiation and therapeutic implications. *Int. J. Clin. Exp. Pathol.* **3**, 691–705.

Arda, H. E., Li, L., Tsai, J., Torre, E. A., Rosli, Y., Peiris, H., Spitale, R. C., Dai, C., Gu, X., Qu, K., et al. (2016). Age-Dependent Pancreatic Gene Regulation Reveals Mechanisms Governing Human β Cell Function. *Cell Metab.* **23**, 909–920.

Artner, I., Hang, Y., Mazur, M., Yamamoto, T., Guo, M., Lindner, J., Magnuson, M. A. and Stein, R. (2010). MafA and MafB regulate genes critical to beta-cells in a unique temporal manner. *Diabetes* **59**, 2530–9.

Balcazar, N., Sathyamurthy, A., Elghazi, L., Gould, A., Weiss, A., Shiojima, I., Walsh, K. and Bernal-Mizrachi, E. (2009). mTORC1 Activation Regulates -Cell Mass and Proliferation by Modulation of Cyclin D2 Synthesis and Stability. *J. Biol. Chem.* **284**, 7832–7842.

Balcazar Morales, N. and Aguilar de Plata, C. (2012). Role of AKT/mTORC1 pathway in pancreatic β-cell proliferation. *Colomb. médica (Cali, Colomb.* **43**, 235–43.

Bliss, C. R. and Sharp, G. W. (1992). Glucose-induced insulin release in islets of young rats: time-dependent potentiation and effects of 2-bromostearate. *Am. J. Physiol. - Endocrinol. Metab.* **263**,.

Blum, B., Hrvatin, S. S. Š., Schuetz, C., Bonal, C., Rezania, A. and Melton, D. A. (2012). Functional beta-cell maturation is marked by an increased glucose threshold and by expression of urocortin 3. *Nat. Biotechnol.* **30**, 261–4.

Crawford, L. A., Guney, M. A., Oh, Y. A., Deyoung, R. A., Valenzuela, D. M., Murphy, A. J., Yancopoulos, G. D., Lyons, K. M., Brigstock, D. R., Economides, A., et al. (2009). Connective tissue growth factor (CTGF) inactivation leads to defects in islet cell lineage allocation and beta-cell proliferation during embryogenesis. *Mol. Endocrinol.* **23**, 324–36.

Doyle, M. J. and Sussel, L. (2007). Nkx2.2 regulates beta-cell function in the mature islet. *Diabetes* **56**, 1999–2007.

Ediger, B. N., Du, A., Liu, J., Hunter, C. S., Walp, E. R., Schug, J., Kaestner, K. H., Stein, R., Stoffers, D. A. and May, C. L. (2014). Islet-1 Is essential for pancreatic β-cell function. *Diabetes* **63**, 4206–17.

Endo, M., Antonyak, M. A. and Cerione, R. A. (2009). Cdc42-mTOR signaling pathway controls Hes5 and Pax6 expression in retinoic acid-dependent neural differentiation. *J. Biol. Chem.* **284**, 5107–18.

Fu, A., Ng, A. C.-H., Depatie, C., Wijesekara, N., He, Y., Wang, G.-S., Bardeesy, N., Scott, F. W., Touyz, R. M., Wheeler, M. B., et al. (2009). Loss of Lkb1 in Adult β Cells Increases β Cell Mass and Enhances Glucose Tolerance in Mice. *Cell Metab.* **10**, 285–295.

Gao, T., McKenna, B., Li, C., Reichert, M., Nguyen, J., Singh, T., Yang, C., Pannikar, A., Doliba, N., Zhang, T., et al. (2014). Pdx1 maintains β cell identity and function by

repressing an α cell program. *Cell Metab.* **19**, 259–71.
González, A. and Hall, M. N. (2017). Nutrient sensing and TOR signaling in yeast and mammals. *EMBO* **15**, 397–408.
Gosmain, Y., Katz, L. S., Masson, M. H., Cheyssac, C., Poisson, C. and Philippe, J. (2013). Pax6 Is Crucial for β-Cell Function, Insulin Biosynthesis, and Glucose-Induced Insulin Secretion. *http://dx.doi.org/10.1210/me.2011-1256*.
Gouzi, M., Kim, Y. H., Katsumoto, K., Johansson, K. and Grapin-Botton, A. (2011). Neurogenin3 initiates stepwise delamination of differentiating endocrine cells during pancreas development. *Dev. Dyn.* **240**, 589–604.
Granot, Z., Swisa, A., Magenheim, J., Stolovich-Rain, M., Fujimoto, W., Manduchi, E., Miki, T., Lennerz, J. K., Stoeckert, C. J., Meyuhas, O., et al. (2009). LKB1 Regulates Pancreatic β Cell Size, Polarity, and Function. *Cell Metab.* **10**, 296–308.
Greiner, T. U., Kesavan, G., Ståhlberg, A. and Semb, H. (2009). Rac1 regulates pancreatic islet morphogenesis. *BMC Dev. Biol.* **9**, 2.
Gu, Y., Lindner, J., Kumar, A., Yuan, W. and Magnuson, M. A. (2011). Rictor/mTORC2 is essential for maintaining a balance between beta-cell proliferation and cell size. *Diabetes* **60**, 827–37.
Hang, Y., Yamamoto, T., Benninger, R. K. P., Brissova, M., Guo, M., Bush, W., Piston, D. W., Powers, A. C., Magnuson, M., Thurmond, D. C., et al. (2014). The MafA transcription factor becomes essential to islet β-cells soon after birth. *Diabetes* **63**, 1994–2005.
Hart, A. W., Mella, S., Mendrychowski, J., van Heyningen, V. and Kleinjan, D. A. (2013). The developmental regulator Pax6 is essential for maintenance of islet cell function in the adult mouse pancreas. *PLoS One* **8**, e54173.
Haschke, F. (2016). Nutritive and Bioactive Proteins in Breast Milk. *Ann Nutr Metab* **69**, 17–26.
Heijboer, A. C., Pijl, H., van den Hoek, A. M., Havekes, L. M., Romijn, J. A. and Corssmit, E. P. M. (2006). Gut-brain axis: Regulation of glucose metabolism. *J. Neuroendocrinol.*
Jonatan, D., Spence, J. R., Method, A. M., Kofron, M., Sinagoga, K., Haataja, L., Arvan, P., Deutsch, G. H. and Wells, J. M. (2014). Sox17 regulates insulin secretion in the normal and pathologic mouse β cell. *PLoS One* **9**, e104675.
Katsuta, H., Aguayo-Mazzucato, C., Katsuta, R., Akashi, T., Hollister-Lock, J., Sharma, A. J., Bonner-Weir, S. and Weir, G. C. (2012). Subpopulations of GFP-Marked Mouse Pancreatic β-Cells Differ in Size, Granularity, and Insulin Secretion. *Endocrinology* **153**, 5180–5187.
Mastracci, T. L. and Sussel, L. (2012). The endocrine pancreas: insights into development, differentiation, and diabetes. *Wiley Interdiscip. Rev. Dev. Biol.* **1**, 609–628.
Millward, D. J. (2012). Knowledge Gained from Studies of Leucine Consumption in Animals and Humans 1–3. *J. Nutr* **142**, 2212–2219.
Mori, H. and Guan, K.-L. (2012). Tissue-Specific Ablation of Tsc1 in Pancreatic Beta-Cells.pp. 407–419.
Nishimura, W., Kondo, T., Salameh, T., El Khattabi, I., Dodge, R., Bonner-Weir, S. and Sharma, A. (2006). A switch from MafB to MafA expression accompanies differentiation to pancreatic beta-cells. *Dev. Biol.* **293**, 526–39.
Okada, T., Liew, C. W., Hu, J., Hinault, C., Michael, M. D., Krtzfeldt, J., Yin, C., Holzenberger, M., Stoffel, M. and Kulkarni, R. N. (2007). Insulin receptors in beta-cells are critical for islet compensatory growth response to insulin resistance.

Proc. Natl. Acad. Sci. U. S. A. **104**, 8977–82.
Pan, F. C. and Wright, C. (2011). Pancreas organogenesis: From bud to plexus to gland. *Dev. Dyn.*
Prado, C. L., Pugh-Bernard, A. E., Elghazi, L., Sosa-Pineda, B. and Sussel, L. (2004). Ghrelin cells replace insulin-producing beta cells in two mouse models of pancreas development. *Proc. Natl. Acad. Sci. U. S. A.* **101**, 2924–9.
Rukstalis, J. M. and Habener, J. F. (2007). Snail2, a mediator of epithelial-mesenchymal transitions, expressed in progenitor cells of the developing endocrine pancreas. *Gene Expr. Patterns* **7**, 471–9.
Sander, M., Neubuser, A., Kalamaras, J., Ee, H. C., Martin, G. R. and German, M. S. (1997). Genetic analysis reveals that PAX6 is required for normal transcription of pancreatic hormone genes and islet development. *Genes Dev.* **11**, 1662–1673.
Schindler, C. E., Partap, U., Patchen, B. K. and Swoap, S. J. (2014). Chronic rapamycin treatment causes diabetes in male mice. *Am. J. Physiol. Regul. Integr. Comp. Physiol.* **307**, R434-43.
Senniappan, S., Alexandrescu, S., Tatevian, N., Shah, P., Arya, V., Flanagan, S., Ellard, S., Rampling, D., Ashworth, M., Brown, R. E., et al. (2014). Sirolimus Therapy in Infants with Severe Hyperinsulinemic Hypoglycemia. *N. Engl. J. Med.* **370**, 1131–1137.
Spence, J. R., Lange, A. W., Lin, S.-C. J., Kaestner, K. H., Lowy, A. M., Kim, I., Whitsett, J. A. and Wells, J. M. (2009). Sox17 regulates organ lineage segregation of ventral foregut progenitor cells. *Dev. Cell* **17**, 62–74.
Stolovich-Rain, M., Enk, J., Vikesa, J., Nielsen, F. C., Saada, A., Glaser, B. and Dor, Y. (2015). Weaning Triggers a Maturation Step of Pancreatic β Cells. *Dev. Cell* **32**, 535–545.
Taylor, B. L., Benthuysen, J. and Sander, M. (2015). Postnatal β-cell proliferation and mass expansion is dependent on the transcription factor Nkx6.1. *Diabetes* **64**, 897–903.
Thorens, B. (2015). GLUT2, glucose sensing and glucose homeostasis. *Diabetologia* **58**, 221–32.
Thorrez, L., Laudadio, I., Van Deun, K., Quintens, R., Hendrickx, N., Granvik, M., Lemaire, K., Schraenen, A., Van Lommel, L., Lehnert, S., et al. (2011). Tissue-specific disallowance of housekeeping genes: the other face of cell differentiation. *Genome Res.* **21**, 95–105.
van der Meulen, T., Donaldson, C. J., Cáceres, E., Hunter, A. E., Cowing-Zitron, C., Pound, L. D., Adams, M. W., Zembrzycki, A., Grove, K. L. and Huising, M. O. (2015). Urocortin3 mediates somatostatin-dependent negative feedback control of insulin secretion. *Nat. Med.* **21**, 769–76.
Wang, J., Yang, X. and Zhang, J. (2016). Bridges between mitochondrial oxidative stress, ER stress and mTOR signaling in pancreatic β cells. *Cell. Signal.* **28**, 1099–1104.
Wijesekara, N., Dai, F. F., Hardy, A. B., Giglou, P. R., Bhattacharjee, A., Koshkin, V., Chimienti, F., Gaisano, H. Y., Rutter, G. A. and Wheeler, M. B. (2010). Beta cell-specific Znt8 deletion in mice causes marked defects in insulin processing, crystallisation and secretion. *Diabetologia* **53**, 1656–1668.
Wilcox, C. L., Terry, N. A., Walp, E. R., Lee, R. A. and May, C. L. (2013). Pancreatic α-cell specific deletion of mouse Arx leads to α-cell identity loss. *PLoS One* **8**, e66214.
Yang, B., Treweek, J. B., Kulkarni, R. P., Deverman, B. E., Chen, C.-K., Lubeck, E., Shah, S., Cai, L. and Gradinaru, V. (2014). Single-cell phenotyping within

transparent intact tissue through whole-body clearing. *Cell* **158**, 945–58.
Zhang, H., Malo, C., Boyle, C. R. and Buddington, R. K. (1998). Diet influences development of the pig (Sus scrofa) intestine during the first 6 hours after birth. *J. Nutr.* **128**, 1302–10.

Figures

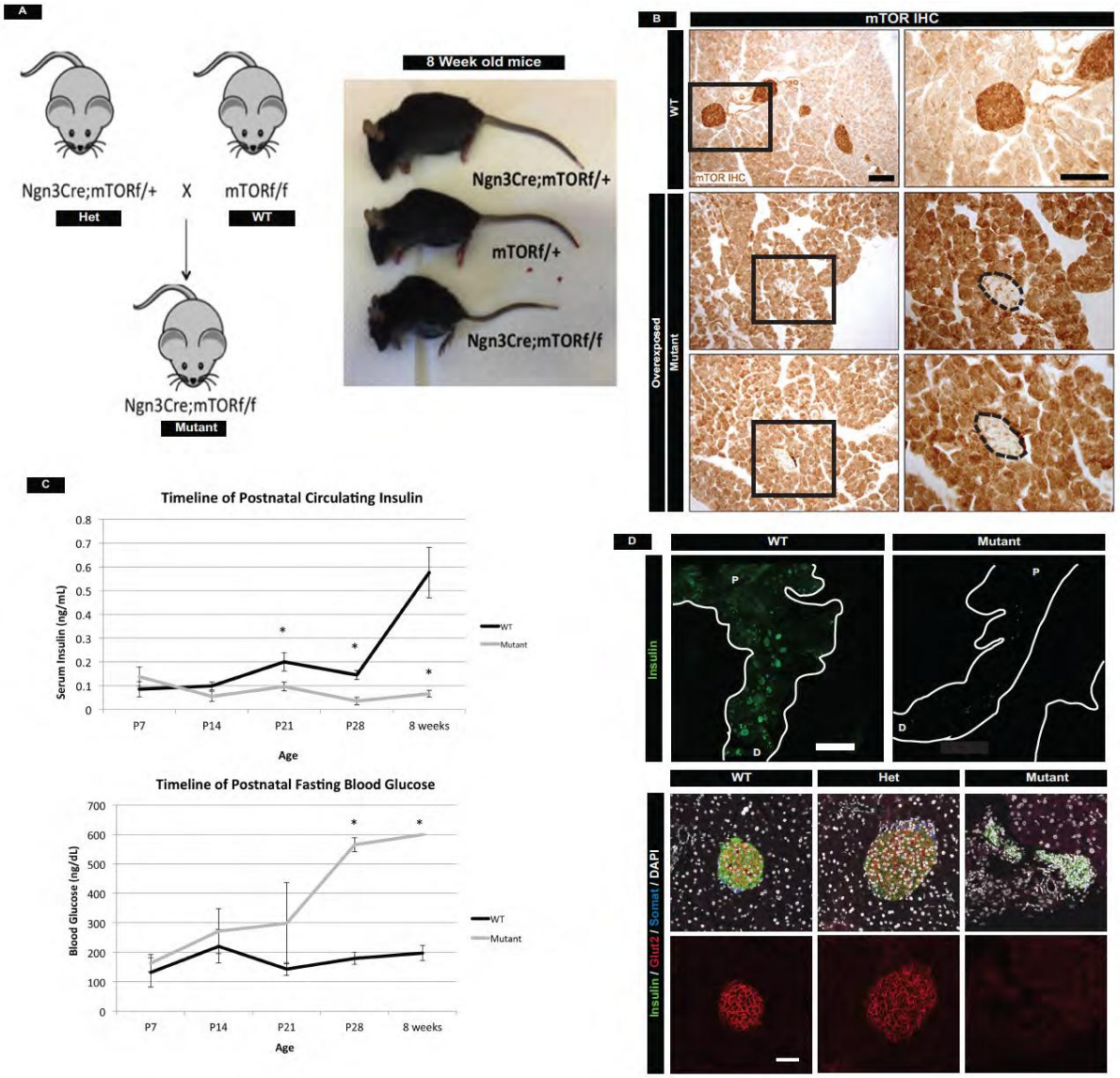

Figure 1. Deletion of mTOR in the endocrine pancreas leads to loss of islet cell mass and hyperglycemia in adult mice.
(A) Schematic of breeding *Neurog3^{Cre};mTOR$^{f/f}$* (mutant) mice. Heterozygous mice were bred to mTOR f/f mice to obtain mutants. At 8 weeks of age, mutant mice are significantly smaller than their wildtype littermates. Both male and female mutants perish just after 8 weeks of age**. (B)** mTOR protein in WT and mutant islets. mTOR is efficiently deleted from islets of mutant mice as compared to WT control mice. Bottom panels are overexposed immunohistochemistry to highlight deletion of mTOR in islets**.** Scale bars, 100 μm. **(C)** Timeline of fasting blood glucose and fasted circulating insulin levels in wildtype and mTOR mutants. Increased glucose levels and reduced insulin are

first detected at P14, worsen at P21, and all mutants are unable to regulate fasted glucose levels at 28 days of life. Values in graphs represent mean ± S.E.M; * $P < 0.05$. **(D) Top:** Whole mount immunofluorescence staining of insulin in the adult pancreas show reduction in the number of islets in mutant mice. P, proximal. D, distal. Scale bar, 1500 μm **Bottom:** Analysis of insulin, somatostatin and Glut2 protein in adult islets. Mutant islets are morphologically distorted and have no detectable Glut2 protein. Scale bar, 50 μm. See also Figures S1,S2, Videos S1,S2, and Table S3 for numbers of animals used.

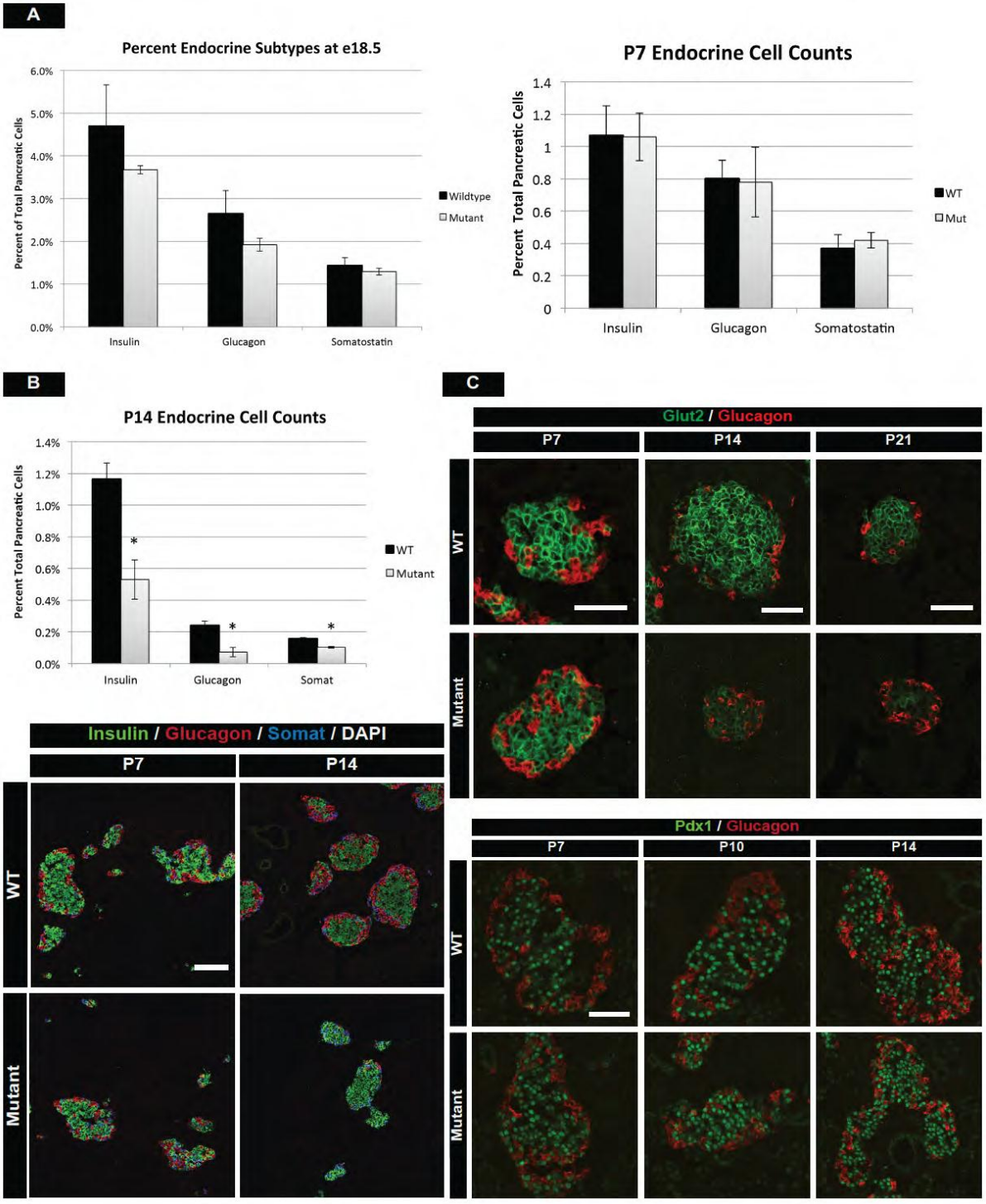

Figure 2. mTOR is required after birth for islet development
(A) Quantifying the percent of β, α, and δ cell populations at e18.5 **(left)** and P7 **(right)** in mTOR mutants. No significant change in islet mass is observed at these stages. **(B) Top:** However, flow cytometry at P14 reveals reduced cell counts for all mutant islet subtypes, as compared to wildtype littermates**. Bottom:** P7 and P14 hormone immunofluorescence of wildtype and mTOR mutant islets. Globally, mutant islets are indistinguishable from wildtype islets at P7. One week later, mutants have noticeably fewer endocrine cells. **(C)** Immunofluorescence for Glut2 in β cells reveals normal glucose-sensing mechanisms at P7, reduced expression beginning at P14, and virtually

absent Glut2 protein at P21. Despite lower cell counts and glucose transporters, β cells retain normal Pdx1 protein levels, indicating retention of endocrine identity. Scale bar, 50 μm. Values in graphs represent mean ± S.E.M; * $P < 0.05$. See also Figures S3,S4 and Table S3 for numbers of animals used.

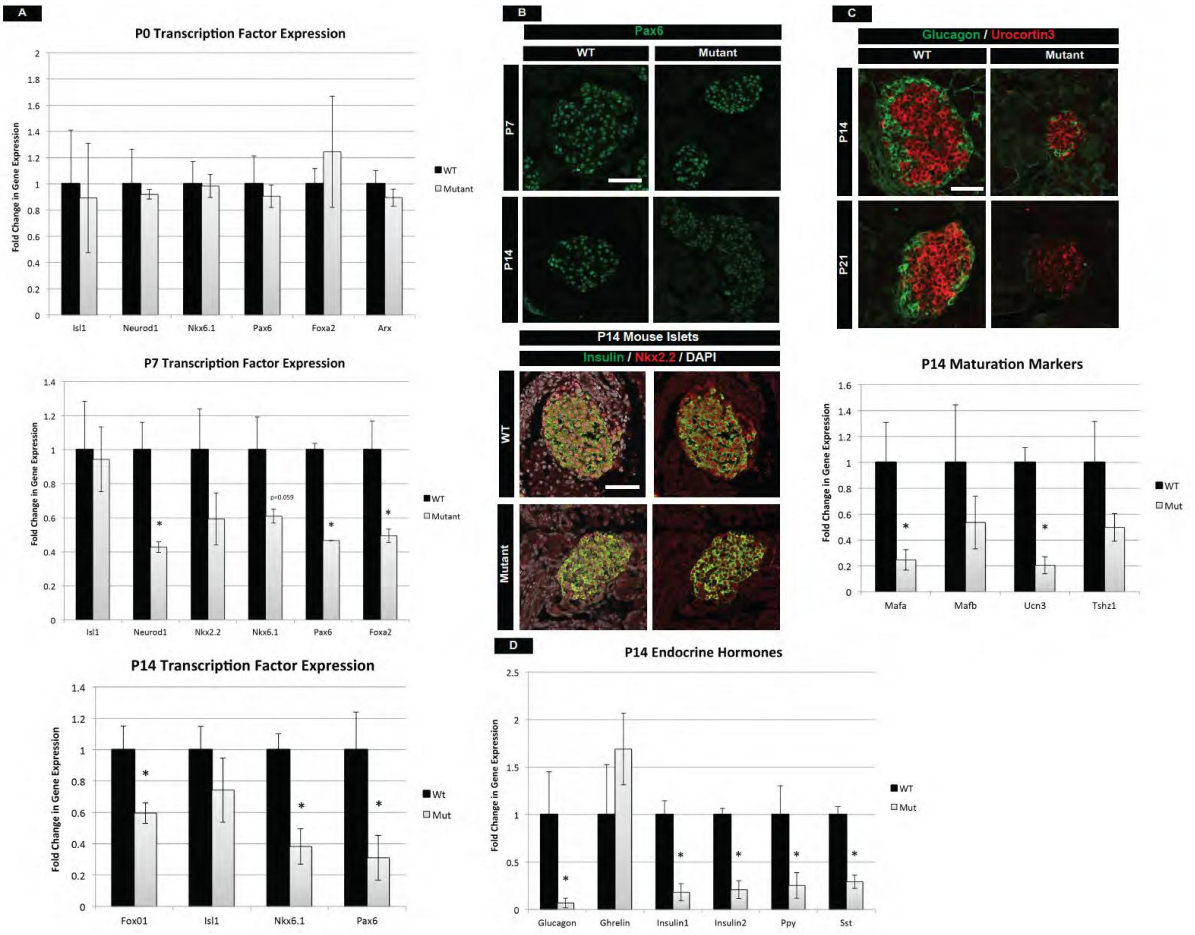

Figure 3. mTOR mutants have compromised postnatal maturation.
(A) qPCR for essential transcription factors required for growth and maturation in the postnatal islet. While no difference is seen at birth, loss of these TF's occurs in the first two weeks of life. **(B)** In conjunction, protein levels of Pax6 and Nkx2.2 are significantly reduced at P14. Scale bar, 50 μm. **(C)** Maturation markers *Ucn3* and *Mafa* are reduced in β cells at P14. Ucn3 protein continues to decrease at P21, indicative of a continued loss of maturity in mTOR mutant islets. Scale bar, 50 μm. **(D)** qPCR analysis of P14 pancreatic hormones. Decreased mRNA levels of all islet hormones is observed. A trend of increasing *Ghrelin* expression is also seen, indicative of a maturation defect. See also Figure S5. Values in graphs represent mean ± S.E.M; * $P < 0.05$. See Table S3 for numbers of animals used.

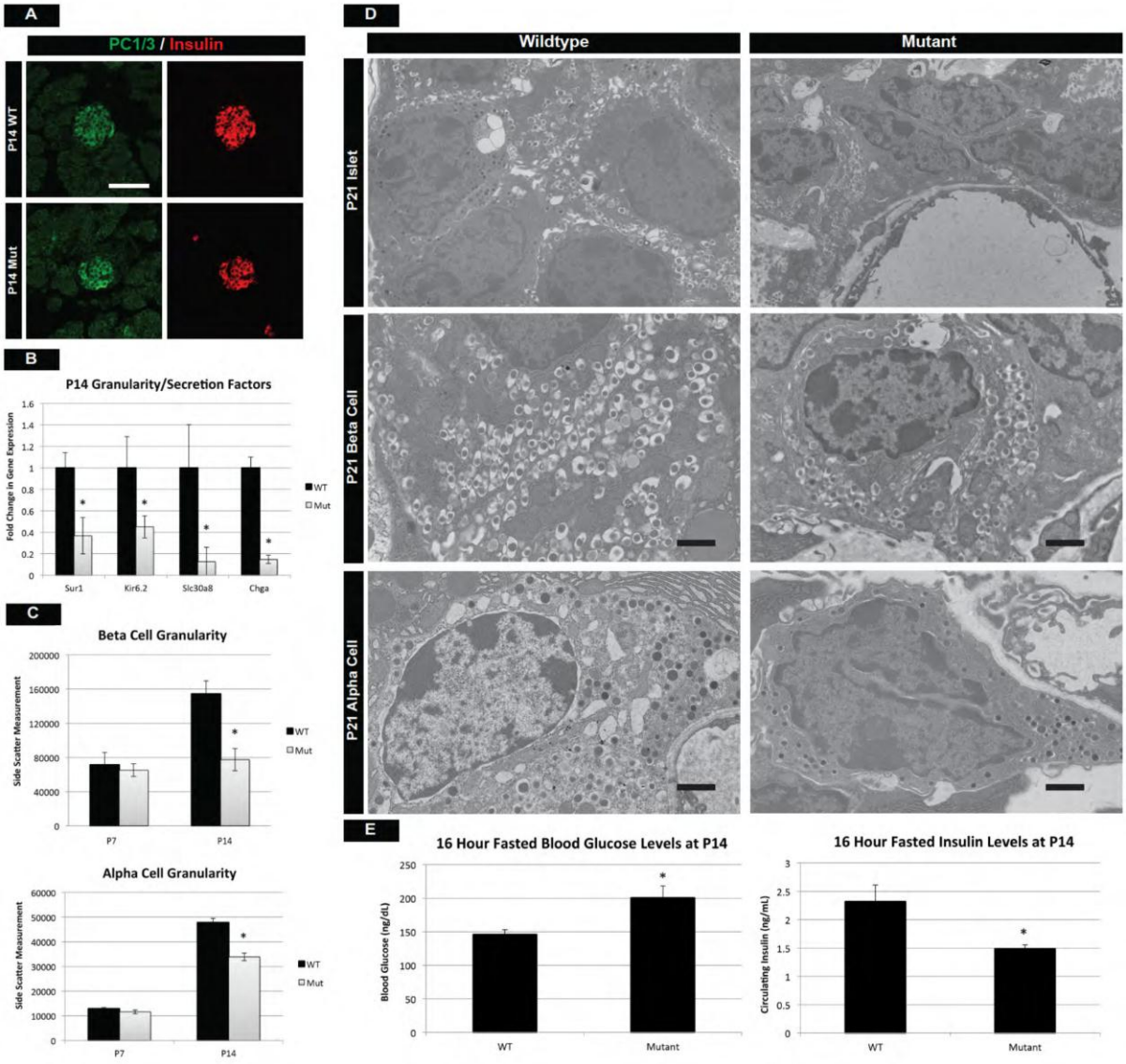

Figure 4. Mutant islet cells show reduced granularity and cellular function.
(A) Pro-hormone convertase 1/3 (PC1/3) staining reveals proper insulin-processing machinery in β cells. However, **(B)** qPCR for endocrine transporters and granularity show significant reduction in mRNA for zinc transporter *Slc30a8*, which is involved in β cell granule formation. This is also reflected in the decreased transcription of chromograninA (*Chga*), a marker of intracellular vesicles. In addition, components making up a K^+ transporter necessary for insulin release are also down-regulated. **(C)** Assessment of α and β cell granularity by average side-scatter measurements reveals normal granule formation at P7, but attenuated granularity at P14. **(D)** EM at P21 confirms that mutant β and α cells have decreased number of insulin and glucagon granules, respectively. Scale bar, 1 μm. **(E)** These defects culminate in the inability of mutant β cells to respond to fasting glucose requirements at P14. See also Figures S5. Values in graphs represent mean ± S.E.M; * $P < 0.05$. See Table S3 for numbers of animals used.

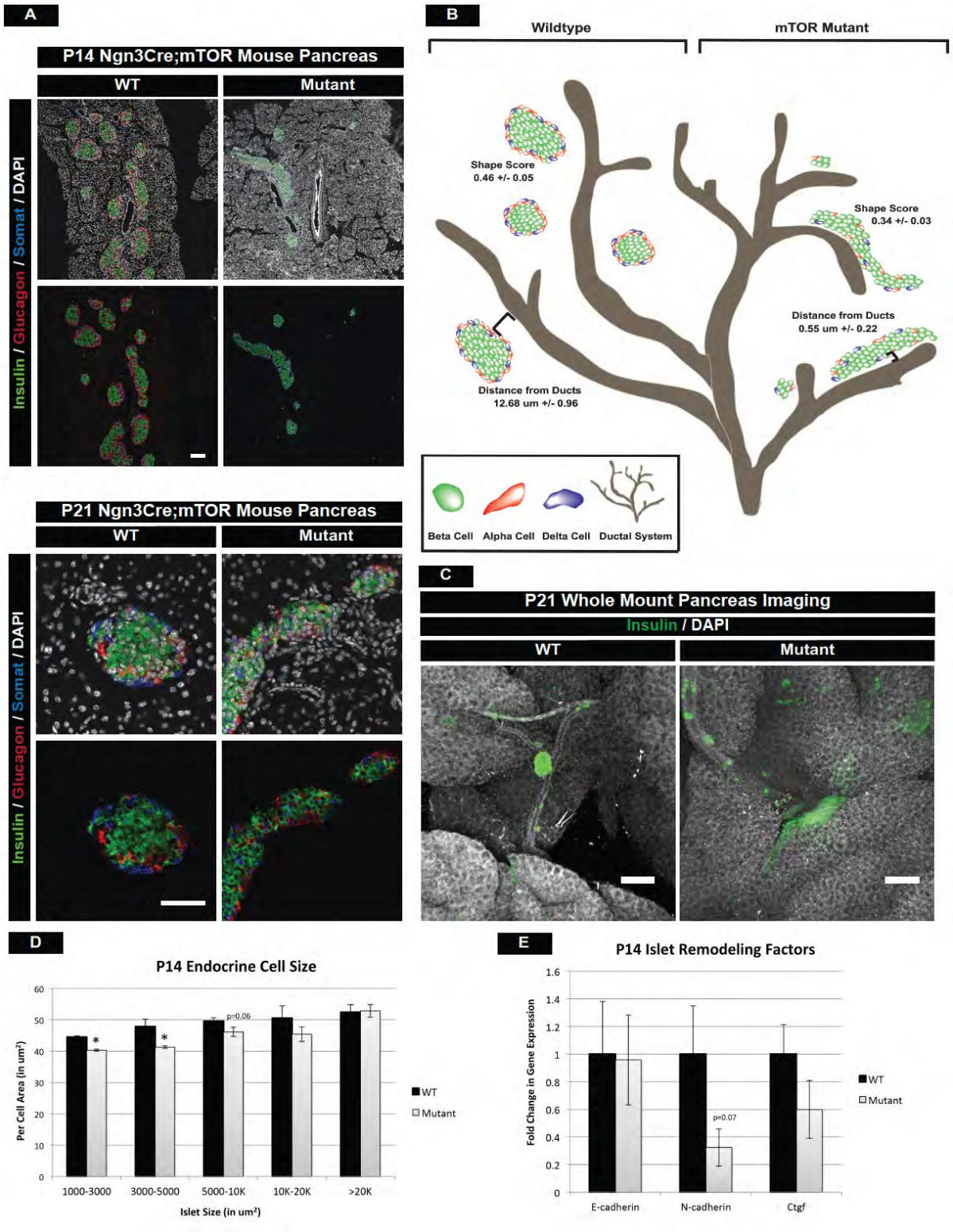

Figure 5. mTOR mutant islets display islet architecture and morphogenesis defects.

(A) P14 and P21 hormone immunofluorescence of islets, highlighting morphological defects**.** Larger mutant islets exhibit abnormally elongated architecture and both small and larger islets remain clustered close to ducts. The morphological defects did not resolve at P21 (bottom panels). Scale bars, top: 100 μm, bottom: 50 μm **(B)** Schematic of normal islet architecture in P14 wildtype animals (left) and shape score in large islets

(>5000 μm^2) compared to that of mTOR mutant islets (right). Also quantified is the distance of large islets (10-20K μm^2) from ductal structures within wildtype and mutant pancreatic tissue. Large islets remain in close proximity to the ducts in mTOR mutant animals. **(C)** Whole-mount immunofluorescence staining of P21 wildtype and mutant islets confirms persistent morphological and migration defects in mTOR mutants. Scale bars, 200 μm. **(D)** Endocrine cell size is also perturbed and correlates with islet size in mTOR mutants. **(E)** qPCR for cell-adhesion and remodeling factors in islets. While no significant difference is seen in *E-cadherin* expression, slight decreases in *N-cadherin* and *Ctgf* may contribute to islet architecture defects. Values in graphs represent mean ± S.E.M; * $P < 0.05$. See also Figure S6, Videos S3,S4, and Table S3 for numbers of animals used.

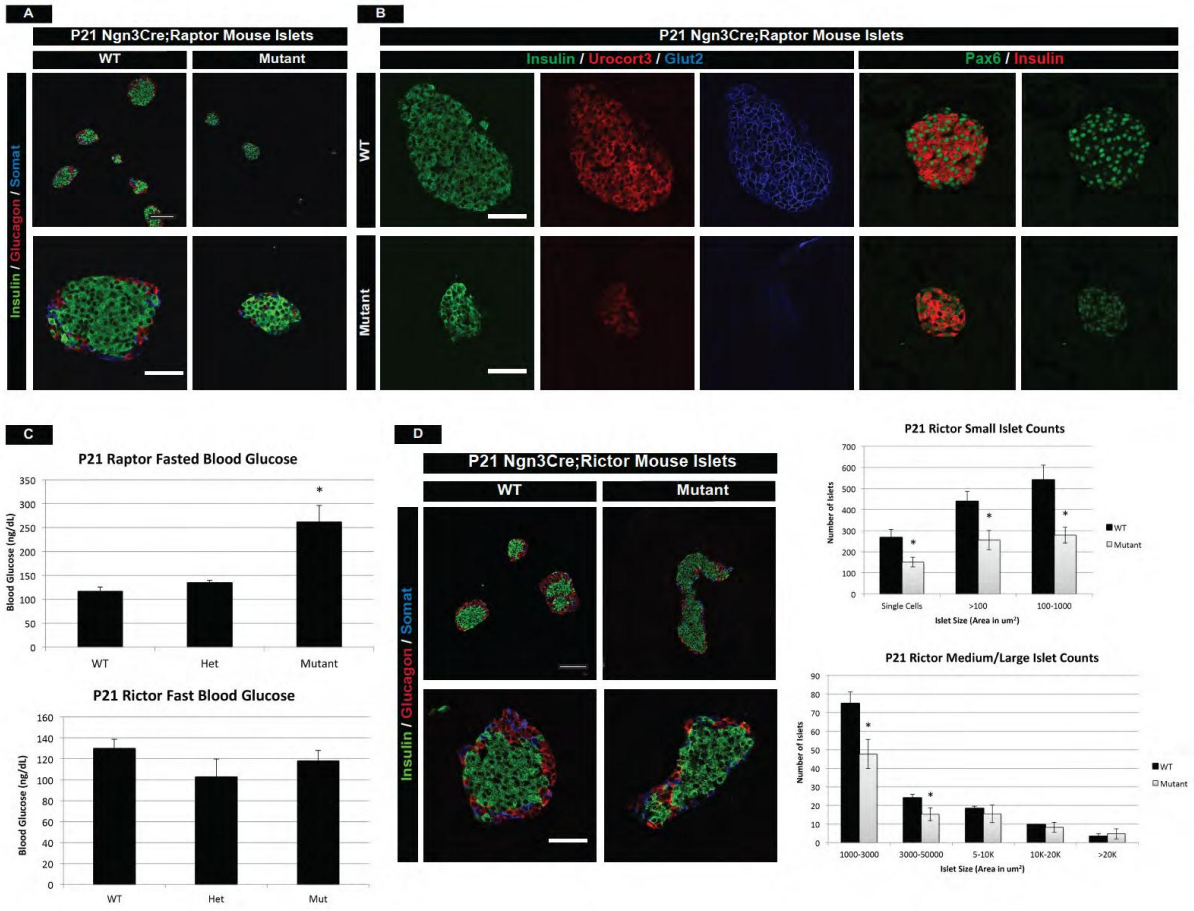

Figure 6. mTOR complexes Rictor and Raptor have distinct roles in postnatal islet development.

(A) Islet hormone immunofluorescence highlights smaller and fewer islets in Raptor mutants as compared to wildtype at P21**. (B)** Immunofluorescence for maturation and functional markers Ucn3 and Glut2 demonstrate reduced Ucn3 and virtually absent Glut2 protein in Raptor-mutant β cells. In addition, Raptor-mutant β cells have reduced Pax6 expression at P21. **(C)** Analysis of fasted blood glucose levels identifies increased blood glucose in Raptor mutant animals, yet normal levels in Rictor mutants at 3 weeks of age. **(D) Left:** Immunofluorescence for Rictor-mutant islets shows a slight morphological defect present in larger islets. **Right:** Quantification of islet number based on islet size. Lower islet counts are indicative of an islet mass defect. Scale bars, 50 μm. Values in graphs represent mean ± S.E.M; * $P < 0.05$. See also Figure S7 and Table S3 for number of animals used.

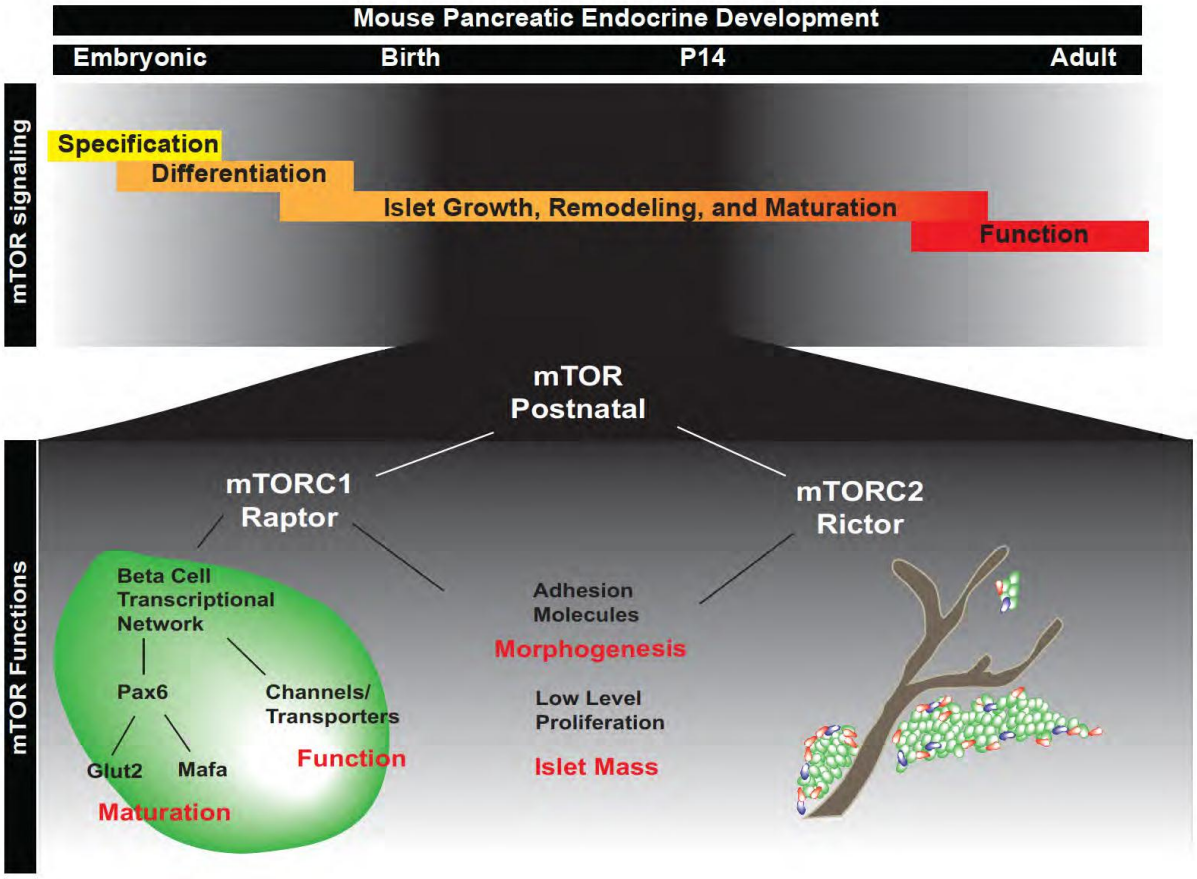

Figure 7. Model of mTOR's role in postnatal islet morphogenesis, maturation and function.

Top Panel: Stages of embryonic and postnatal development of the endocrine pancreas. mTOR signaling is essential in the first two weeks of postnatal life, the time in which endocrine cells undergo morphogenesis into islets and mature into fully functional β cells. **Bottom Panel:** During postnatal islet development, mTOR signaling is required for islet morphogenesis and β-cell maturation. Our data indicate morphogenesis is regulated by both mTORC1 (Raptor) and mTORC2 (Rictor), as a robust phenotype is only seen with deletion of both complexes. In addition, both complexes influence islet mass. However, mTORC1 is the main complex influencing postnatal islet development. C1 signaling is required specifically for maturation and function of endocrine cells within the pancreas and regulates these processes, in part, via Pax6. These signals potentiate cellular maturation and functional mechanisms within the cell.

Supplemental Figures

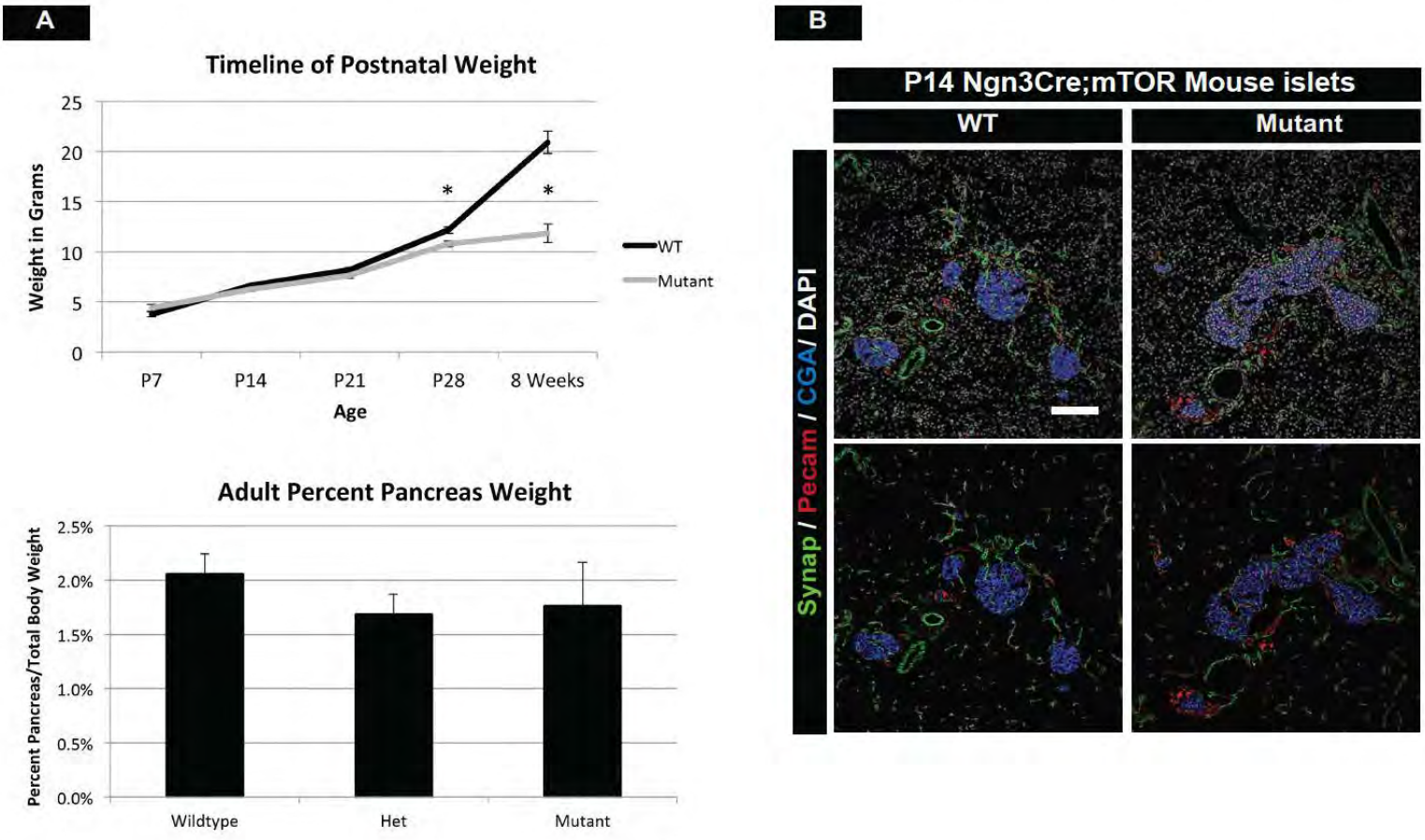

Figure S1. Related to Figure 1: Analysis of animal and total pancreas weight, vascularization and innervation of islets.
(A) Timeline of postnatal weight gain in wildtype and mTOR mutants. Only after mutants are severely diabetic is there a significant decrease in weight. Pancreas weight is still proportional to total body weight in the adult**.** Values in graphs represent mean ± S.E.M; * $P < 0.05$. **(B)** Vascularization and innervation of mTOR mutant islets is comparable to wildtype at P14. Immunostaining of vasculature (PECAM) and innervation (Synaptophysin). Scale bars, 50 μm. See Table S3 for number of animals used.

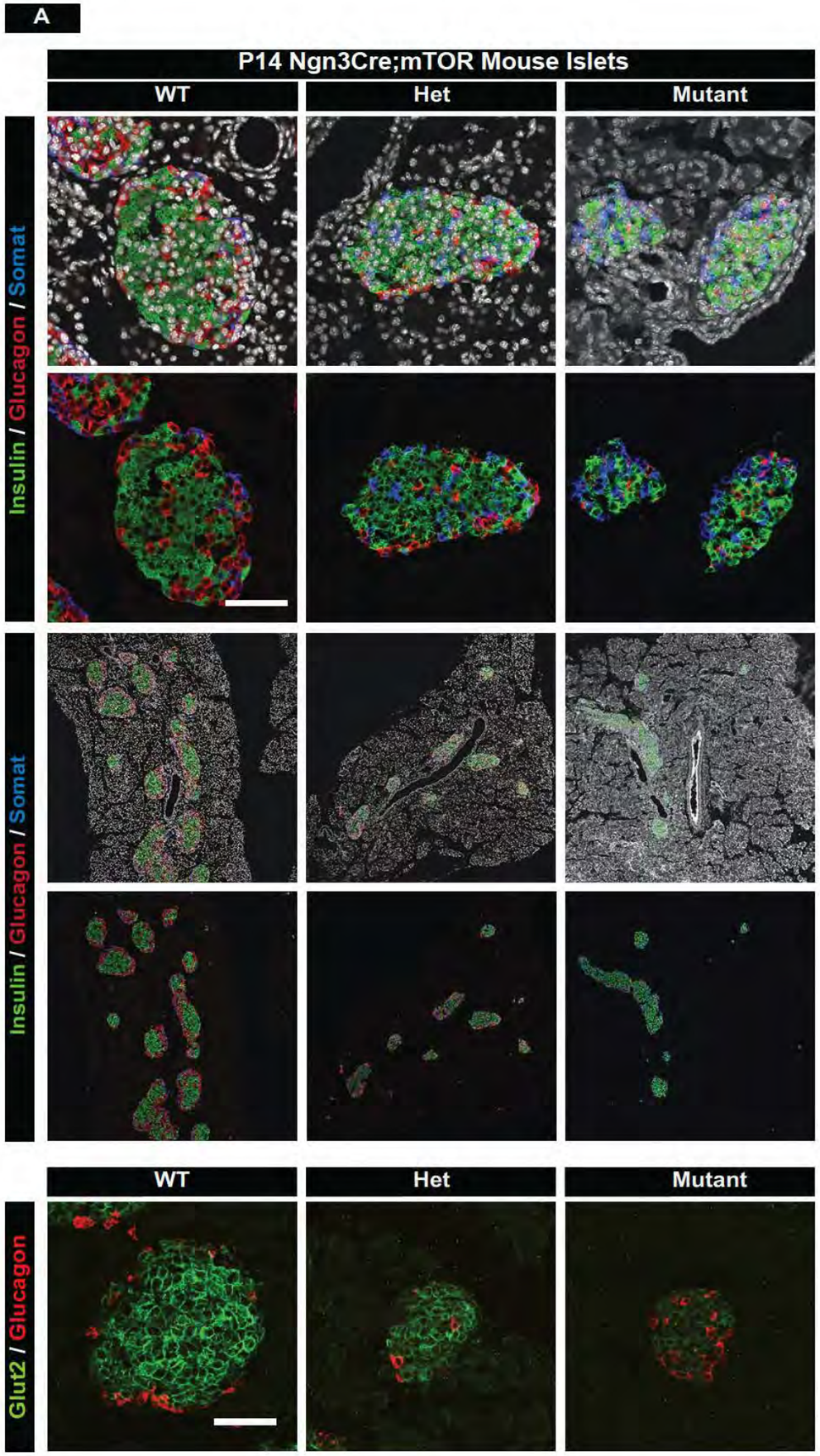

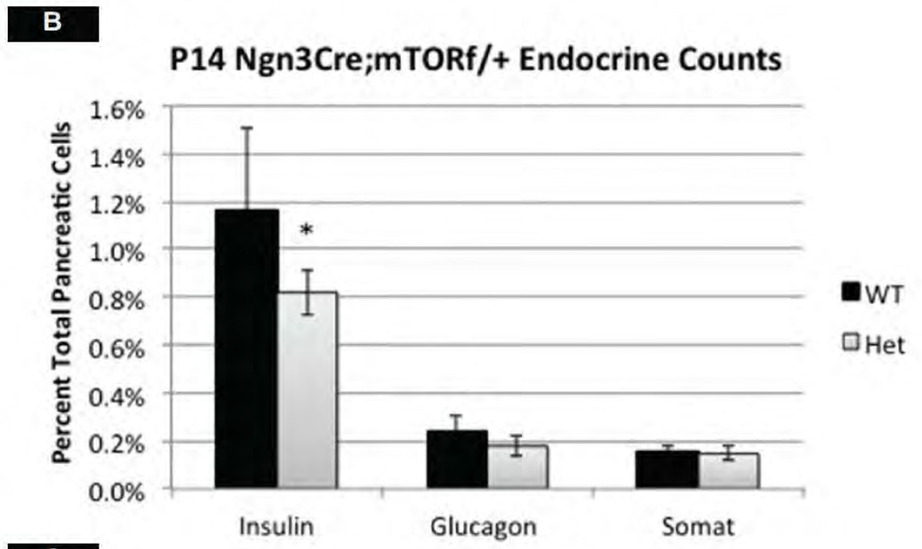

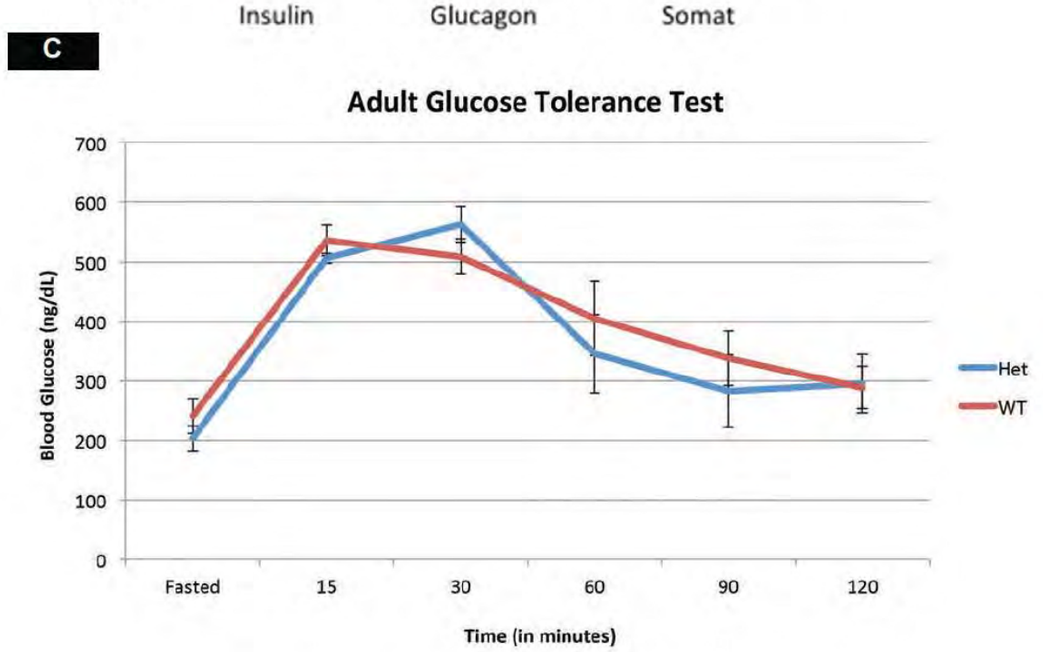

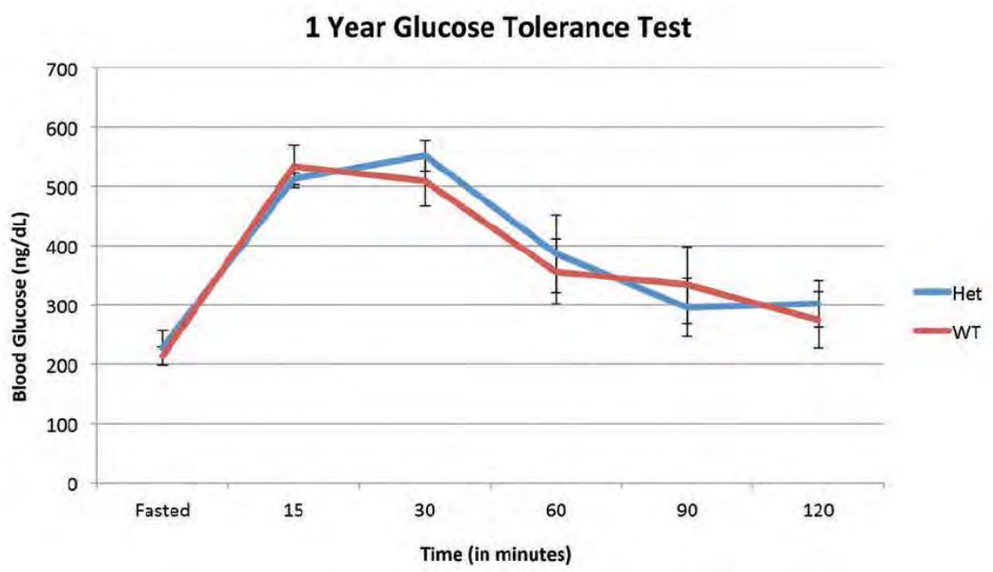

Figure S2. Related to Figure 1: mTOR heterozygous mice display altered β-cell mass, but do not exhibit a functional phenotype.
(A) Immunofluorescence of wildtype, heterozygous, and mTOR mutant P14 islets**. (B)** Quantification of cell numbers at P14 in wildtype and heterozygous mice using flow cytometry. There is a small, but significant decrease in β cells of mTOR heterozygous islets, however this does not lead to aberrant glucose regulation at 8 weeks or one year of age. **(C)** Glucose tolerance test in wildtype and heterozygous mice. Top: 8 weeks old. Bottom: 1 year old. Scale bars, 50 μm. Values in graphs represent mean ± S.E.M; * $P < 0.05$. See Table S3 for number of animals used.

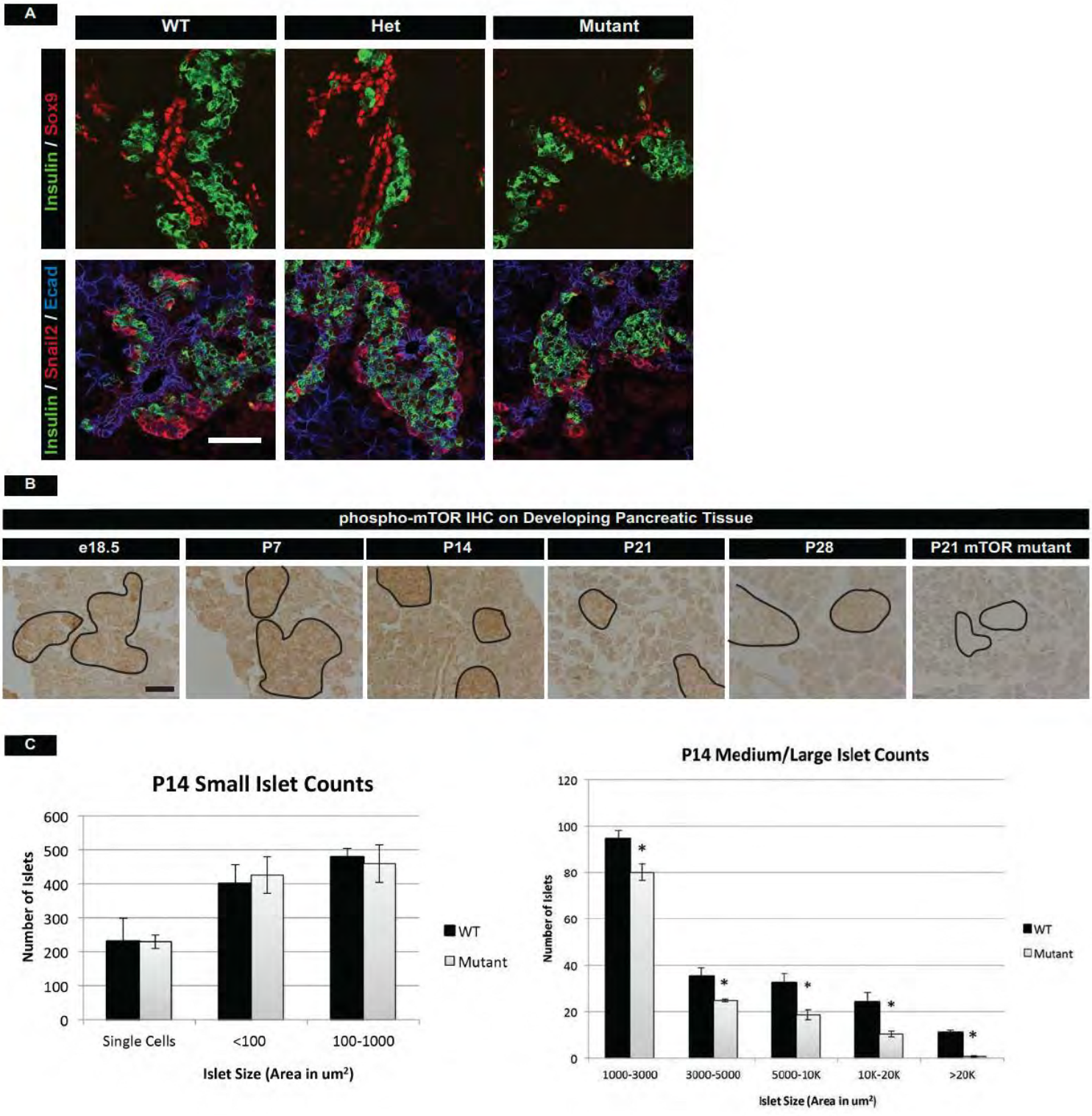

Figure S3. Related to Figure 2: mTOR is not required for embryonic islet development.
(A) Endocrine cell migration and islet morphogenesis are comparable between wildtype and mutant animals at e18.5. Insulin positive cells down-regulate E-cadherin and migrate out of the Sox9 positive duct, organizing into pre-islet clusters. Snail2 is observed at the leading edges of the migrating cells. Scale bars, 50 μm. **(B)** Active mTOR (phospho-mTOR) staining in developing pancreatic tissue from embryonic day 18.5 to postnatal day 28. High levels of active mTOR are observed in islets (outlined) in the first two weeks after birth. Scale bar, 50 μm. **(C)** Islet counts for P14 wildtype and mutant pancreatic tissue. No difference is observed in small islet counts at this stage, but medium and large islet numbers are decreased, indicative of an islet mass defect. See Table S3 for number of animals used.

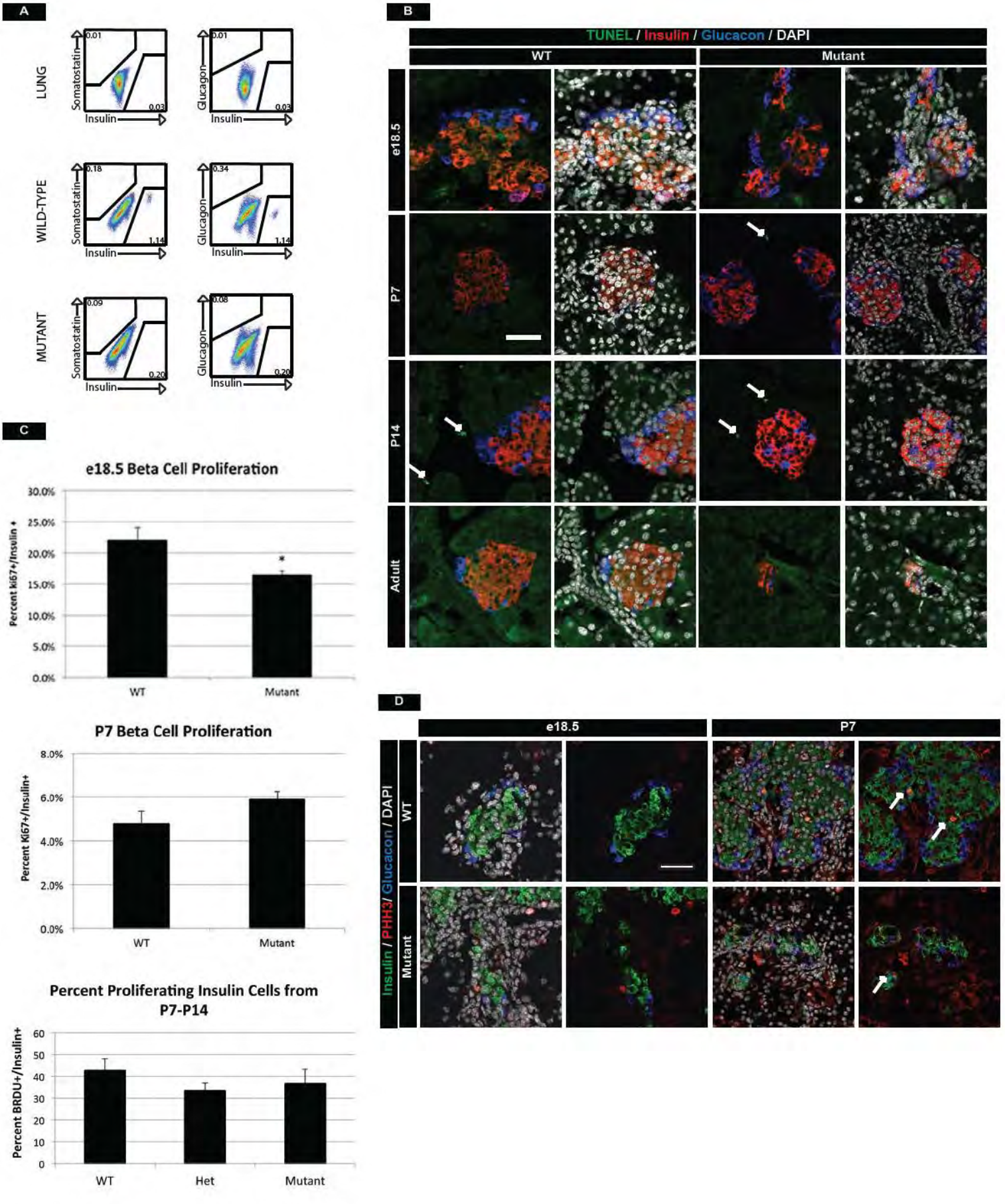

Figure S4. Related to Figure 2: Analysis of apoptosis and cell proliferation in wildtype and mTOR mutant islets during perinatal development.
(A) Representative FACS plots highlighting efficient staining of endocrine populations at P21 via flow cytometry. Isotype control: lung **(B)** Comparable levels of apoptosis in wildtype and mTOR mutant islets. Representative TUNEL stains of wildtype and mutant islets from e18.5 to adult. Arrows indicate TUNEL positive cells**.** Scale bar, 50 μm. **(C) Top:** Proliferation as assessed by Ki67 staining indicates a defect at e18.5 in mTOR mutants. **Middle:** Proliferation at P7 (Ki67) **Bottom:** At P14, islets are assessed for incorporation BRDU in β cells by flow cytometry as a measure of proliferation from 1-2 weeks of life. No statistical difference in global proliferation from 1-2 weeks of life is detected. **(D)** PHH3 stains at e18.5 and P7 is consistent with reduced proliferation in late embryonic/early postnatal life. Arrows indicate insulin/PHH3 double positive cells. Scale bar, 50 μm. **(D)** Values in graphs represent mean ± S.E.M. * $P < 0.05$. See Table S3 for number of animals used.

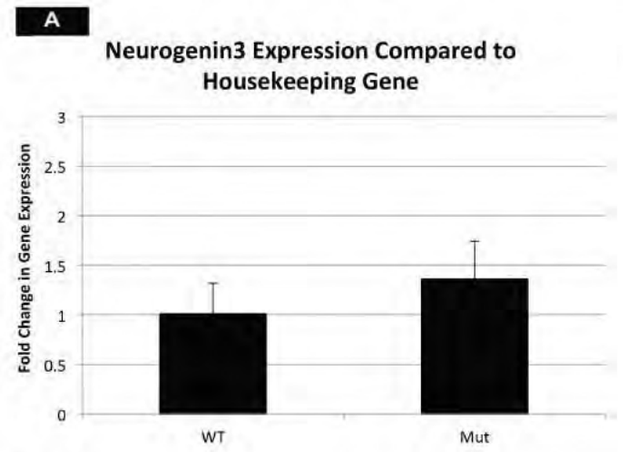

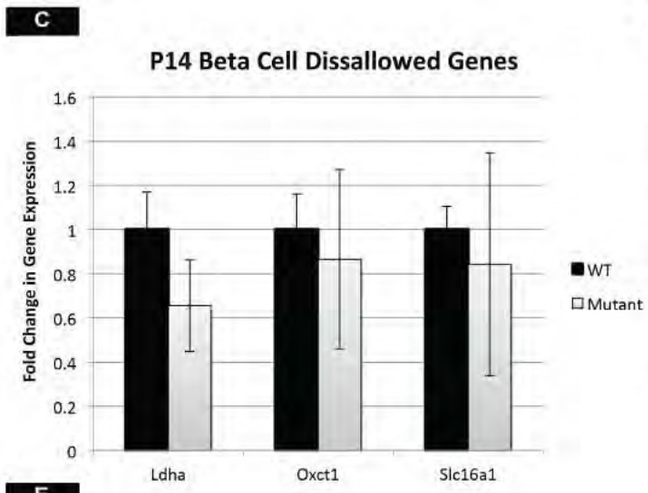

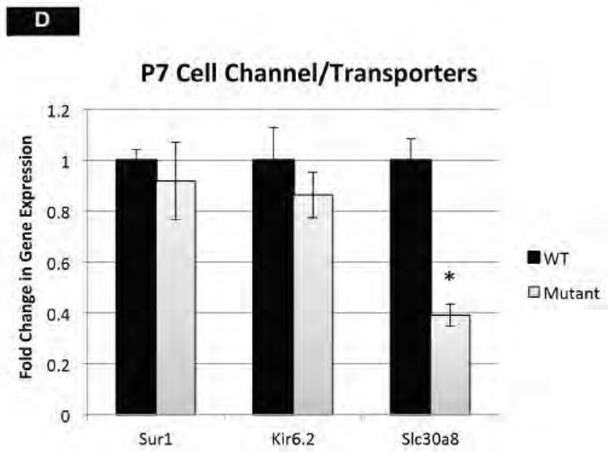

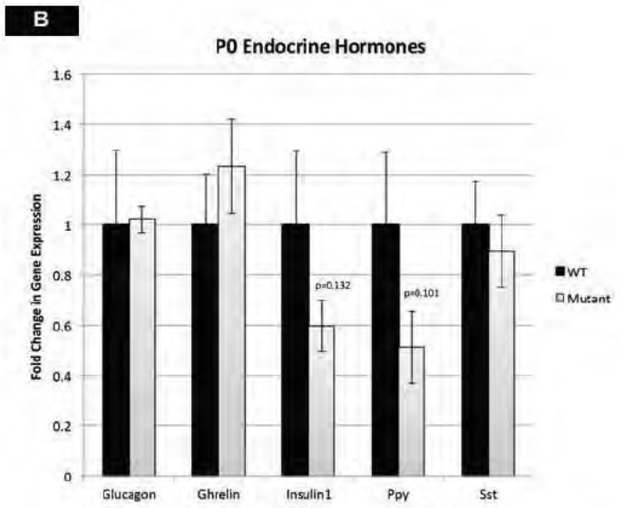

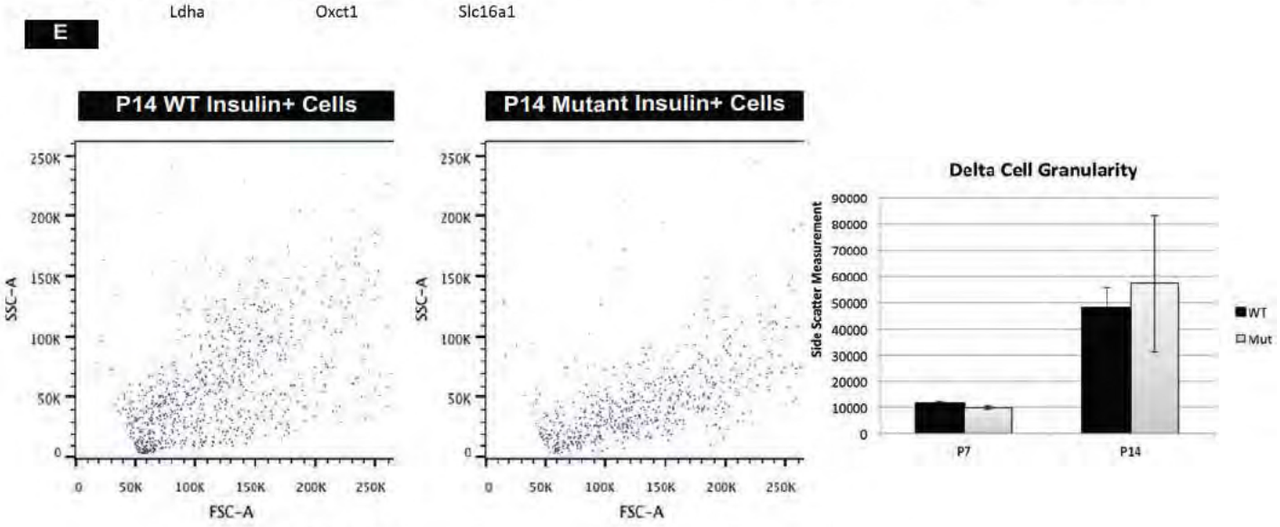

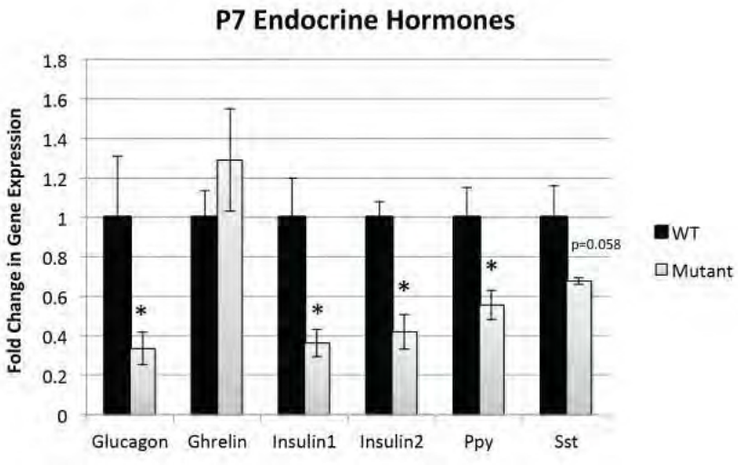

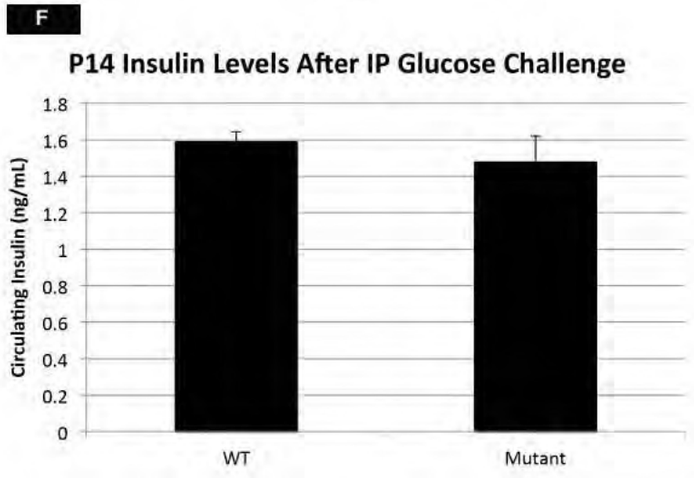

Figure S5. Related to Figures 3/4: Characterization of postnatal gene expression, granularity, and function in mTOR mutants.
(A) qPCR data are normalized to Neurogenin3, which has no change in gene expression when compared to housekeeping gene Hprt1 **(B)** qPCR for P0 and P7 endocrine hormones. While no significant difference is seen just after birth, 1-week later hormones are significantly down in mTOR mutants. **(C)** Despite a maturation defect in mTOR mutant islets at P14, by qPCR there are no increases in selectively disallowed genes. **(D)** qPCR for endocrine cell channels and transporters reveals normal levels of components of the Na/K^+ channel, but significant reductions in zinc transporter, *Slc30a8* at P7. **(E)** Representative side-scatter (SSC) plots for wildtype and mutant insulin+ cells. Note a collective decrease in SSC measurements in mutant β cells. However, this does not seem to be the case for somatostatin positive cells within mutant islets. **(F)** A glucose challenge at P14 indicates that despite maturation defects, β cells are able to secrete comparable levels of insulin in response to high levels of glucose. Values in graphs represent mean ± S.E.M. * $P < 0.05$. See Table S3 for number of animals used.

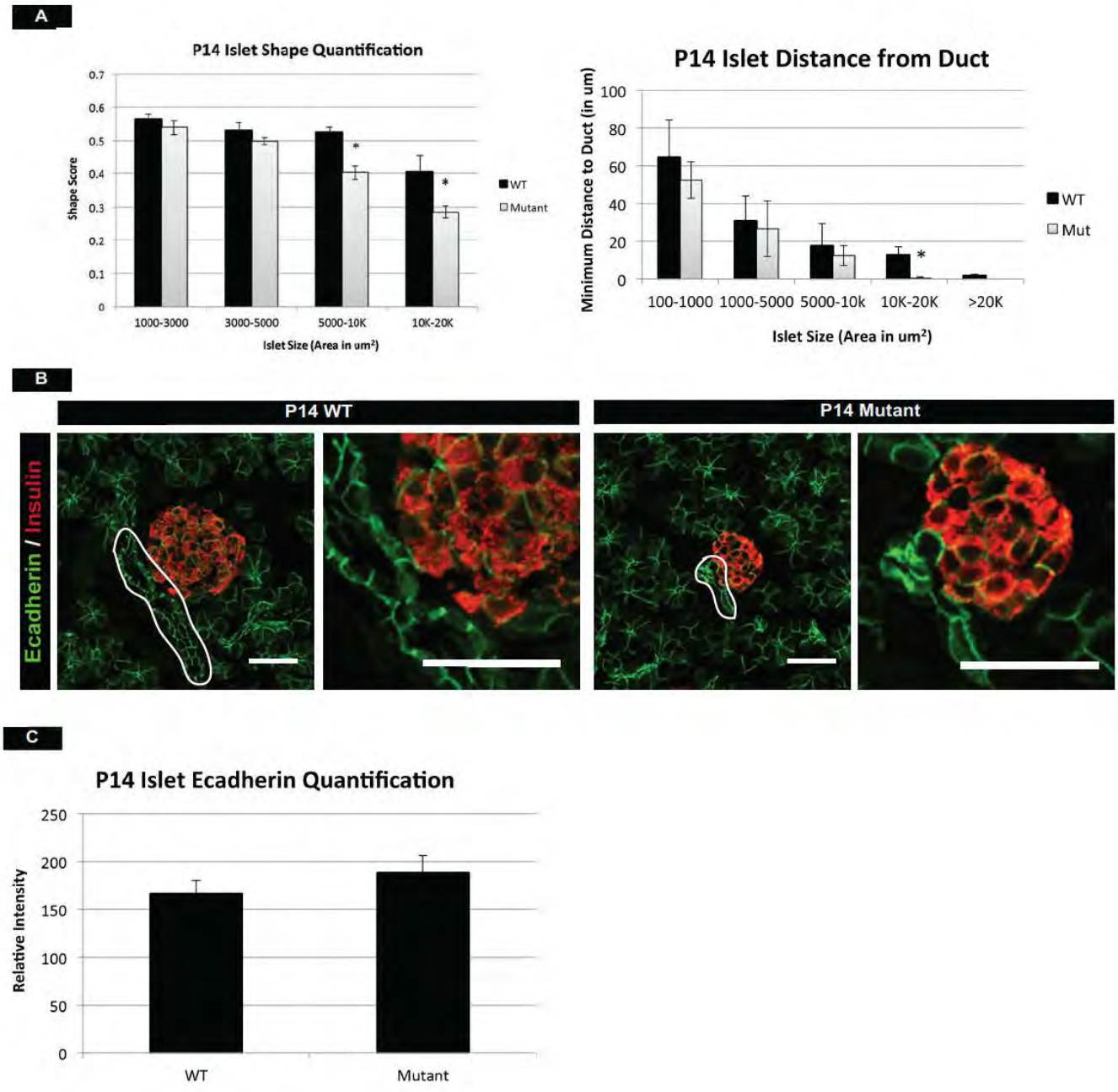

Figure S6. Related to Figure 5: Characterization of morphogenesis defects in mTOR mutants.
(A) Right: Graphical representation of islet shape quantification. Mutant islets with a larger area have lower shape scores, indicative of a morphology defect**. Left:** Quantification of islet distance from ductal structures. Islets were segregated based on size. Large islets in mTOR mutants remained in close proximity to ducts. **(B)** Increased expression of E-cadherin between islet endocrine cells and in conjunction with nearby ductal structures is observed in P14 mutant pancreatic tissue as compared to wildtype. Ducts outlined in white. **(C)** Quantification of E-cadherin immunofluorescence intensity in wildtype and mTOR mutant islets at P14. A trend of increased expression could account for morphogenesis and migration defects observed in mutant animals. Values in graphs represent mean ± S.E.M; * $P < 0.05$. See Table S3 for number of animals used.

A

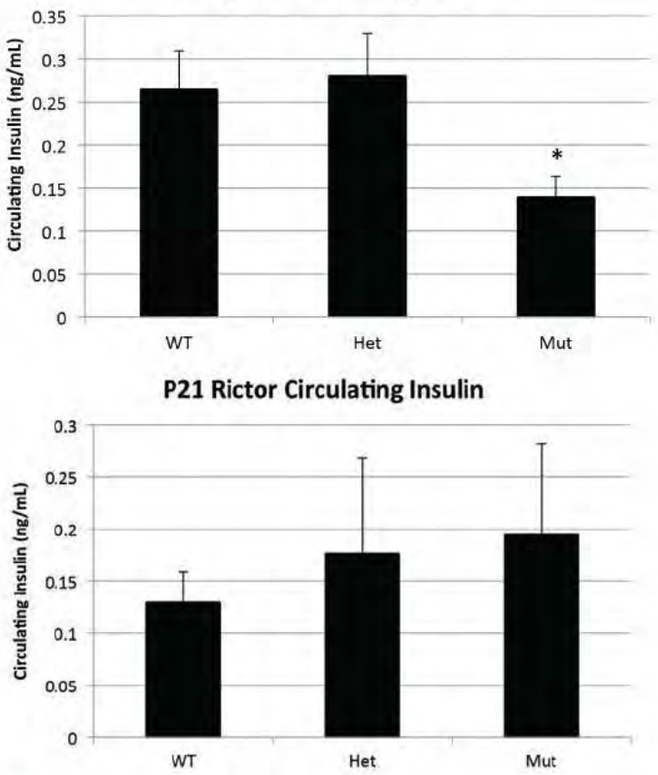
P21 Raptor Circulating Insulin
Circulating Insulin (ng/mL)
0.35
0.3
0.25
0.2
0.15
0.1
0.05
0
*
WT
Het
Mut
P21 Rictor Circulating Insulin
Circulating Insulin (ng/mL)
0.3
0.25
0.2
0.15
0.1
0.05
0
WT
Het
Mut

B

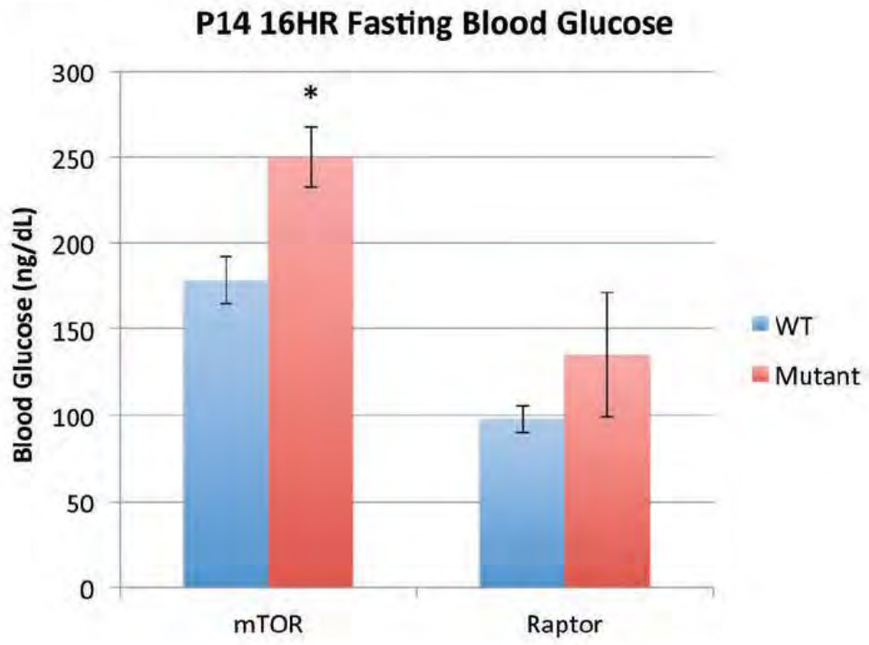
P14 16HR Fasting Blood Glucose
Blood Glucose (ng/dL)
300
250
200
150
100
50
0
*
mTOR
Raptor
WT
Mutant

C

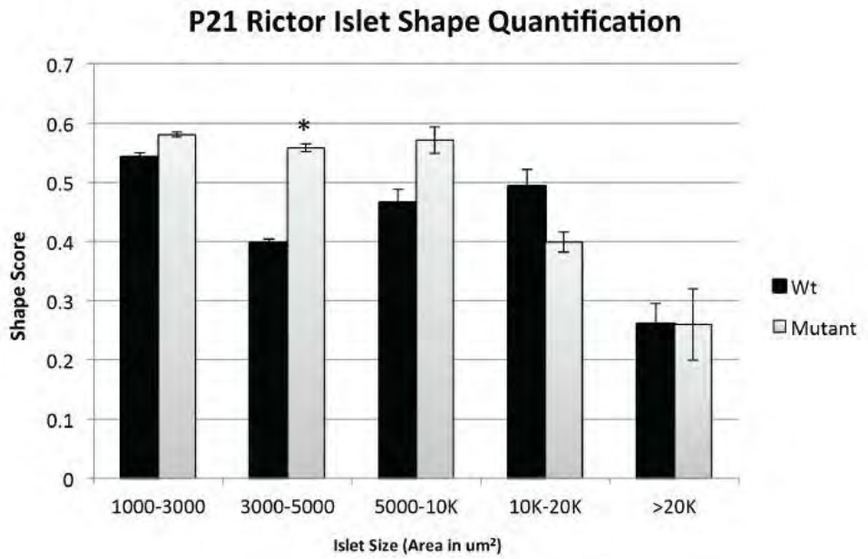
P21 Rictor Islet Shape Quantification
Shape Score
0.7
0.6
0.5
0.4
0.3
0.2
0.1
0
*
1000-3000
3000-5000
5000-10K
10K-20K
>20K
Islet Size (Area in um²)
Wt
Mutant

D

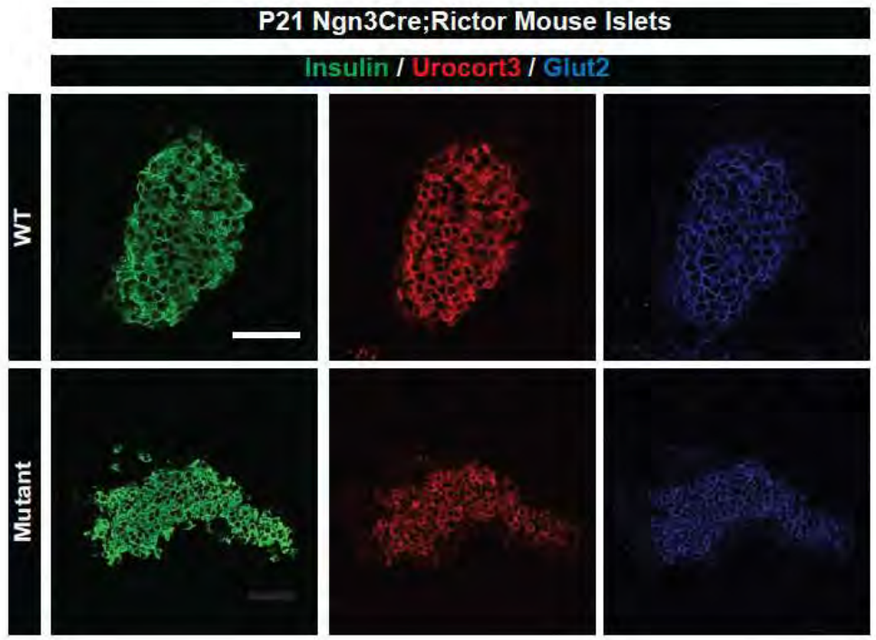
P21 Ngn3Cre;Rictor Mouse Islets
Insulin / Urocort3 / Glut2
WT
Mutant

Figure S7. Related to Figure 6: Raptor/Rictor play distinct roles in postnatal islet development.
(A) Circulating insulin levels in wildtype, heterozygous, and Raptor/Rictor mutant animals at P21. While Rictor animals maintain normal insulin levels, Raptor mutants have significantly less. **(B)** 16-hour fasting blood glucose readings for P14 mTOR and Raptor mutant mice. While a significant increase in fasting blood glucose levels is seen in mTOR mutants, Raptor mutants do not show a significant phenotype at this stage. This indicates latency in the Raptor functional phenotype. **(C)** Rictor islet-shape quantification reveals the presence, but overall fewer morphologically distorted islets compared to mTOR mutant mice. **(D)** Immunofluorescence for maturation and functional markers Ucn3 and Glut2 also show comparable levels between Rictor mutant and WT islets at P21. Islet hormone immunofluorescence at P21 highlights another abnormally shaped islet in Rictor mutants. Values in graphs represent mean ± S.E.M; * $P < 0.05$. See Table S3 for number of animals used.

Movies

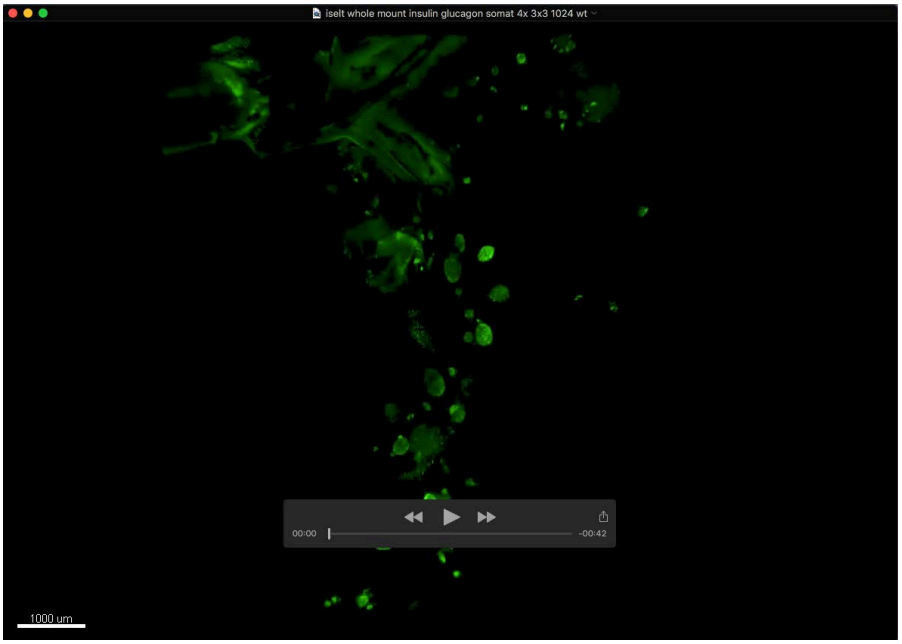

Movie S1. Adult wildtype islet whole-mount staining.
Whole mount immunofluorescence of 8-week old wildtype mice. Insulin is shown in green, highlighting many round islets within this section of the pancreas. Movie was generated using Imaris software.

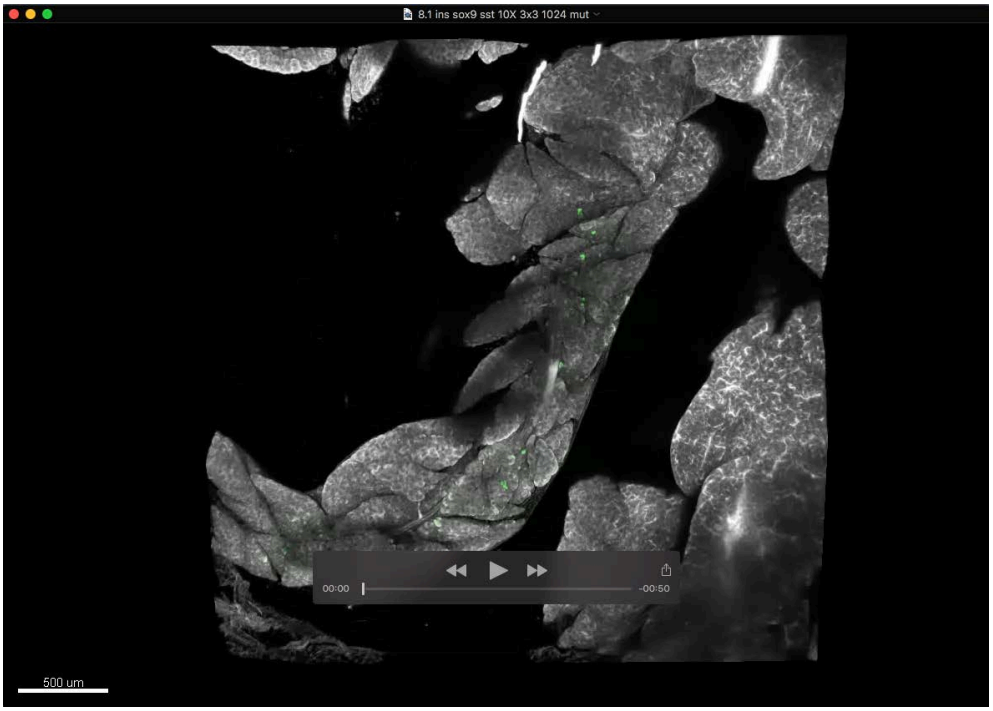

Movie S2. Adult mutant islet whole-mount staining.
Whole mount immunofluorescence of 8-week old mTOR mutant mice. Insulin is shown in green, emphasizing a loss of β cell mass in mutant animals. Movie was generated using Imaris software.

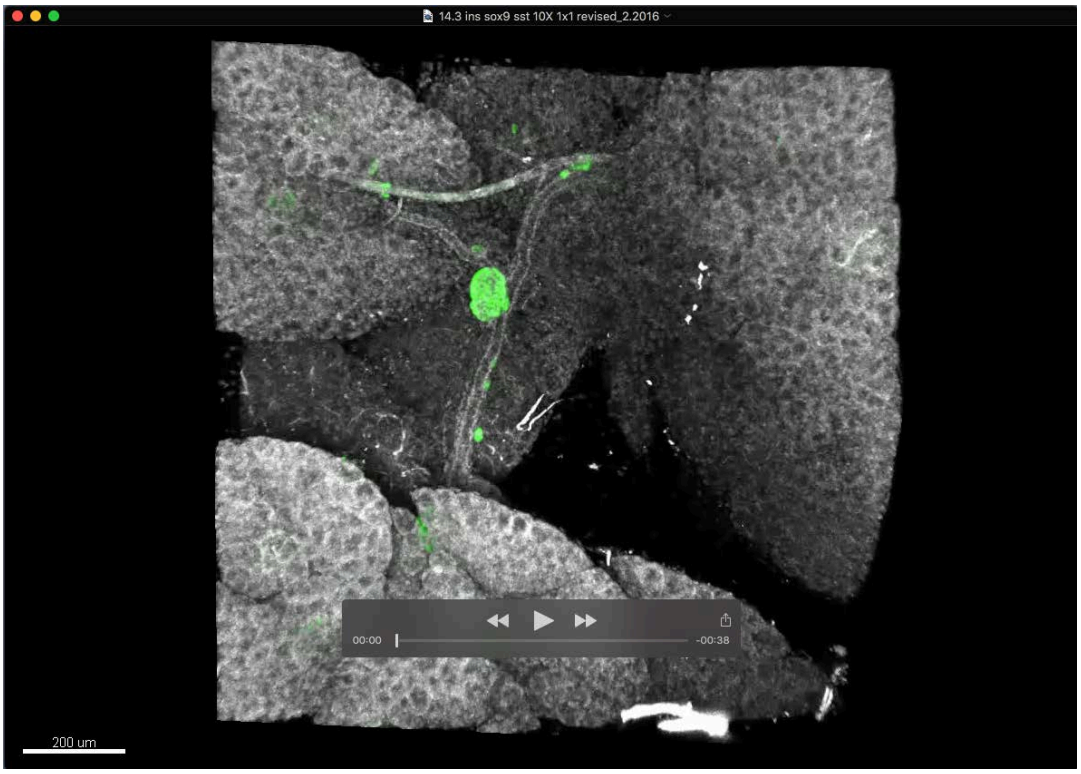

Movie S3. P21 Wildtype islet whole-mount staining.
Whole mount immunofluorescence of 3-week old wildtype mice. Insulin is shown in green to highlight a central, round islet present. Movie was generated using Imaris software.

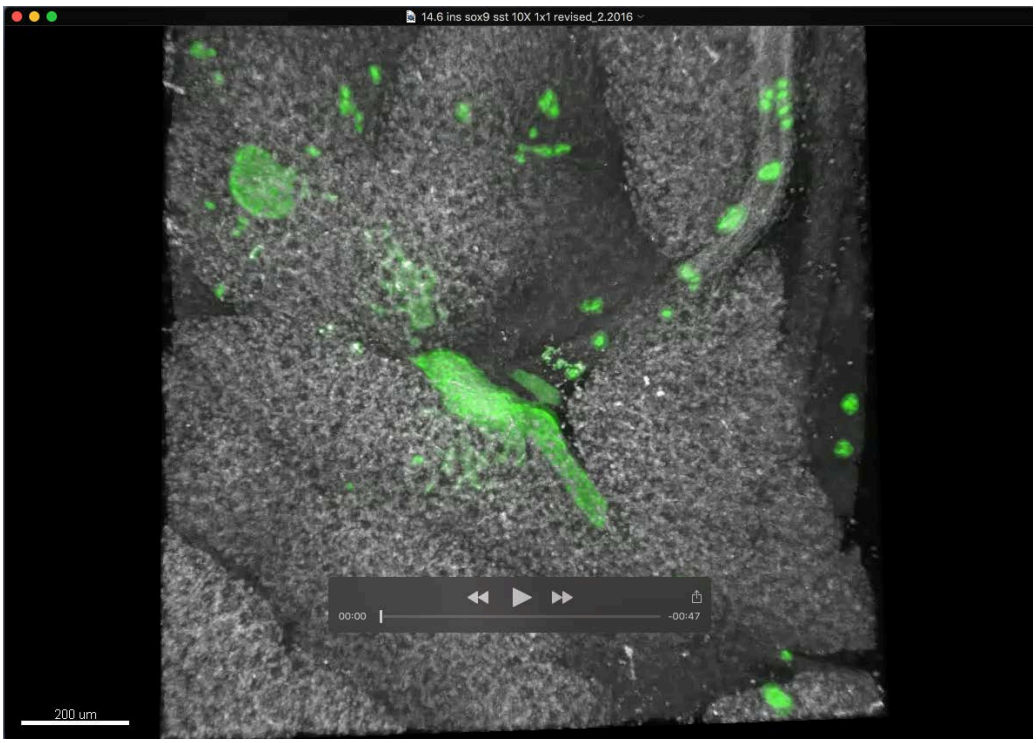

Movie S4. P21 Mutant islet whole-mount staining.
Whole mount immunofluorescence of 3-week old mTOR mutant mice. Insulin is shown in green to highlight an elongated, dysmorphic islet at the center of the movie. Also present are smaller islets, which remain close to the ductal structures in mutant mice. Movie was generated using Imaris software.

Supplemental Methods

Mice

Neurog3Cre mice (Schonhoff et al., 2004) were obtained from Jax and maintained as hemizygous on a C57/BL6 background. mTORf/f, Rictorf/f, and Raptorf/f mice were obtained from the Zheng lab and have been previously described (Gangloff et al., 2004; Sengupta et al., 2010; Shiota et al., 2006). A list of genotyping primers can be found in Table S2. Tissue and/or blood samples were collected at time points including e18.5, P0, P7, P10, P14, P21, P28, and 8 weeks of age.

Tissue Processing

Whole pancreas was isolated from mice and washed with cold 1x PBS. Tissue was fixed in 4% PFA overnight at 4° and then washed 3x with PBS. Tissue was then placed in 30% sucrose overnight at 4°.

Samples were washed briefly with 1x PBS, embedded using O.C.T Compound (Tissue-Tek), and frozen. Blocks were serial sectioned at 8 microns.

For electron microscopy analysis, isolated pancreatic tissue was processed as previously described (Jonatan et al., 2014). Tissue was imaged using a Hitachi H-7650 Transmission Electron Microscope equipped with an AMT 2k x 2k tem CCD digital camera.

Circulating Insulin and Glucose

Mice were anesthetized using Isofluorane and blood was collected using a cardiac puncture and placed in a MiniCollect KEDTA tube (Fisher Scientific) with Aprotinin (Fisher Bioreagents) and DPPIV inhibitor (Millipore). Blood was centrifuged for ten minutes at 4° and serum was collected for ELISA analysis.

Glucose Tolerance Tests

For glucose tolerance tests, mice were fasted for 16 hours prior to the experiment. Mice were weighed and fasted blood glucose was taken using a TrueTrack glucometer. 2 g/kg weight of 20% D-glucose was administered to mice and readings were taken at 15, 30, 60, 90, and 120 minutes after intraperitoneal (IP) injection.

IP glucose tolerance test was performed by fasting mice for 16 hours prior to injection. 2 g/kg of 20% D-glucose was administered at that time and mice were monitored for 30 minutes after IP injection. At that time blood serum was collected, processed, and analyzed using methods and materials indicated above.

Immunostaining and Imaging

A full list of antibodies can be found in the Table S1. Slides were rehydrated in 1x PBS and then put in blocking buffer (10% normal donkey serum + 0.5% Triton in 1x PBS) for 1 hour. Primary antibodies were diluted in blocking buffer and incubated overnight at 4°. Slides were washed 3 times in 1x PBS. Secondary antibodies were diluted in blocking buffer and applied to the slides for 1 hour at room temperature. Fluoromount-G (SouthernBiotech) was applied to slides and they were cover slipped. Slides were imaged using a Nikon Confocal A1 inverted microscope. Image analysis and quantification was done using Nikon Elements and Imaris software.

For IHC, frozen sections were rinsed in 1xPBS after thawing. Antigen retrieval was done using 10 mM Citrate buffer and then slides were treated in 3% H_20_2 for 15 minutes. Slides were rinsed and then blocked for 1 hour in 1x PBS + 0.1% Tween 20 + 5% BSA + 5% NDS. Primary antibodies were applied overnight in blocking solution. Slides were rinsed and secondary antibodies were applied for 1 hour. Vector Labs AB reagent was used for 30 minutes on slides, after which Vector Labs DAB reagent was used to develop the stain. The reaction was quenched using water and slides were mounted using Fluromount-G (SouthernBiotech).

Morphogenesis and Migration analysis

For quantification, NIS-Elements software was used to threshold a binary layer based on pixel intensity for each channel. A combined binary layer was created to account for all islet subtypes (Insulin + Glucagon + Somatostatin). From that combined binary layer, we then calculated the circularity, convexity, and elongation of each islet according to the standard mathematical definitions below, all of which are standard functions available in NIS-Elements:

Circularity = $4\times\pi\times\frac{Area}{Perimeter^2}$

Convexity = $\frac{Area}{Convex\ Hull\ Area}$

Elongation = $\frac{Max\ Feret}{Min\ Feret}$

We also extracted data on the islet area and number of nuclei per islet. Total, the number of islets analyzed for mTOR wildtype mice was 593 and 404 for mutant mice (size >100um$^{2)}$. The number of islets analyzed

based on large islet size (5000-20Kum^2) was 171 and 87 for wildtype and mutant mice, respectively. This culminated in 94,546 wildtype cells and 53,748 mutant cells analyzed across 3 biological replicates per group. Shape score was calculated through the following equation: $\frac{1}{Elongation} \times Circularity \times \frac{1}{Convexity}$. Islets were categorized based on area and graphed accordingly.

Ductal analysis was similar to the above protocol. P14 serial sectioned pancreatic tissue was stained for ductal marker, DBA and pan-endocrine marker, ChromograninA. NIS-Elements software calculated the distance of CGA positive islets from the nearest DBA positive ductal structure using the binary layers and thresholds set in the software for the two stains.

Whole-Mount Pancreas Staining

Whole pancreas from mice was dissected and washed with cold 1x PBS. Tissue was then fixed overnight in 4% PFA at 4°. Tissue was washed in cold 1x PBS to remove fixation solution. Tissue was placed in a 50mL conical tube containing A4P0 solution (4% acrylamide + 2.5mg/mL Va-044), oxygen removed, and placed in a 37° water bath overnight. A4P0 solution was decanted off and tissue was incubated in 8% SDS solution until cleared. Tissue was washed in 1x PBS for one day to remove SDS. Primary antibodies were diluted in blocking buffer and tissue was incubated in solution at 4° for 3 days. Pancreas samples were washed with 5x for 1hour with 1x PBS and then the same staining protocol was applied for secondary antibodies.

Flow Cytometry Cellular Dissociation Protocol

Tissue was minced in 37° Red Blood Cell Lysis Buffer for 10 minutes. Tissue was centrifuged and washed in cold Hanks Buffer Salt Solution (HBSS) and incubated in digest solution (2 g/L collagen Type1, 0.2 g/L soybean trypsin inhibitor, 0.5 ug/mL DNase 1 in HBSS) at 37° for 35 minutes. Tissue was washed in cold HBSS and incubated in Trypsin solution for 10 minutes at room temperature. Cells were washed and resuspended in HBSS and filtered through a 40 micron cell strainer and then fixed using Cytofix/Cytoperm solution (BD Biosciences) on ice for 20 minutes. Cells were washed in Perm/Wash buffer (BD Biosciences) and spun down. Primary antibodies were diluted in Perm/Wash buffer and incubated for 40 minutes on ice. Secondary antibodies were also diluted in Perm solution and incubated at room temperature in the dark for 15 minutes.

Supplemental Tables

Table S1: Primary and Secondary Antibodies

Primary Antibody	**Source**	**Catalog Number**	**Dilution**
Rat anti-BrdU	Abcam	Ab6326-250	1:100
Goat anti-Somatostatin	Santa Cruz	SC-7819	1:200
Rabbit anti-cleaved Caspase 3	Cell Signaling	9661	1:200
Goat anti-Glut2	Santa Cruz	SC-7580	1:500
Mouse anti-Glucagon	Sigma	G2654	1:500
Rabbit anti-Glucagon	Zymed	18-0064	1:500
Rabbit anti-mTOR	Cell Signaling	7C10	1:200

Rabbit anti-Uroctortin3	Phoenix Pharmaceuticals	H-019-29	1:500
Rabbit anti-Ki67	Abcam	Ab15580	1:500
Rabbit anti-Nkx2.2	Tom Jessell Lab	110722	1:2000
Rat anti-PECAM	BD Biosciences	553371	1:150
Rabbit anti-SOX9	Santa Cruz	Sc-20095	1:100
Goat anti-Pdx1	Abcam	Ab94931	1:5000
Bio anti-DBA	Vector	B-1035	1:100
Guinea Pig anti-Insulin	DAKO	A0564	1:1000
Rabbit anti-Phospho-mTOR	Cell Signaling	D9C2	1:100
Mouse anti-PHH3	Abcam	Ab14955-100	1:200
Goat anti-Ghrelin	Santa-Cruz	Sc-10368	1:200
Guinea Pig anti-Synaptophysin	Synaptic Systems	101 004	1:1000
Goat anti-ChromograninA	Santa Cruz	Sc-1488	1:200
Rabbit anti-Sox9	EMD Millipore	AB5535	1:5000
Rabbit anti-Snail2	Abcam	Ab85931	1:100
Rabbit anti-PC1/3	EMD Millipore	AB10553	1:500
Rabbit anti-Pax6	Covance	PRB-278P	1:500
Rat anti-Ecad	R&D	MAB7481	1:500

Secondary Antibody	**Source**	Dilution
Donkey anti-rabbit 546	Invitrogen	1:500
Donkey anti-rat 647	Invitrogen	1:500
Donkey anti-goat 546	Invitrogen	1:500
Donkey anti-rabbit 488	Invitrogen	1:500
Donkey anti-guinea pig 488	Invitrogen	1:500
Donkey anti-guinea pig 546	Invitrogen	1:500

Donkey anti-goat 647	Invitrogen	1:500
Donkey anti-goat 488	Invitrogen	1:500
Donkey anti-rabbit 647	Invitrogen	1:500
Donkey anti-mouse 647	Invitrogen	1:500
Donkey anti-mouse Cy3	Jackson Immuno	1:500
PE anti-mouse	Biolegend	1:100
Goat anti-guinea pig	Invitrogen	1:500

Table S2: Primer list for genotyping

Mouse	**Forward Primer**	**Reverse Primer**
Ngn3Cre	ATT TGC CTG CAT TAC CGG TC	AGA GAC GGA AAT CCA TCG CTC G
mTOR	TTA TGT TTG ATA ATT GCA GTT TTG GCT AGC AGT	TTT AGG ACT CCT TCT GTG ACA TAC ATT TCC T
Rictor	ACT GAA TAT GTT CAT GGT TGT G	GAA GTT ATT CAG ATG GCC CAG C
Raptor	CTC AGT AGT GGT ATG TGC TCA G	GGG TAC AGT ATG TCA GCA CAG

Table S3: Significance and N values

Figure	**Description**	**P value**	**Number of animals**
1C	Fasting BGL P7	0.2243	7 WT, 6 Mut
	Fasting BGL P14	0.2741	15 WT, 5 Mut
	Fasting BGL P21	0.1882	5 WT, 3 Mut
	Fasting BGL P28	0.000003	7 WT, 3 Mut
	Fasting BGL 8 weeks	0.00005	3 WT 3 Mut
1C	Circ Insulin P7	0.1717	3 WT, 5 Mut
	Circ Insulin P14	0.1565	6 WT, 3 Mut
	Circ Insulin P21	0.0206	5 WT, 5 Mut
	Circ Insulin P28	0.0044	8 WT, 2 Mut
	Circ Insuiln 8 weeks	0.0016	3 WT 3 Mut
2A	e18.5 Endocrine Count Insulin	0.1778	5 WT, 4 Mut
	e18.5 Endocrine Count Glucagon	0.1287	5 WT, 4 Mut
	e18.5 Endocrine Count Somatostain	0.2706	5 WT, 4 Mut
2A	P7 Endocrine Count Insulin	0.4558	3 WT, 5 Mut
	P7 Endocrine Count Glucagon	0.2016	3 WT, 5 Mut
	P7 Endocrine Count Somatostatin	0.0930	3 WT, 5 Mut
2B	P14 Endocrine Count Insulin	0.0016	11 WT, 5 Mut
	P14 Endocrine Count Glucagon	0.0039	6 WT, 3 Mut
	P14 Endocrine Count Somatostatin	0.0010	6 WT, 3 Mut

3A	P0 TF Isl1	0.4317	3 WT, 3 Mut
	P0 TF Neurod1	0.3901	3 WT, 3 Mut
	P0 TF Nkx6.1	0.4676	3 WT, 3 Mut
	P0 TF Pax6	0.3531	3 WT, 3 Mut
	P0 TF Foxa2	0.3042	3 WT, 3 Mut
	P0 TF Arx	0.2160	3 WT, 3 Mut
3A	P7 TF Isl1	0.4387	3 WT, 3 Mut
	P0 TF Neurod1	0.0124	3 WT, 3 Mut
	P0 TF Nkx2.2	0.1123	3 WT, 3 Mut
	P0 TF Nkx6.1	0.0597	3 WT, 3 Mut
	P0 TF Pax6	7.14E-05	3 WT, 3 Mut
	P0 TF Foxa2	0.0215	3 WT, 3 Mut
3A	P14 TF FoxO1	0.0348	3 WT 3 Mut
	P14 TF Isl1	0.1835	3 WT, 3 Mut
	P14 TF Nkx6.1	0.0077	3 WT, 3 Mut
	P14 TF Pax6	0.0344	3 WT, 3 Mut
3C	P14 Maturation Mafa	0.0387	3 WT, 3 Mut
	P14 Maturation Mafb	0.1985	3 WT, 3 Mut
	P14 Maturation Ucn3	0.0019	3 WT, 3 Mut
	P14 Maturation Tshz1	0.1034	3 WT, 3 Mut
3D	P14 Hormone Glucagon	0.0545	3 WT, 3 Mut
	P14 Hormone Ghrelin	0.1732	3 WT, 3 Mut
	P14 Hormone Insulin1	0.0043	3 WT, 3 Mut
	P14 Hormone Insulin2	0.0011	3 WT, 3 Mut
	P14 Hormone Ppy	0.0440	3 WT, 3 Mut
	P14 Hormone Sst	0.0014	3 WT, 3 Mut
4B	P14 Transporter Sur1	0.0040	3 WT 3 Mut
	P14 Transporter Kir6.2	0.0186	3 WT 3 Mut
	P14 Transporter Slc30a8	0.0117	3 WT, 3 Mut
	P14 Vesicle Marker Chga	0.0006	3 WT, 3 Mut
4C	Beta Cell Granularity P7	0.3658	3 WT, 5 Mut
	Beta Cell Granularity P14	0.0161	3 WT, 2 Mut
	Alpha Cell Granularity P7	0.1358	3 WT, 5 Mut
	Alpha Cell Granularity P14	0.0049	3 WT, 2 Mut
4E	16 Hour Fasted Blood Glucose at P14	0.0032	11 WT, 9 Mut
	16 Hour Fasted Insulin at P14	0.0132	5 WT, 5 Mut
5D	P14 Endocrine Cell Size 1000-3000	0.0009	3 WT, 3 Mut
	P14 Endocrine Cell Size 3000-5000	0.0320	3 WT, 3 Mut
	P14 Endocrine Cell Size 5000-10K	0.0684	3 WT, 3 Mut
	P14 Endocrine Cell Size 10K-20K	0.1589	3 WT, 3 Mut

	P14 Endocrine Cell Size >20K	0.4567	3 WT, 3 Mut
5E	P14 Islet Remodeling Factors E-cadherin	0.4686	3 WT, 3 Mut
	P14 Islet Remodeling Factors N-cadherin	0.0731	3 WT, 3 Mut
	P14 Islet Remodeling Factors Ctgf	0.1259	3 WT, 3 Mut
6C	P21 Raptor Fasted BGL (Het)	0.0784	5 WT, 7 Het
	P21 Raptor Fasted BGL (Mut)	0.0218	5 WT, 4 Mut
	P21 Rictor Fasted BGL (Het)	0.1179	7 WT, 4 Het
	P21 Rictor Fasted BGL (Mut)	0.2181	7 WT, 4 Mut
6D	P21 Rictor Single Cells	0.0191	3 WT, 3 Mut
	P21 Rictor >100	0.0208	3 WT, 3 Mut
	P21 Rictor 100-1000	0.0082	3 WT, 3 Mut
	P21 Rictor 1000-3000	0.0249	3 WT, 3 Mut
	P21 Rictor 3000-5000	0.0536	3 WT, 3 Mut
	P21 Rictor 5000-10K	0.3204	3 WT, 3 Mut
	P21 Rictor 10K-20K	0.3361	3 WT, 3 Mut
	P21 Rictor >20K	0.3501	3 WT, 3 Mut
Supp Figure 1A	Postnatal Weight P7	0.0886	7 WT, 7 Mut
	Postnatal Weight P14	0.3407	15 WT, 5 Mut
	Postnatal Weight P21	0.1179	5 WT, 3 Mut
	Postnatal Weight P28	0.0123	5 WT, 2 Mut
	Postnatal Weight 8 Weeks	0.0004	4 WT, 4 Mut
	Adult Percent Pancreas Weight (WT)	N/A	4 WT
	Adult Percent Pancreas Weight (Het)	0.0986	4 Het
	Adult Percent Pancreas Weight (Mut)	0.2662	4 Mut
Supp Figure 2B	P14 Endocrine Count Insulin	0.0041	11 WT, 6 Het
	P14 Endocrine Count Glucagon	0.0601	11 WT, 6 Het
	P14 Endocrine Count Somatostatin	0.2275	11 WT, 6 Het
Supp Figure 2C	Adult Glucose Tolerance Test Fasted	0.1711	4 WT, 4 Het
	Adult Glucose Tolerance Test 15	0.1555	4 WT, 4 Het
	Adult Glucose Tolerance Test 30	0.1229	4 WT, 4 Het
	Adult Glucose Tolerance Test 60	0.2681	4 WT, 4 Het
	Adult Glucose Tolerance Test 90	0.2480	4 WT, 4 Het
	Adult Glucose Tolerance Test 120	0.4594	4 WT, 4 Het
	1 Year Glucose Tolerance Test Fasted	0.3463	3 WT, 5 Het
	1 Year Glucose Tolerance Test 15	0.3075	3 WT, 5 Het
	1 Year Glucose Tolerance Test 30	0.2176	3 WT, 5 Het
	1 Year Glucose Tolerance Test 60	0.3698	3 WT, 5 Het
	1 Year Glucose Tolerance Test 90	0.3308	3 WT, 5 Het
	1 Year Glucose Tolerance Test 120	0.3384	3 WT, 5 Het
Supp Figure 3C	P14 Single Cells	0.4983	3WT, 3 Mut
	P14 <100	0.3781	3WT, 3 Mut

	P14 100-1000	0.3891	3WT, 3 Mut
	P14 1000-3000	0.0265	3 WT, 3 Mut
	P14 3000-5000	0.0223	3 WT, 3 Mut
	P14 1000-10K	0.0161	3 WT, 3 Mut
	P14 10K-20K	0.0136	3 WT, 3 Mut
	P14 >20K	0.0003	3 WT, 3 Mut
Supp Figure 4C	e18.5 Beta Cell Proliferation Ki67	0.0189	3 WT, 3 Mut
	P7 Beta Cell Proliferation Ki67	0.0977	3 WT, 3 Mut
	Percent Proliferation (WT)	N/A	7 WT
	Percent Proliferation (Het)	0.1688	5 Het
	Percent Proliferation (Mut)	0.2627	3 Mut
Supp Figure 5A	P14 Neurogenin3 Expression	0.2604	3WT, 3 Mut
Supp Figure 5B	P0 Hormone Glucagon	0.4728	3 WT, 3 Mut
	P0 Hormone Ghrelin	0.2242	3 WT, 3 Mut
	P0 Hormone Insulin1	0.1322	3 WT, 3 Mut
	P0 Hormone Ppy	0.1009	3 WT, 3 Mut
	P0 Hormone Sst	0.3295	3 WT, 3 Mut
	P7 Hormone Glucagon	0.0531	3 WT, 3 Mut
	P7 Hormone Ghrelin	0.1888	3 WT, 3 Mut
	P7 Hormone Insulin1	0.0193	3 WT, 3 Mut
	P7 Hormone Insulin2	0.0041	3 WT, 3 Mut
	P7 Hormone Ppy	0.0292	3 WT, 3 Mut
	P7 Hormone Sst	0.0584	3 WT, 3 Mut
Supp Figure 5C	P14 Disallowed Gene Ldha	0.1345	3 WT, 3 Mut
	P14 Disallowed Gene Oxct1	0.3868	3 WT, 3 Mut
	P14 Disallowed Gene Slc16a1	0.3696	3 WT, 3 Mut
Supp Figure 5D	P7 Channel/Transporter Sur1	0.3179	3 WT, 3 Mut
	P7 Channel/Transporter Kir6.2	0.2184	3 WT, 3 Mut
	P7 Channel/Transporter Slc30a8	0.0015	3 WT, 3 Mut
Supp Figure 5E	Delta Cell Granularity P7	0.1141	3 WT, 5 Mut
	Delta Cell Granularity P14	0.3930	3 WT, 2 Mut
Supp Figure 5F	Insulin After IP Glucose	0.2457	6 WT, 4 Mut
Supp Figure 6A	P14 Shape 1000-3000	0.2027	3 WT, 3 Mut
	P14 Shape 3000-5000	0.1442	3 WT, 3 Mut
	P14 Shape 5000-10K	0.0044	3 WT, 3 Mut

	P14 Shape 10K-20K	0.0465	3 WT, 3 Mut
	P14 Distance 100-1000	0.3112	3 WT, 3 Mut
	P14 Distance 1000-5000	0.4321	3 WT, 3 Mut
	P14 Distance 5000-10K	0.3587	3 WT, 3 Mut
	P14 Distance 10K-20K	0.0246	3 WT, 3 Mut
	P14 Distance >20K	0.0580	3 WT, 3 Mut
Supp Figure 6C	P14 E-cadherin Quantification	0.1975	3 WT, 3 Mut
Supp Figure 7A	P21 Raptor Circulating Insulin (Het)	0.4114	5 WT, 7 Het
	P21 Raptor Circulating Insulin (Mut)	0.0254	5 WT, 4 Mut
	P21 Rictor Circulating Insulin (Het)	0.4590	7 WT, 4 Het
	P21 Rictor Circulating Insulin (Mut)	0.2638	7 WT, 4 Mut
Supp Figure 7B	P14 16 Hour Fast mTOR	0.0068	18 WT, 4 Mut
	P14 16 Hour Fast Raptor	0.2060	7 WT, 3 Mut
Supp Figure 7C	P21 Rictor Shape 1000-3000	0.1513	3 WT, 3 Mut
	P21 Rictor Shape 3000-5000	0.0405	3 WT, 3 Mut
	P21 Rictor Shape 5000-10K	0.2967	3 WT, 3 Mut
	P21 Rictor Shape 10K-20K	0.1174	3 WT, 3 Mut
	P21 Rictor Shape >20K	0.4951	3 WT, 3 Mut

Supplemental References

Gangloff, Y.-G., Mueller, M., Dann, S. G., Svoboda, P., Sticker, M., Spetz, J.-F., Um, S. H., Brown, E. J., Cereghini, S., Thomas, G., et al. (2004). Disruption of the mouse mTOR gene leads to early postimplantation lethality and prohibits embryonic stem cell development. *Mol. Cell. Biol.* **24**, 9508–16.

Jonatan, D., Spence, J. R., Method, A. M., Kofron, M., Sinagoga, K., Haataja, L., Arvan, P., Deutsch, G. H. and Wells, J. M. (2014). Sox17 regulates insulin secretion in the normal and pathologic mouse β cell. *PLoS One* **9**, e104675.

Schonhoff, S. E., Giel-Moloney, M. and Leiter, A. B. (2004). Neurogenin 3-expressing progenitor cells in the gastrointestinal tract differentiate into both endocrine and non-endocrine cell types. *Dev. Biol.* **270**, 443–54.

Sengupta, S., Peterson, T. R., Laplante, M., Oh, S. and Sabatini, D. M. (2010). mTORC1 controls fasting-induced ketogenesis and its modulation by ageing. *Nature* **468**, 1100–1104.

Shiota, C., Woo, J.-T., Lindner, J., Shelton, K. D. and Magnuson, M. A. (2006). *Multiallelic Disruption of the rictor Gene in Mice Reveals that mTOR Complex 2 Is Essential for Fetal Growth and Viability*.

Supplemental Figures

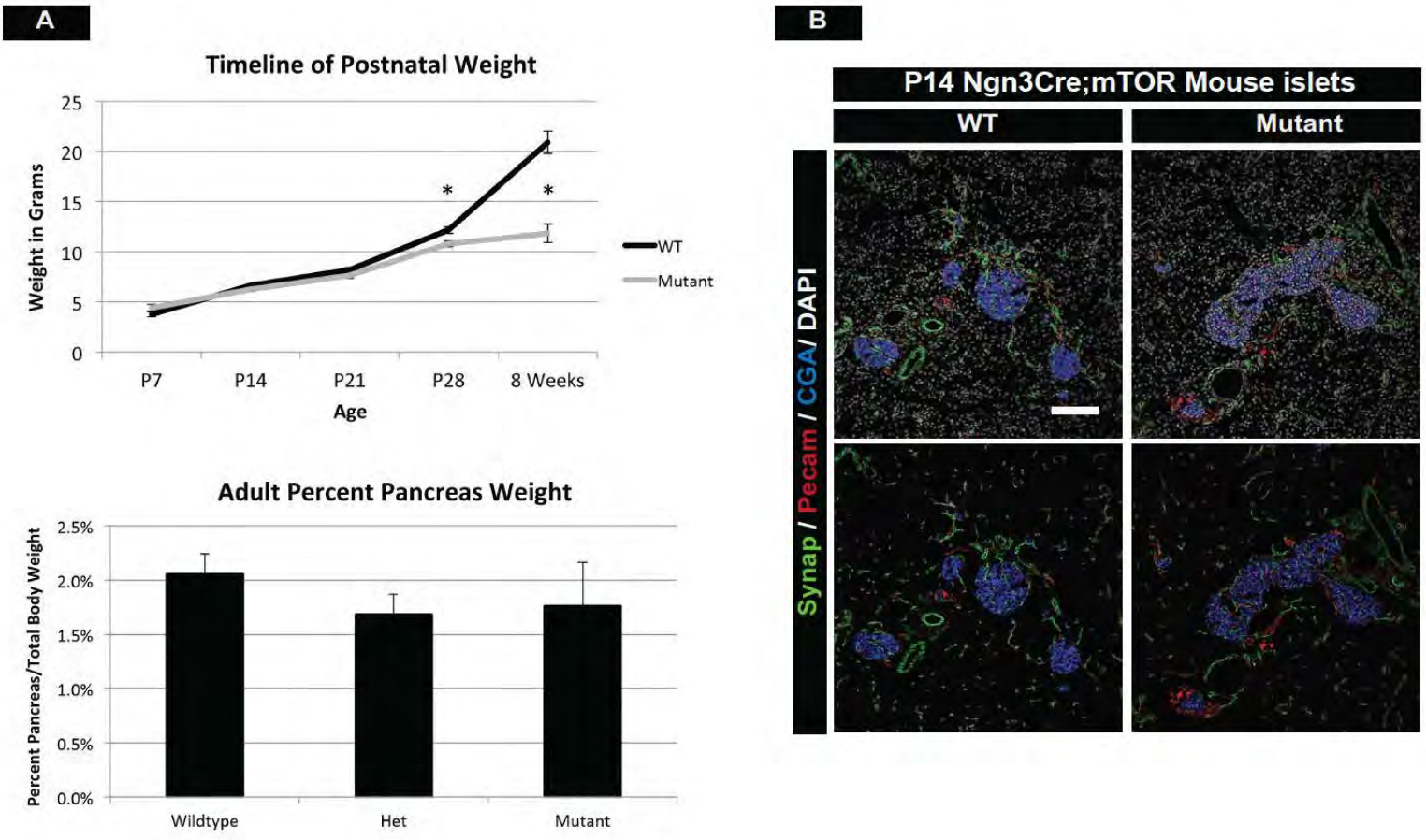

Figure S1. Related to Figure 1: Analysis of animal and total pancreas weight, vascularization and innervation of islets.
(A) Timeline of postnatal weight gain in wild type and mTOR mutants. Only after mutants are severely diabetic is there a significant decrease in weight. Pancreas weight is still proportional to total body weight in the adult**.** Values in graphs represent mean ± S.E.M; * $P < 0.05$. **(B)** Vascularization and innervation of mTOR mutant islets is comparable to wildtype at P14. Immunostaining of vasculature (PECAM1) and innervation (synaptophysin). Scale bars, 50 μm. See Table S3 for number of animals used.

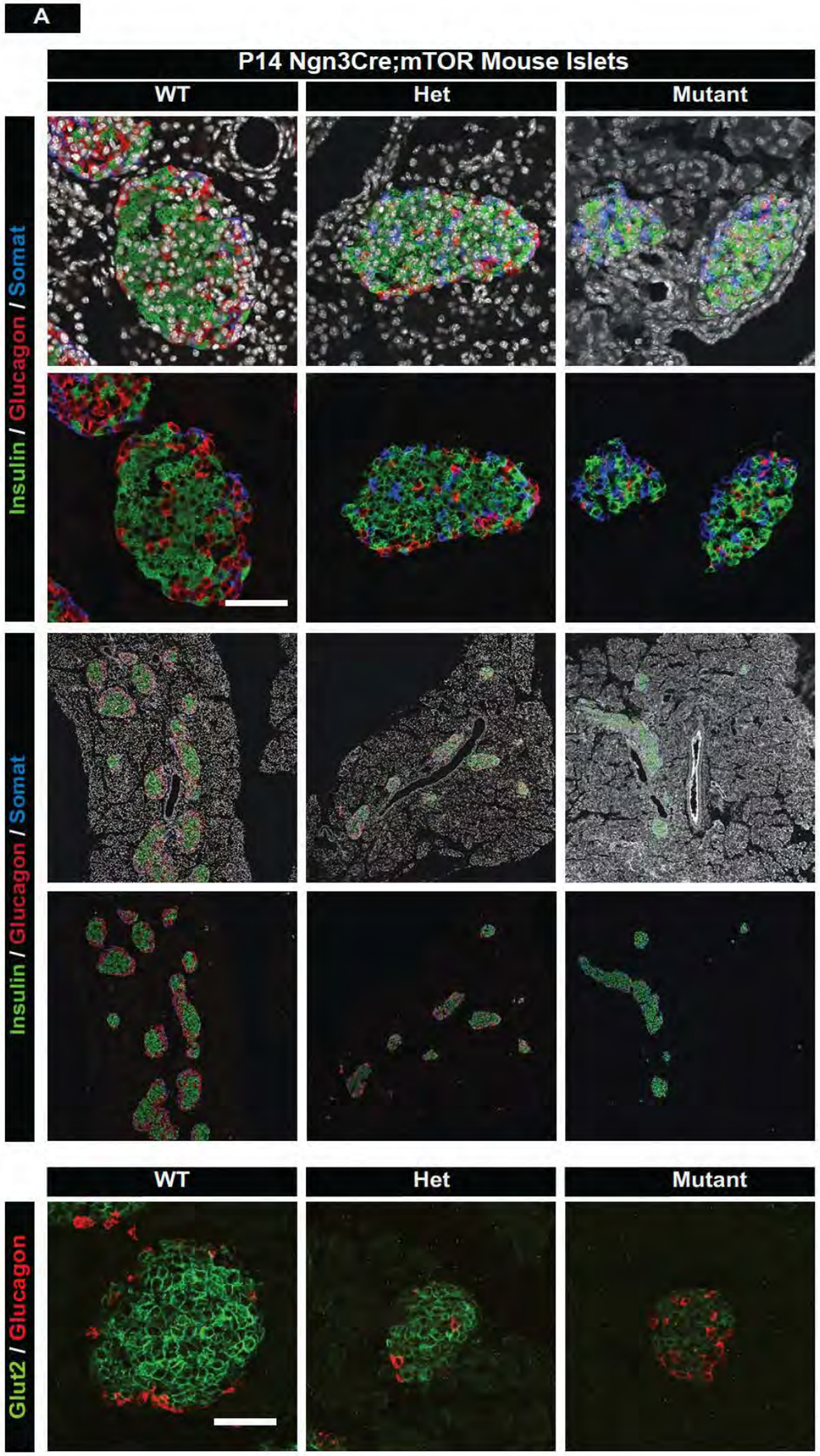

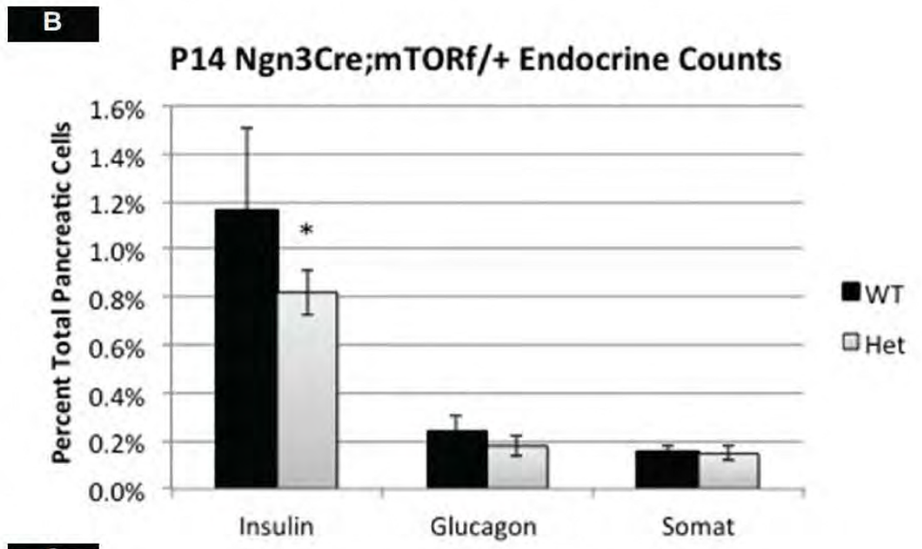

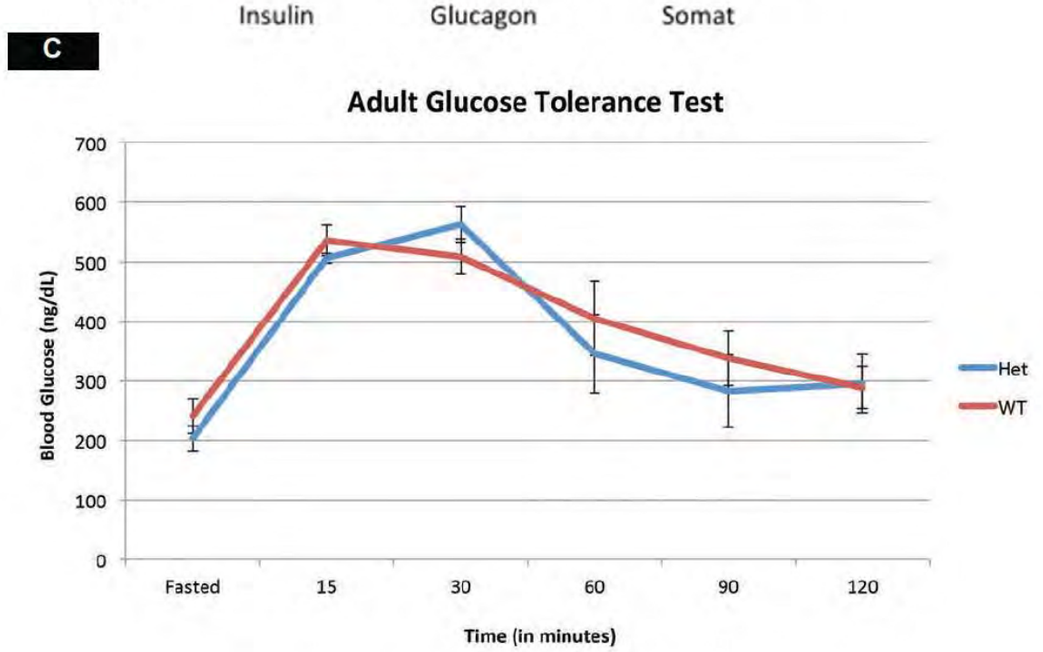

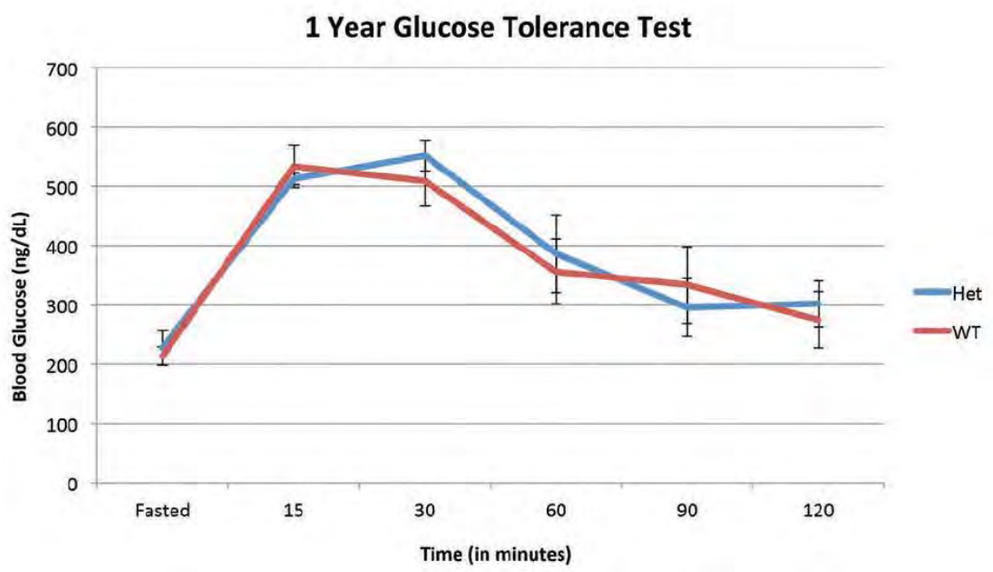

Figure S2. Related to Figure 1: mTOR heterozygous mice display altered β-cell mass, but do not exhibit a functional phenotype.
(A) Immunofluorescence of wild-type, heterozygous, and mTOR mutant P14 islets**. (B)** Quantification of cell numbers at P14 in wild-type and heterozygous mice using flow cytometry. There is a small, but significant decrease in β cells of mTOR heterozygous islets, however this does not lead to aberrant glucose regulation at 8 weeks or one year of age. **(C)** Glucose tolerance test in wild-type and heterozygous mice. Top: 8 weeks old. Bottom: 1 year old. Scale bars, 50 μm. Values in graphs represent mean ± S.E.M; * $P < 0.05$. See Table S3 for number of animals used.

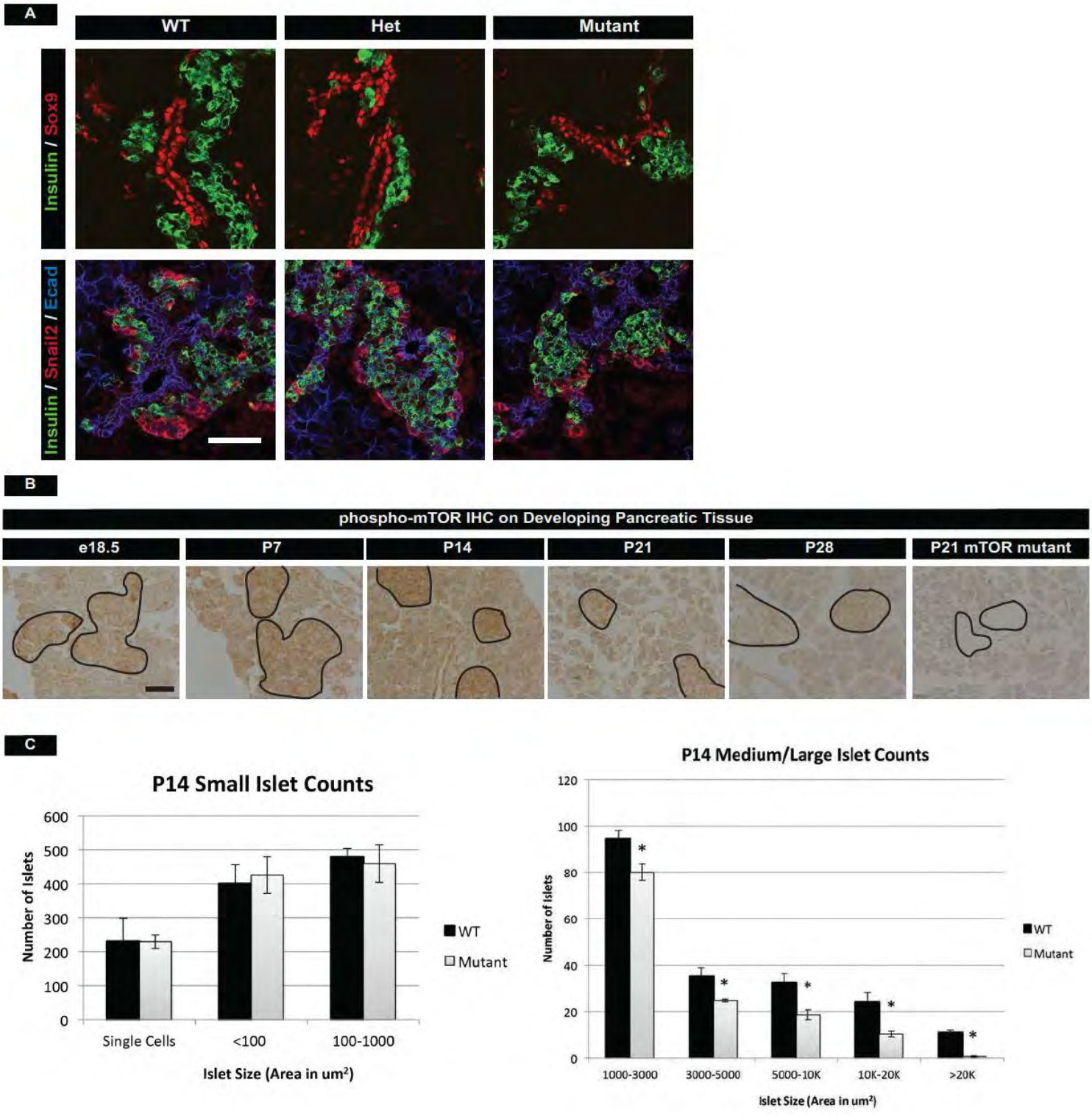

Figure S3. Related to Figure 2: mTOR is not required for embryonic islet development. **(A)** Endocrine cell migration and islet morphogenesis are comparable between wild-type and mutant animals at e18.5. Insulin positive cells down-regulate E-cadherin and migrate out of the Sox9 positive duct, organizing into pre-islet clusters. Snail2 is observed at the leading edges of the migrating cells. Scale bars, 50 μm. **(B)** Active mTOR (phospho-mTOR) staining in developing pancreatic tissue from embryonic day 18.5 to postnatal day 28. High levels of active mTOR are observed in islets (outlined) in the first two weeks after birth. Scale bar, 50 μm. **(C)** Islet counts for P14 wild-type and mutant pancreatic tissue. No difference is observed in small islet counts at this stage, but medium and large islet numbers are decreased, indicative of an islet mass defect. See Table S3 for number of animals used.

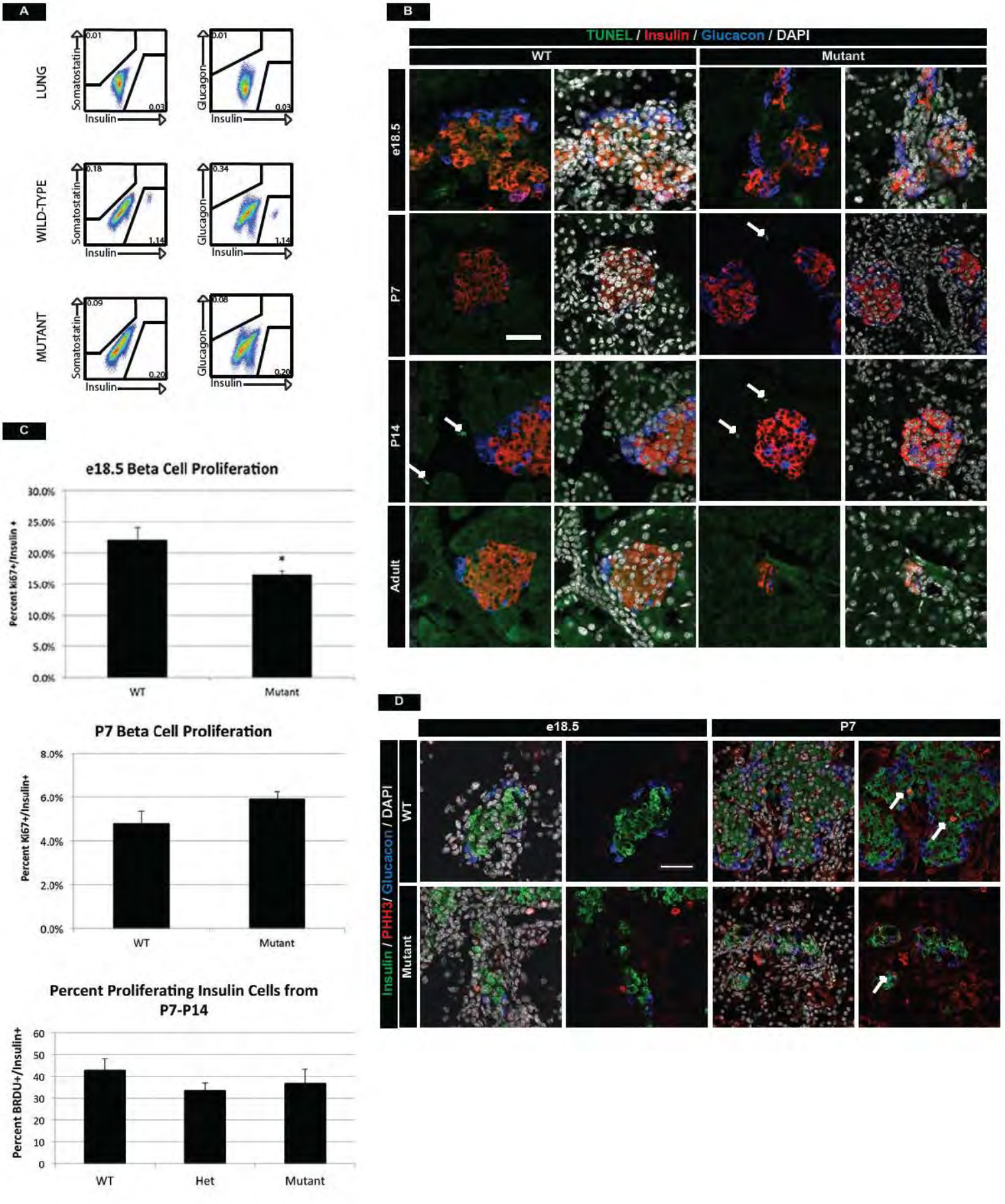

Figure S4. Related to Figure 2: Analysis of apoptosis and cell proliferation in wildtype and mTOR mutant islets during perinatal development.
(A) Representative FACS plots highlighting efficient staining of endocrine populations at P21 via flow cytometry. Isotype control: lung **(B)** Comparable levels of apoptosis in wild-type and mTOR mutant islets. Representative TUNEL stains of wildtype and mutant islets from e18.5 to adult. Arrows indicate TUNEL positive cells**.** Scale bar, 50 μm. **(C) Top:** Proliferation as assessed by Ki67 staining indicates a defect at e18.5 in mTOR mutants. **Middle:** Proliferation at P7 (Ki67) **Bottom:** At P14, islets are assessed for incorporation BRDU in β cells by flow cytometry as a measure of proliferation from 1-2 weeks of life. No statistical difference in global proliferation from 1-2 weeks of life is detected. **(D)** PHH3 stains at e18.5 and P7 is consistent with reduced proliferation in late embryonic/early postnatal life. Arrows indicate insulin/PHH3 double positive cells. Scale bar, 50 μm. **(D)** Values in graphs represent mean ± S.E.M. * $P < 0.05$. See Table S3 for number of animals used.

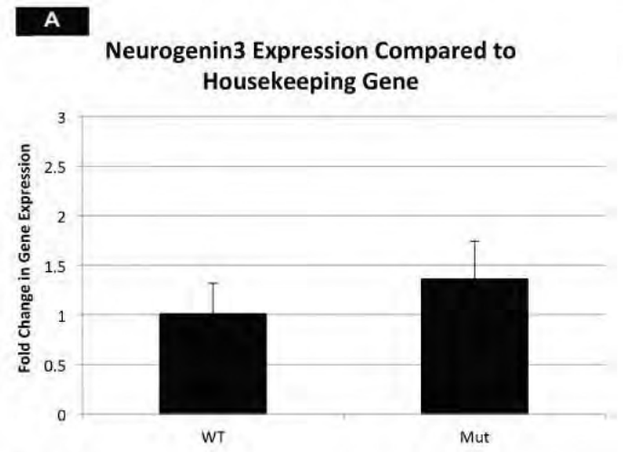

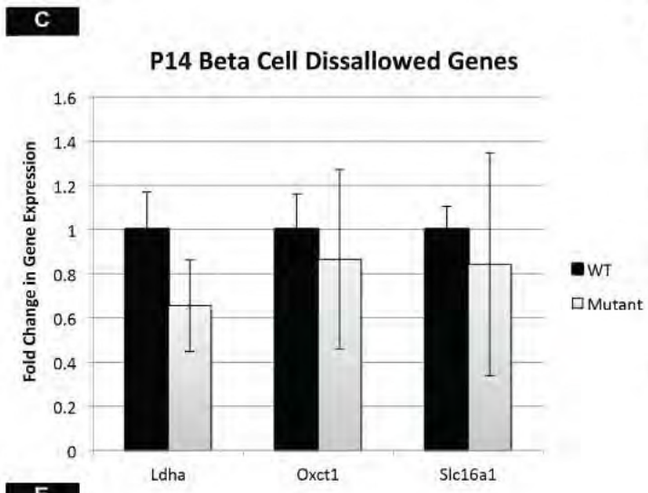

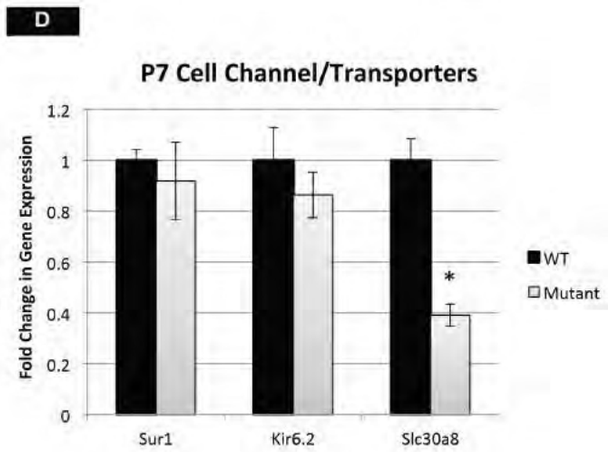

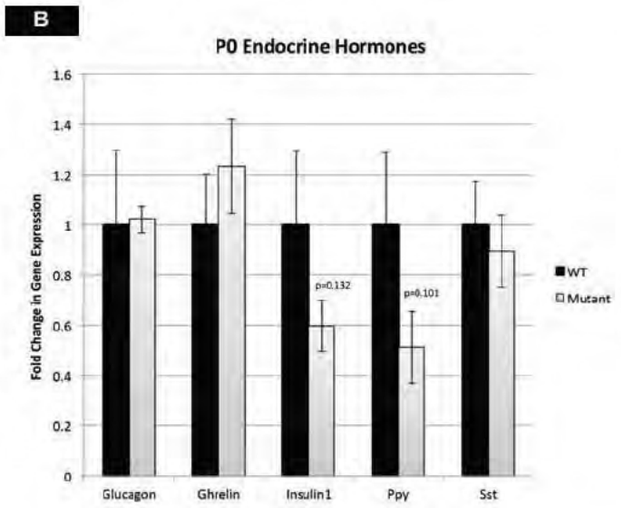

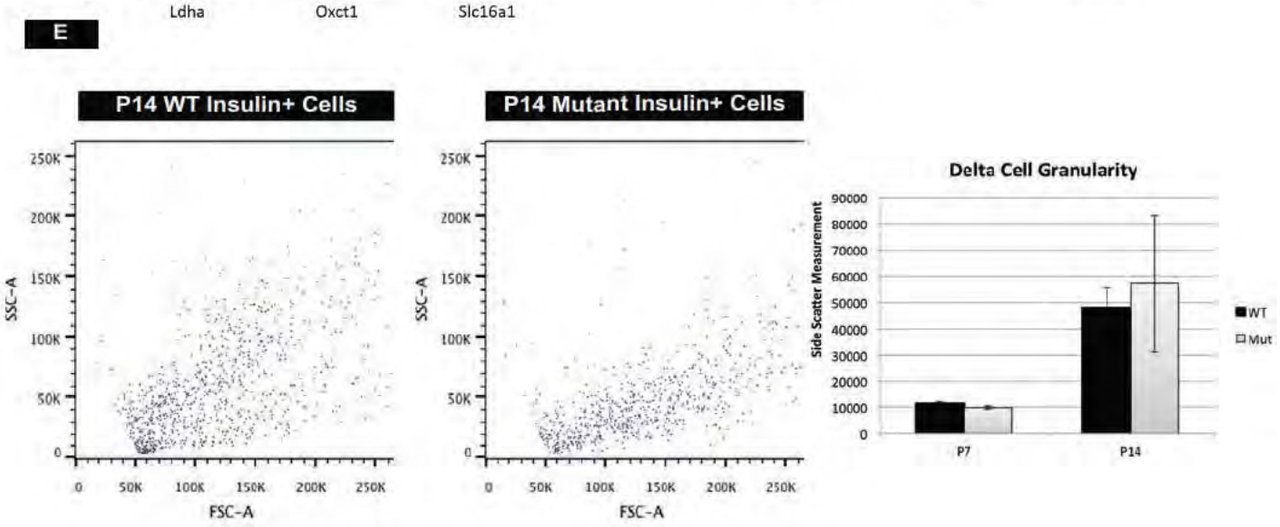

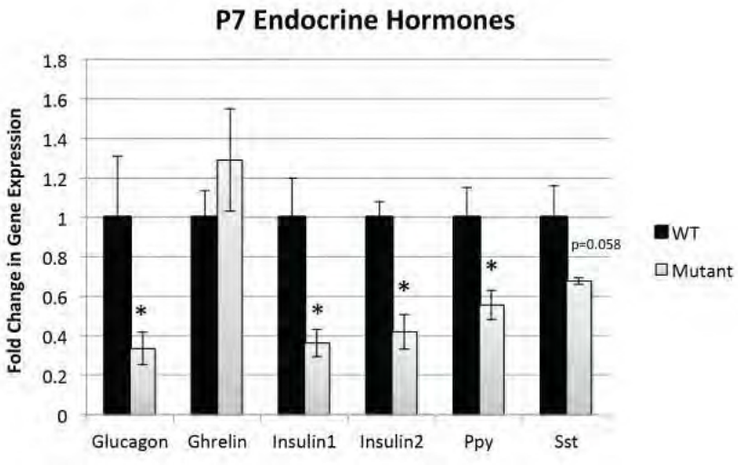

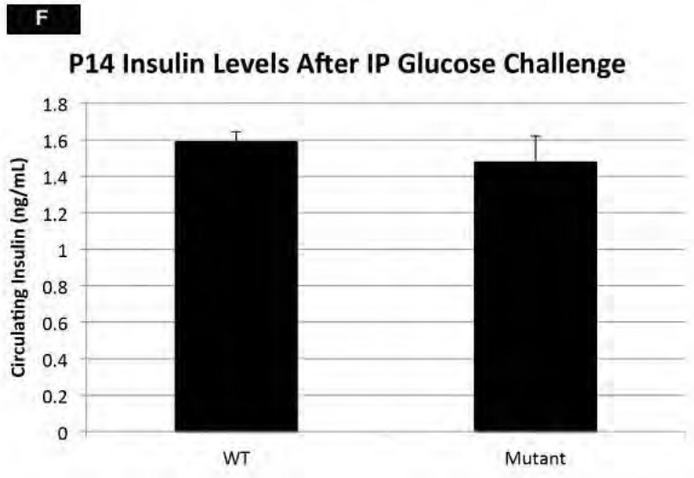

Figure S5. Related to Figures 3/4: Characterization of postnatal gene expression, granularity, and function in mTOR mutants.
(A) qPCR data are normalized to *Ngn3* (neurogenin 3), which has no change in gene expression when compared to housekeeping gene *Hprt1* **(B)** qPCR for P0 and P7 endocrine hormones. While no significant difference is seen just after birth, 1-week later hormones are significantly down in mTOR mutants. **(C)** Despite a maturation defect in mTOR mutant islets at P14, by qPCR there are no increases in selectively disallowed genes. **(D)** qPCR for endocrine cell channels and transporters reveals normal levels of components of the Na/K^+ channel, but significant reductions in zinc transporter, *Slc30a8* at P7. **(E)** Representative side-scatter (SSC) plots for wildtype and mutant insulin+ cells. Note a collective decrease in SSC measurements in mutant β cells. However, this does not seem to be the case for somatostatin positive cells within mutant islets. **(F)** A glucose challenge at P14 indicates that despite maturation defects, β cells are able to secrete comparable levels of insulin in response to high levels of glucose. Values in graphs represent mean ± S.E.M. * $P < 0.05$. See Table S3 for number of animals used.

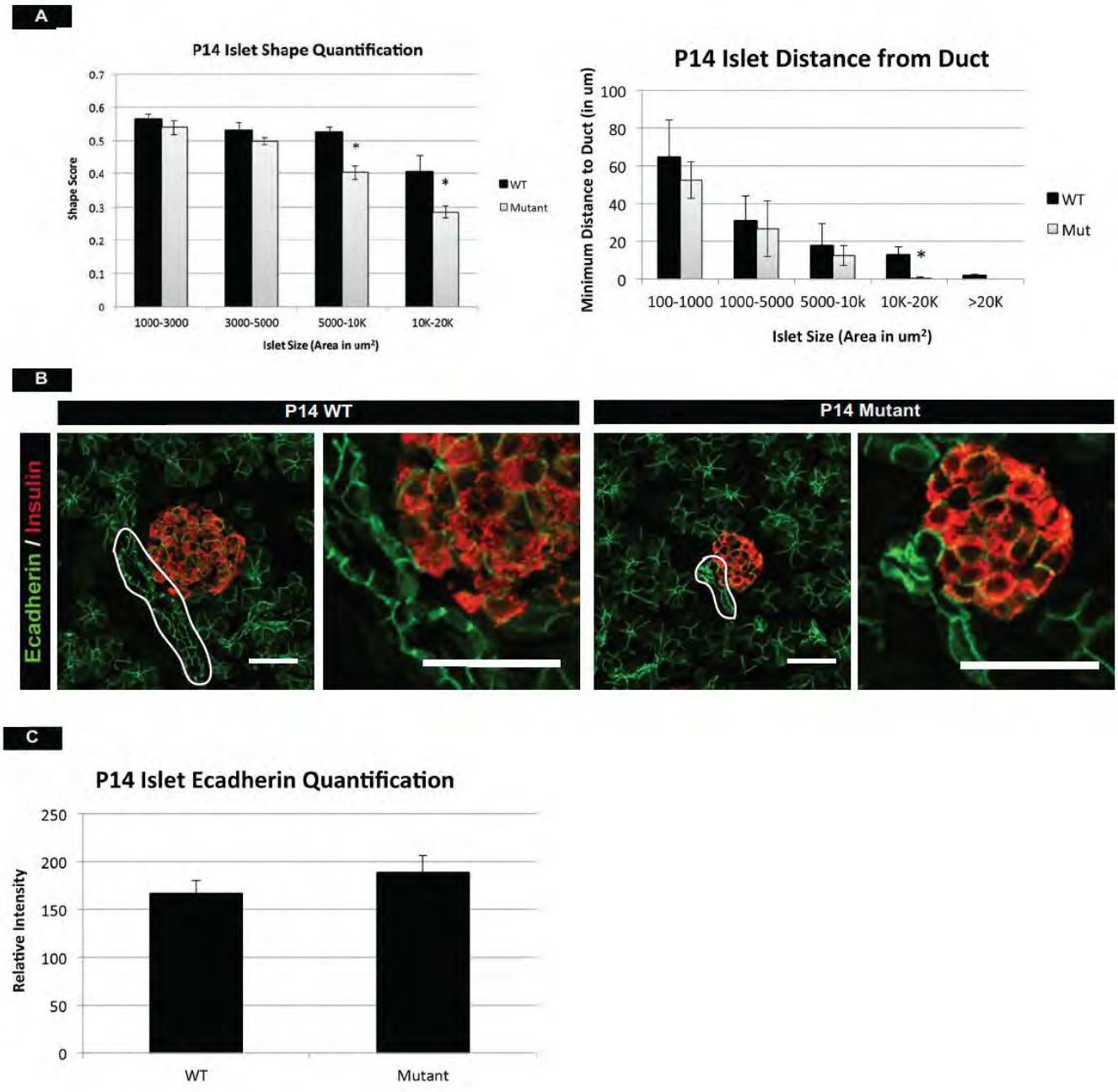

Figure S6. Related to Figure 5: Characterization of morphogenesis defects in mTOR mutants.
(A) Right: Graphical representation of islet shape quantification. Mutant islets with a larger area have lower shape scores, indicative of a morphology defect**. Left:** Quantification of islet distance from ductal structures. Islets were segregated based on size. Large islets in mTOR mutants remained in close proximity to ducts. **(B)** Increased expression of E-cadherin between islet endocrine cells and in conjunction with nearby ductal structures is observed in P14 mutant pancreatic tissue as compared to wildtype. Ducts outlined in white. **(C)** Quantification of E-cadherin immunofluorescence intensity in wildtype and mTOR mutant islets at P14. A trend of increased expression could account for morphogenesis and migration defects observed in mutant animals. Values in graphs represent mean ± S.E.M; * $P < 0.05$. See Table S3 for number of animals used.

A

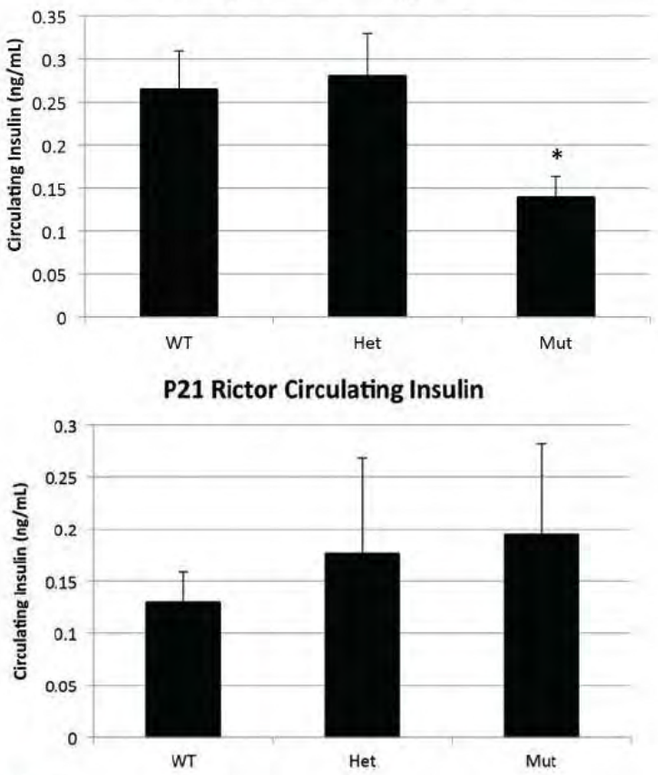
P21 Raptor Circulating Insulin
Circulating Insulin (ng/mL)
0.35
0.3
0.25
0.2
0.15
0.1
0.05
0
*
WT
Het
Mut
P21 Rictor Circulating Insulin
Circulating Insulin (ng/mL)
0.3
0.25
0.2
0.15
0.1
0.05
0
WT
Het
Mut

B

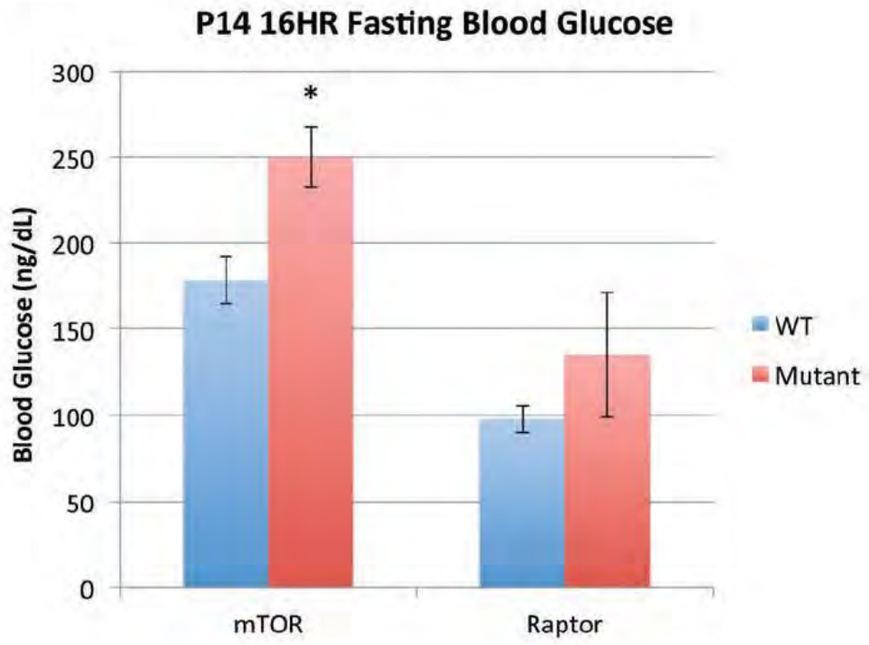
P14 16HR Fasting Blood Glucose
Blood Glucose (ng/dL)
300
250
200
150
100
50
0
*
mTOR
Raptor
WT
Mutant

C

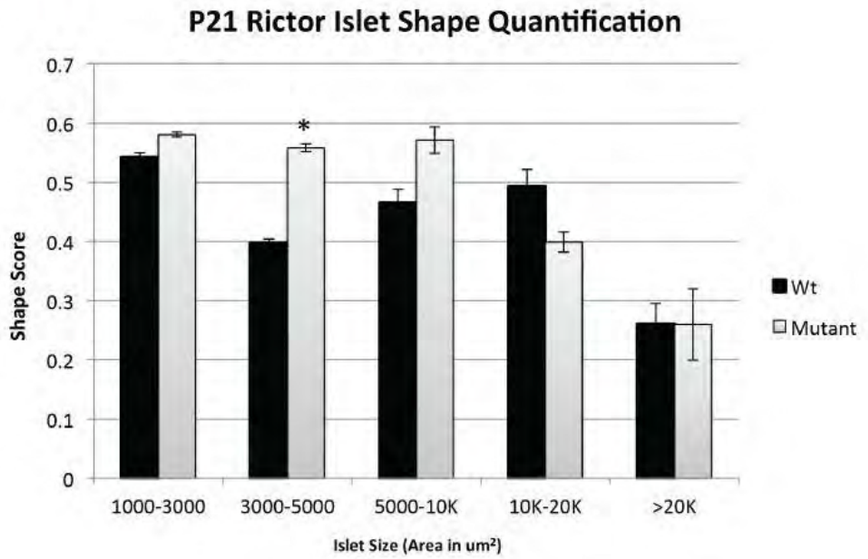
P21 Rictor Islet Shape Quantification
Shape Score
0.7
0.6
0.5
0.4
0.3
0.2
0.1
0
*
1000-3000
3000-5000
5000-10K
10K-20K
>20K
Islet Size (Area in um²)
Wt
Mutant

D

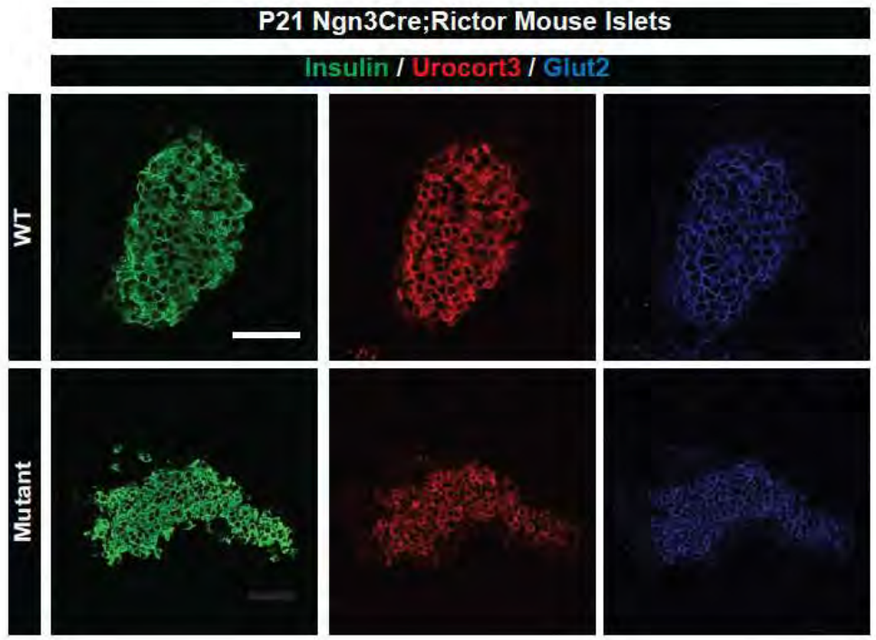
P21 Ngn3Cre;Rictor Mouse Islets
Insulin / Urocort3 / Glut2
WT
Mutant

Figure S7. Related to Figure 6: mTORC1/2 (Raptor/Rictor) play distinct roles in postnatal islet development.
(A) Circulating insulin levels in wild-type, heterozygous, and Raptor/Rictor mutant animals at P21. While Rictor animals maintain normal insulin levels, Raptor mutants have significantly less. **(B)** 16-hour fasting blood glucose readings for P14 mTOR and Raptor mutant mice. While a significant increase in fasting blood glucose levels is seen in mTOR mutants, Raptor mutants do not show a significant phenotype at this stage. This indicates latency in the Raptor functional phenotype. **(C)** Rictor islet-shape quantification reveals the presence, but overall fewer morphologically distorted islets compared to mTOR mutant mice. **(D)** Immunofluorescence for maturation and functional markers Ucn3 and Glut2 also show comparable levels between Rictor mutant and wild-type islets at P21. Islet hormone immunofluorescence at P21 highlights another abnormally shaped islet in Rictor mutants. Values in graphs represent mean ± S.E.M; * $P < 0.05$. See Table S3 for number of animals used.

Movies

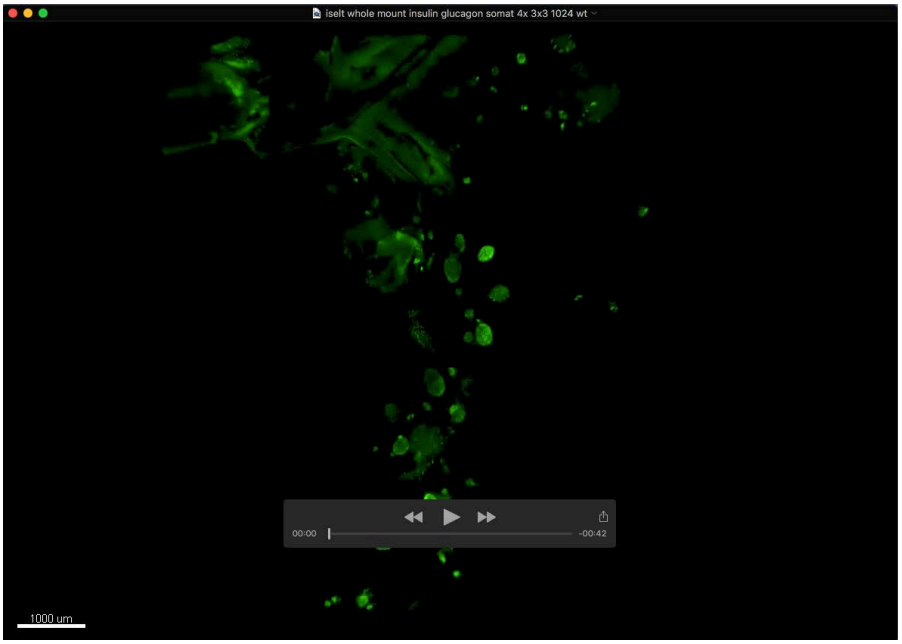

Movie 1. Adult wild-type islet whole-mount staining.
Whole mount immunofluorescence of 8-week old wild-type mice. Insulin is shown in green, highlighting many round islets within this section of the pancreas. Movie was generated using Imaris software.

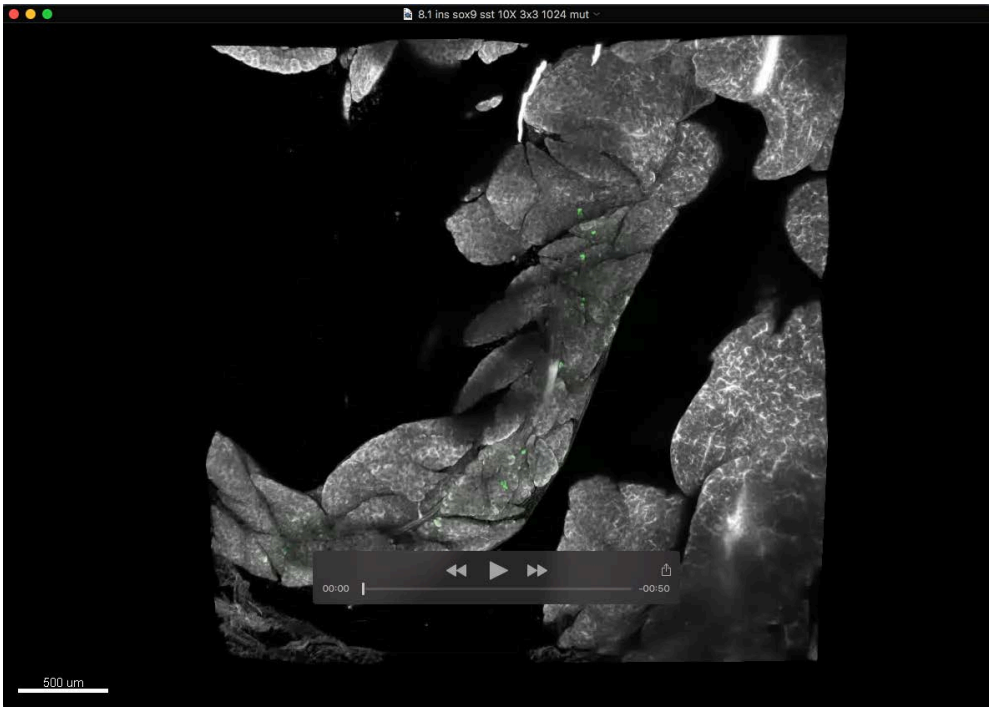

Movie 2. Adult mutant islet whole-mount staining.
Whole mount immunofluorescence of 8-week old mTOR mutant mice. Insulin is shown in green, emphasizing a loss of β cell mass in mutant animals. Movie was generated using Imaris software.

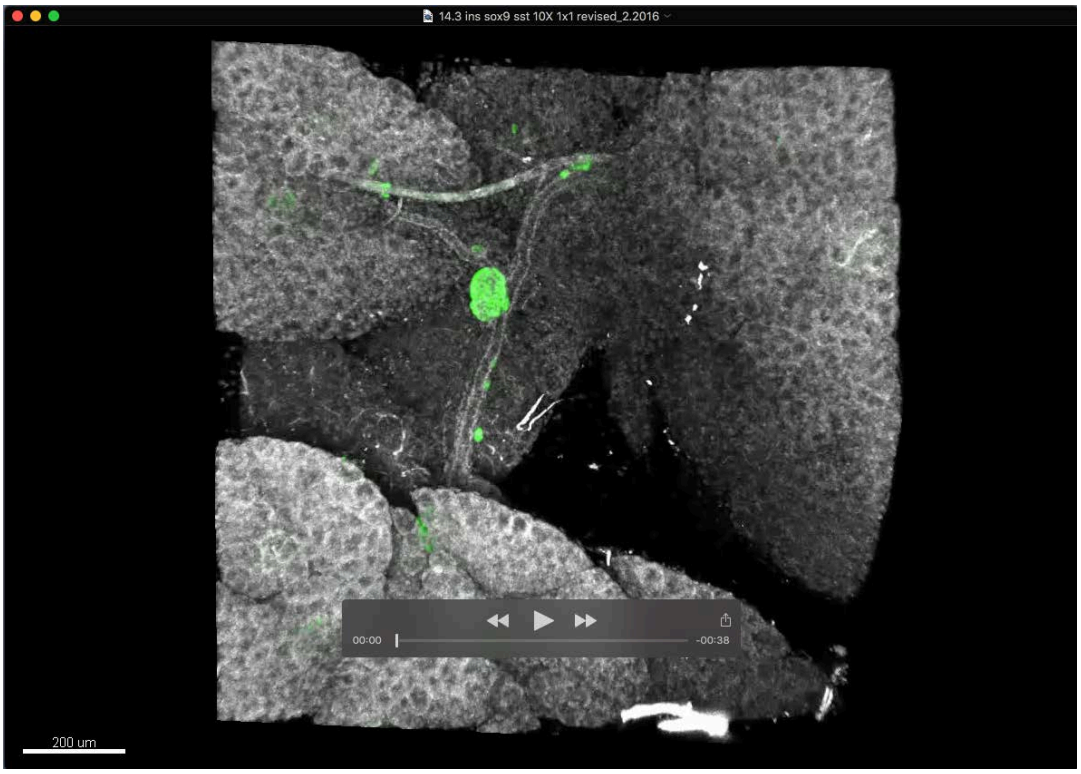

Movie 3. P21 Wild-type islet whole-mount staining.
Whole mount immunofluorescence of 3-week old wildtype mice. Insulin is shown in green to highlight a central, round islet present. Movie was generated using Imaris software.

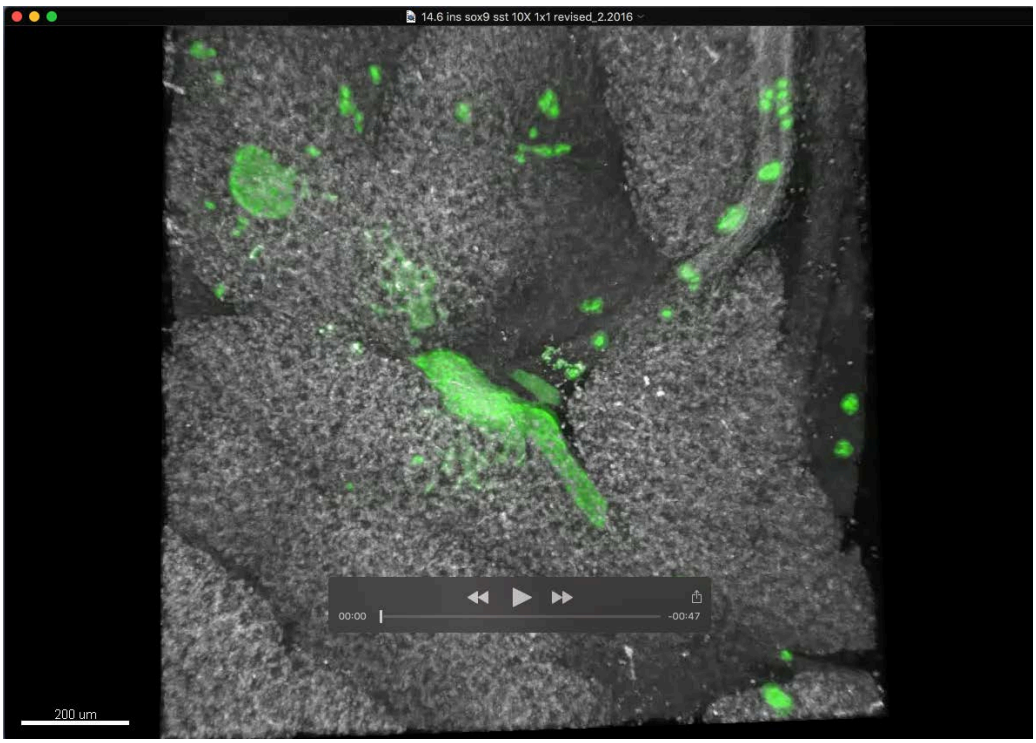

Movie 4. P21 Mutant islet whole-mount staining.
Whole mount immunofluorescence of 3-week old mTOR mutant mice. Insulin is shown in green to highlight an elongated, dysmorphic islet at the center of the movie. Also present are smaller islets, which remain close to the ductal structures in mutant mice. Movie was generated using Imaris software.

Supplemental Methods

Mice

Neurog3^{Cre} mice (Schonhoff et al., 2004) were obtained from Jax and maintained as hemizygous on a C57/BL6 background. *mTOR*$^{f/f}$, *Rictor*$^{f/f}$, and *Raptor*$^{f/f}$ mice were obtained from the Zheng lab and have been previously described (Gangloff et al., 2004; Sengupta et al., 2010; Shiota et al., 2006). A list of genotyping primers can be found in Table S2. Tissue and/or blood samples were collected at time points including e18.5, P0, P7, P10, P14, P21, P28, and 8 weeks of age.

Tissue Processing

Whole pancreas was isolated from mice and washed with cold 1x PBS. Tissue was fixed in 4% PFA overnight at 4° and then washed 3x with PBS. Tissue was then placed in 30% sucrose overnight at 4°.

Samples were washed briefly with 1x PBS, embedded using O.C.T Compound (Tissue-Tek), and frozen. Blocks were serial sectioned at 8 microns.

For electron microscopy analysis, isolated pancreatic tissue was processed as previously described (Jonatan et al., 2014). Tissue was imaged using a Hitachi H-7650 Transmission Electron Microscope equipped with an AMT 2k x 2k tem CCD digital camera.

Circulating Insulin and Glucose

Mice were anesthetized using Isofluorane and blood was collected using a cardiac puncture and placed in a MiniCollect KEDTA tube (Fisher Scientific) with Aprotinin (Fisher Bioreagents) and DPPIV inhibitor (Millipore). Blood was centrifuged for ten minutes at 4° and serum was collected for ELISA analysis.

Glucose Tolerance Tests

For glucose tolerance tests, mice were fasted for 16 hours prior to the experiment. Mice were weighed and fasted blood glucose was taken using a TrueTrack glucometer. 2 g/kg weight of 20% D-glucose was administered to mice and readings were taken at 15, 30, 60, 90, and 120 minutes after intraperitoneal (IP) injection.

IP glucose tolerance test was performed by fasting mice for 16 hours prior to injection. 2 g/kg of 20% D-glucose was administered at that time and mice were monitored for 30 minutes after IP injection. At that time blood serum was collected, processed, and analyzed using methods and materials indicated above.

Immunostaining and Imaging

A full list of antibodies can be found in the Table S1. Slides were rehydrated in 1x PBS and then put in blocking buffer (10% normal donkey serum + 0.5% Triton in 1x PBS) for 1 hour. Primary antibodies were diluted in blocking buffer and incubated overnight at 4°. Slides were washed 3 times in 1x PBS. Secondary antibodies were diluted in blocking buffer and applied to the slides for 1 hour at room temperature. Fluoromount-G (SouthernBiotech) was applied to slides and they were cover slipped. Slides were imaged using a Nikon Confocal A1 inverted microscope. Image analysis and quantification was done using Nikon Elements and Imaris software.

For IHC, frozen sections were rinsed in 1xPBS after thawing. Antigen retrieval was done using 10 mM Citrate buffer and then slides were treated in 3% H_20_2 for 15 minutes. Slides were rinsed and then blocked for 1 hour in 1x PBS + 0.1% Tween 20 + 5% BSA + 5% NDS. Primary antibodies were applied overnight in blocking solution. Slides were rinsed and secondary antibodies were applied for 1 hour. Vector Labs AB reagent was used for 30 minutes on slides, after which Vector Labs DAB reagent was used to develop the stain. The reaction was quenched using water and slides were mounted using Fluromount-G (SouthernBiotech).

Morphogenesis and Migration analysis

For quantification, NIS-Elements software was used to threshold a binary layer based on pixel intensity for each channel. A combined binary layer was created to account for all islet subtypes (Insulin + Glucagon + Somatostatin). From that combined binary layer, we then calculated the circularity, convexity, and elongation of each islet according to the standard mathematical definitions below, all of which are standard functions available in NIS-Elements:

Circularity = $4\times\pi\times\frac{Area}{Perimeter^2}$

Convexity = $\frac{Area}{Convex\ Hull\ Area}$

Elongation = $\frac{Max\ Feret}{Min\ Feret}$

We also extracted data on the islet area and number of nuclei per islet. Total, the number of islets analyzed for mTOR wildtype mice was 593 and 404 for mutant mice (size >100um$^{2)}$. The number of islets analyzed

based on large islet size (5000-20Kum^2) was 171 and 87 for wildtype and mutant mice, respectively. This culminated in 94,546 wild-type cells and 53,748 mutant cells analyzed across 3 biological replicates per group. Shape score was calculated through the following equation: $\frac{1}{Elongation} \times Circularity \times \frac{1}{Convexity}$. Islets were categorized based on area and graphed accordingly.

Ductal analysis was similar to the above protocol. P14 serial sectioned pancreatic tissue was stained for ductal marker, DBA and pan-endocrine marker, ChromograninA. NIS-Elements software calculated the distance of CGA positive islets from the nearest DBA positive ductal structure using the binary layers and thresholds set in the software for the two stains.

Whole-Mount Pancreas Staining

Whole pancreas from mice was dissected and washed with cold 1x PBS. Tissue was then fixed overnight in 4% PFA at 4°. Tissue was washed in cold 1x PBS to remove fixation solution. Tissue was placed in a 50mL conical tube containing A4P0 solution (4% acrylamide + 2.5mg/mL Va-044), oxygen removed, and placed in a 37° water bath overnight. A4P0 solution was decanted off and tissue was incubated in 8% SDS solution until cleared. Tissue was washed in 1x PBS for one day to remove SDS. Primary antibodies were diluted in blocking buffer and tissue was incubated in solution at 4° for 3 days. Pancreas samples were washed with 5x for 1hour with 1x PBS and then the same staining protocol was applied for secondary antibodies.

Flow Cytometry Cellular Dissociation Protocol

Tissue was minced in 37° Red Blood Cell Lysis Buffer for 10 minutes. Tissue was centrifuged and washed in cold Hanks Buffer Salt Solution (HBSS) and incubated in digest solution (2 g/L collagen Type1, 0.2 g/L soybean trypsin inhibitor, 0.5 ug/mL DNase 1 in HBSS) at 37° for 35 minutes. Tissue was washed in cold HBSS and incubated in Trypsin solution for 10 minutes at room temperature. Cells were washed and resuspended in HBSS and filtered through a 40 micron cell strainer and then fixed using Cytofix/Cytoperm solution (BD Biosciences) on ice for 20 minutes. Cells were washed in Perm/Wash buffer (BD Biosciences) and spun down. Primary antibodies were diluted in Perm/Wash buffer and incubated for 40 minutes on ice. Secondary antibodies were also diluted in Perm solution and incubated at room temperature in the dark for 15 minutes.

Supplemental Tables

Table S1: Primary and Secondary Antibodies

Primary Antibody	**Source**	**Catalog Number**	**Dilution**
Rat anti-BrdU	Abcam	Ab6326-250	1:100
Goat anti-Somatostatin	Santa Cruz	SC-7819	1:200
Rabbit anti-cleaved Caspase 3	Cell Signaling	9661	1:200
Goat anti-Glut2	Santa Cruz	SC-7580	1:500
Mouse anti-Glucagon	Sigma	G2654	1:500
Rabbit anti-Glucagon	Zymed	18-0064	1:500
Rabbit anti-mTOR	Cell Signaling	7C10	1:200

Rabbit anti-Uroctortin3	Phoenix Pharmaceuticals	H-019-29	1:500
Rabbit anti-Ki67	Abcam	Ab15580	1:500
Rabbit anti-Nkx2.2	Tom Jessell Lab	110722	1:2000
Rat anti-PECAM	BD Biosciences	553371	1:150
Rabbit anti-SOX9	Santa Cruz	Sc-20095	1:100
Goat anti-Pdx1	Abcam	Ab94931	1:5000
Bio anti-DBA	Vector	B-1035	1:100
Guinea Pig anti-Insulin	DAKO	A0564	1:1000
Rabbit anti-Phospho-mTOR	Cell Signaling	D9C2	1:100
Mouse anti-PHH3	Abcam	Ab14955-100	1:200
Goat anti-Ghrelin	Santa-Cruz	Sc-10368	1:200
Guinea Pig anti-Synaptophysin	Synaptic Systems	101 004	1:1000
Goat anti-ChromograninA	Santa Cruz	Sc-1488	1:200
Rabbit anti-Sox9	EMD Millipore	AB5535	1:5000
Rabbit anti-Snail2	Abcam	Ab85931	1:100
Rabbit anti-PC1/3	EMD Millipore	AB10553	1:500
Rabbit anti-Pax6	Covance	PRB-278P	1:500
Rat anti-Ecad	R&D	MAB7481	1:500

Secondary Antibody	**Source**	Dilution
Donkey anti-rabbit 546	Invitrogen	1:500
Donkey anti-rat 647	Invitrogen	1:500
Donkey anti-goat 546	Invitrogen	1:500
Donkey anti-rabbit 488	Invitrogen	1:500
Donkey anti-guinea pig 488	Invitrogen	1:500
Donkey anti-guinea pig 546	Invitrogen	1:500

Donkey anti-goat 647	Invitrogen	1:500
Donkey anti-goat 488	Invitrogen	1:500
Donkey anti-rabbit 647	Invitrogen	1:500
Donkey anti-mouse 647	Invitrogen	1:500
Donkey anti-mouse Cy3	Jackson Immuno	1:500
PE anti-mouse	Biolegend	1:100
Goat anti-guinea pig	Invitrogen	1:500

Table S2: Primer list for genotyping

Mouse	Forward Primer	Reverse Primer
Ngn3^{Cre}	ATT TGC CTG CAT TAC CGG TC	AGA GAC GGA AAT CCA TCG CTC G
mTOR$^{f/f}$	TTA TGT TTG ATA ATT GCA GTT TTG GCT AGC AGT	TTT AGG ACT CCT TCT GTG ACA TAC ATT TCC T
Rictor$^{f/f}$	ACT GAA TAT GTT CAT GGT TGT G	GAA GTT ATT CAG ATG GCC CAG C
Raptor$^{f/f}$	CTC AGT AGT GGT ATG TGC TCA G	GGG TAC AGT ATG TCA GCA CAG

Table S3: Significance and N values

Figure	Description	P value	Number of animals
1C	Fasting BGL P7	0.2243	7 WT, 6 Mut
	Fasting BGL P14	0.2741	15 WT, 5 Mut
	Fasting BGL P21	0.1882	5 WT, 3 Mut
	Fasting BGL P28	0.000003	7 WT, 3 Mut
	Fasting BGL 8 weeks	0.00005	3 WT 3 Mut
1C	Circ Insulin P7	0.1717	3 WT, 5 Mut
	Circ Insulin P14	0.1565	6 WT, 3 Mut
	Circ Insulin P21	0.0206	5 WT, 5 Mut
	Circ Insulin P28	0.0044	8 WT, 2 Mut
	Circ Insuiln 8 weeks	0.0016	3 WT 3 Mut
2A	e18.5 Endocrine Count Insulin	0.1778	5 WT, 4 Mut
	e18.5 Endocrine Count Glucagon	0.1287	5 WT, 4 Mut
	e18.5 Endocrine Count Somatostain	0.2706	5 WT, 4 Mut
2A	P7 Endocrine Count Insulin	0.4558	3 WT, 5 Mut
	P7 Endocrine Count Glucagon	0.2016	3 WT, 5 Mut
	P7 Endocrine Count Somatostatin	0.0930	3 WT, 5 Mut
2B	P14 Endocrine Count Insulin	0.0016	11 WT, 5 Mut
	P14 Endocrine Count Glucagon	0.0039	6 WT, 3 Mut
	P14 Endocrine Count Somatostatin	0.0010	6 WT, 3 Mut

3A	P0 TF Isl1	0.4317	3 WT, 3 Mut
	P0 TF Neurod1	0.3901	3 WT, 3 Mut
	P0 TF Nkx6.1	0.4676	3 WT, 3 Mut
	P0 TF Pax6	0.3531	3 WT, 3 Mut
	P0 TF Foxa2	0.3042	3 WT, 3 Mut
	P0 TF Arx	0.2160	3 WT, 3 Mut
3A	P7 TF Isl1	0.4387	3 WT, 3 Mut
	P0 TF Neurod1	0.0124	3 WT, 3 Mut
	P0 TF Nkx2.2	0.1123	3 WT, 3 Mut
	P0 TF Nkx6.1	0.0597	3 WT, 3 Mut
	P0 TF Pax6	7.14E-05	3 WT, 3 Mut
	P0 TF Foxa2	0.0215	3 WT, 3 Mut
3A	P14 TF FoxO1	0.0348	3 WT 3 Mut
	P14 TF Isl1	0.1835	3 WT, 3 Mut
	P14 TF Nkx6.1	0.0077	3 WT, 3 Mut
	P14 TF Pax6	0.0344	3 WT, 3 Mut
3C	P14 Maturation Mafa	0.0387	3 WT, 3 Mut
	P14 Maturation Mafb	0.1985	3 WT, 3 Mut
	P14 Maturation Ucn3	0.0019	3 WT, 3 Mut
	P14 Maturation Tshz1	0.1034	3 WT, 3 Mut
3D	P14 Hormone Glucagon	0.0545	3 WT, 3 Mut
	P14 Hormone Ghrelin	0.1732	3 WT, 3 Mut
	P14 Hormone Insulin1	0.0043	3 WT, 3 Mut
	P14 Hormone Insulin2	0.0011	3 WT, 3 Mut
	P14 Hormone Ppy	0.0440	3 WT, 3 Mut
	P14 Hormone Sst	0.0014	3 WT, 3 Mut
4B	P14 Transporter Sur1	0.0040	3 WT 3 Mut
	P14 Transporter Kir6.2	0.0186	3 WT 3 Mut
	P14 Transporter Slc30a8	0.0117	3 WT, 3 Mut
	P14 Vesicle Marker Chga	0.0006	3 WT, 3 Mut
4C	Beta Cell Granularity P7	0.3658	3 WT, 5 Mut
	Beta Cell Granularity P14	0.0161	3 WT, 2 Mut
	Alpha Cell Granularity P7	0.1358	3 WT, 5 Mut
	Alpha Cell Granularity P14	0.0049	3 WT, 2 Mut
4E	16 Hour Fasted Blood Glucose at P14	0.0032	11 WT, 9 Mut
	16 Hour Fasted Insulin at P14	0.0132	5 WT, 5 Mut
5D	P14 Endocrine Cell Size 1000-3000	0.0009	3 WT, 3 Mut
	P14 Endocrine Cell Size 3000-5000	0.0320	3 WT, 3 Mut
	P14 Endocrine Cell Size 5000-10K	0.0684	3 WT, 3 Mut
	P14 Endocrine Cell Size 10K-20K	0.1589	3 WT, 3 Mut

	P14 Endocrine Cell Size >20K	0.4567	3 WT, 3 Mut
5E	P14 Islet Remodeling Factors E-cadherin	0.4686	3 WT, 3 Mut
	P14 Islet Remodeling Factors N-cadherin	0.0731	3 WT, 3 Mut
	P14 Islet Remodeling Factors Ctgf	0.1259	3 WT, 3 Mut
6C	P21 Raptor Fasted BGL (Het)	0.0784	5 WT, 7 Het
	P21 Raptor Fasted BGL (Mut)	0.0218	5 WT, 4 Mut
	P21 Rictor Fasted BGL (Het)	0.1179	7 WT, 4 Het
	P21 Rictor Fasted BGL (Mut)	0.2181	7 WT, 4 Mut
6D	P21 Rictor Single Cells	0.0191	3 WT, 3 Mut
	P21 Rictor >100	0.0208	3 WT, 3 Mut
	P21 Rictor 100-1000	0.0082	3 WT, 3 Mut
	P21 Rictor 1000-3000	0.0249	3 WT, 3 Mut
	P21 Rictor 3000-5000	0.0536	3 WT, 3 Mut
	P21 Rictor 5000-10K	0.3204	3 WT, 3 Mut
	P21 Rictor 10K-20K	0.3361	3 WT, 3 Mut
	P21 Rictor >20K	0.3501	3 WT, 3 Mut
Supp Figure 1A	Postnatal Weight P7	0.0886	7 WT, 7 Mut
	Postnatal Weight P14	0.3407	15 WT, 5 Mut
	Postnatal Weight P21	0.1179	5 WT, 3 Mut
	Postnatal Weight P28	0.0123	5 WT, 2 Mut
	Postnatal Weight 8 Weeks	0.0004	4 WT, 4 Mut
	Adult Percent Pancreas Weight (WT)	N/A	4 WT
	Adult Percent Pancreas Weight (Het)	0.0986	4 Het
	Adult Percent Pancreas Weight (Mut)	0.2662	4 Mut
Supp Figure 2B	P14 Endocrine Count Insulin	0.0041	11 WT, 6 Het
	P14 Endocrine Count Glucagon	0.0601	11 WT, 6 Het
	P14 Endocrine Count Somatostatin	0.2275	11 WT, 6 Het
Supp Figure 2C	Adult Glucose Tolerance Test Fasted	0.1711	4 WT, 4 Het
	Adult Glucose Tolerance Test 15	0.1555	4 WT, 4 Het
	Adult Glucose Tolerance Test 30	0.1229	4 WT, 4 Het
	Adult Glucose Tolerance Test 60	0.2681	4 WT, 4 Het
	Adult Glucose Tolerance Test 90	0.2480	4 WT, 4 Het
	Adult Glucose Tolerance Test 120	0.4594	4 WT, 4 Het
	1 Year Glucose Tolerance Test Fasted	0.3463	3 WT, 5 Het
	1 Year Glucose Tolerance Test 15	0.3075	3 WT, 5 Het
	1 Year Glucose Tolerance Test 30	0.2176	3 WT, 5 Het
	1 Year Glucose Tolerance Test 60	0.3698	3 WT, 5 Het
	1 Year Glucose Tolerance Test 90	0.3308	3 WT, 5 Het
	1 Year Glucose Tolerance Test 120	0.3384	3 WT, 5 Het
Supp Figure 3C	P14 Single Cells	0.4983	3WT, 3 Mut
	P14 <100	0.3781	3WT, 3 Mut

	P14 100-1000	0.3891	3WT, 3 Mut
	P14 1000-3000	0.0265	3 WT, 3 Mut
	P14 3000-5000	0.0223	3 WT, 3 Mut
	P14 1000-10K	0.0161	3 WT, 3 Mut
	P14 10K-20K	0.0136	3 WT, 3 Mut
	P14 >20K	0.0003	3 WT, 3 Mut
Supp Figure 4C	e18.5 Beta Cell Proliferation Ki67	0.0189	3 WT, 3 Mut
	P7 Beta Cell Proliferation Ki67	0.0977	3 WT, 3 Mut
	Percent Proliferation (WT)	N/A	7 WT
	Percent Proliferation (Het)	0.1688	5 Het
	Percent Proliferation (Mut)	0.2627	3 Mut
Supp Figure 5A	P14 Neurogenin3 Expression	0.2604	3WT, 3 Mut
Supp Figure 5B	P0 Hormone Glucagon	0.4728	3 WT, 3 Mut
	P0 Hormone Ghrelin	0.2242	3 WT, 3 Mut
	P0 Hormone Insulin1	0.1322	3 WT, 3 Mut
	P0 Hormone Ppy	0.1009	3 WT, 3 Mut
	P0 Hormone Sst	0.3295	3 WT, 3 Mut
	P7 Hormone Glucagon	0.0531	3 WT, 3 Mut
	P7 Hormone Ghrelin	0.1888	3 WT, 3 Mut
	P7 Hormone Insulin1	0.0193	3 WT, 3 Mut
	P7 Hormone Insulin2	0.0041	3 WT, 3 Mut
	P7 Hormone Ppy	0.0292	3 WT, 3 Mut
	P7 Hormone Sst	0.0584	3 WT, 3 Mut
Supp Figure 5C	P14 Disallowed Gene Ldha	0.1345	3 WT, 3 Mut
	P14 Disallowed Gene Oxct1	0.3868	3 WT, 3 Mut
	P14 Disallowed Gene Slc16a1	0.3696	3 WT, 3 Mut
Supp Figure 5D	P7 Channel/Transporter Sur1	0.3179	3 WT, 3 Mut
	P7 Channel/Transporter Kir6.2	0.2184	3 WT, 3 Mut
	P7 Channel/Transporter Slc30a8	0.0015	3 WT, 3 Mut
Supp Figure 5E	Delta Cell Granularity P7	0.1141	3 WT, 5 Mut
	Delta Cell Granularity P14	0.3930	3 WT, 2 Mut
Supp Figure 5F	Insulin After IP Glucose	0.2457	6 WT, 4 Mut
Supp Figure 6A	P14 Shape 1000-3000	0.2027	3 WT, 3 Mut
	P14 Shape 3000-5000	0.1442	3 WT, 3 Mut
	P14 Shape 5000-10K	0.0044	3 WT, 3 Mut

	P14 Shape 10K-20K	0.0465	3 WT, 3 Mut
	P14 Distance 100-1000	0.3112	3 WT, 3 Mut
	P14 Distance 1000-5000	0.4321	3 WT, 3 Mut
	P14 Distance 5000-10K	0.3587	3 WT, 3 Mut
	P14 Distance 10K-20K	0.0246	3 WT, 3 Mut
	P14 Distance >20K	0.0580	3 WT, 3 Mut
Supp Figure 6C	P14 E-cadherin Quantification	0.1975	3 WT, 3 Mut
Supp Figure 7A	P21 Raptor Circulating Insulin (Het)	0.4114	5 WT, 7 Het
	P21 Raptor Circulating Insulin (Mut)	0.0254	5 WT, 4 Mut
	P21 Rictor Circulating Insulin (Het)	0.4590	7 WT, 4 Het
	P21 Rictor Circulating Insulin (Mut)	0.2638	7 WT, 4 Mut
Supp Figure 7B	P14 16 Hour Fast mTOR	0.0068	18 WT, 4 Mut
	P14 16 Hour Fast Raptor	0.2060	7 WT, 3 Mut
Supp Figure 7C	P21 Rictor Shape 1000-3000	0.1513	3 WT, 3 Mut
	P21 Rictor Shape 3000-5000	0.0405	3 WT, 3 Mut
	P21 Rictor Shape 5000-10K	0.2967	3 WT, 3 Mut
	P21 Rictor Shape 10K-20K	0.1174	3 WT, 3 Mut
	P21 Rictor Shape >20K	0.4951	3 WT, 3 Mut

Supplemental References

Gangloff, Y.-G., Mueller, M., Dann, S. G., Svoboda, P., Sticker, M., Spetz, J.-F., Um, S. H., Brown, E. J., Cereghini, S., Thomas, G., et al. (2004). Disruption of the mouse mTOR gene leads to early postimplantation lethality and prohibits embryonic stem cell development. *Mol. Cell. Biol.* **24**, 9508–16.

Jonatan, D., Spence, J. R., Method, A. M., Kofron, M., Sinagoga, K., Haataja, L., Arvan, P., Deutsch, G. H. and Wells, J. M. (2014). Sox17 regulates insulin secretion in the normal and pathologic mouse β cell. *PLoS One* **9**, e104675.

Schonhoff, S. E., Giel-Moloney, M. and Leiter, A. B. (2004). Neurogenin 3-expressing progenitor cells in the gastrointestinal tract differentiate into both endocrine and non-endocrine cell types. *Dev. Biol.* **270**, 443–54.

Sengupta, S., Peterson, T. R., Laplante, M., Oh, S. and Sabatini, D. M. (2010). mTORC1 controls fasting-induced ketogenesis and its modulation by ageing. *Nature* **468**, 1100–1104.

Shiota, C., Woo, J.-T., Linder, J., Shelton, K.D. and Magnuson, M.A. (2006). Multiallelic disruption of the rictor gene in mice reveals that mTOR complex 2 is essential for fetal growth and viability. *Dev. Cell* **11,** 583-589.